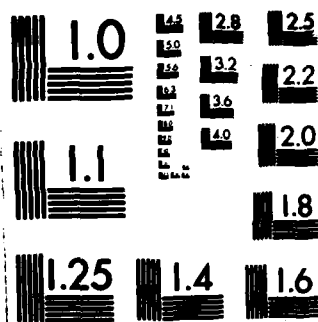AD-A148 065   COMPUTATION OF FLOW AND HEAT TRANSFER IN FLOW AROUND A   1/1
               180-DEG BEND(U) UNIVERSITY OF MANCHESTER INST OF
               SCIENCE AND TECHNOLOGY (ENGL.. B E LAUNDER ET AL.
UNCLASSIFIED   APR 84 N00014-83-G-0021   F/G 20/4   NL

END
DATE
FILMED
85
DTIC

MICROCOPY RESOLUTION TEST CHART
NATIONAL BUREAU OF STANDARDS-1963-A

1 INTRODUCTION

During 1982-83 work progressed on four separate fronts corresponding to both experimental and computational aspects of turbulent flow in 180° bends for both square and round tubes.

The year saw the completion of work on the square sectioned bend and Mr. R.W. Johnson's PhD thesis documenting in great detail the research accomplished will be circulated within two months. Here, therefore, in Section 2 only a short summary will be given. Appendix 1 includes a paper by Chang, Humphrey, Johnson and Launder [1] reporting the outcome of the computational work reported at the 4th Turbulent Shear Flows Symposium in Karlsruhe.

The computational work on flow in circular sectioned ducts has also reached the stage of publication [2,3,4] and copies of these papers are also appended to supplement the summary of computational and experimental research given in Section 3. Finally, Section 4 outlines the work now underway to bring the project to completion.

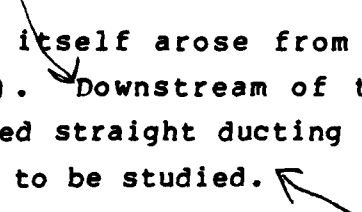# 2 SQUARE SECTIONED BEND

2.1 Experimental Program

2.1.1 Apparatus and Instrumentation

The design and construction of the apparatus was described in some detail in last year's Annual Report [5]. The radius of the bend was 3.35 times the duct hydraulic diameter (D_H), the width of the duct walls being 88.9 mm. Up to 70 hydraulic diameters of flow development were available prior to the bend but the main emphasis of the experiments was directed at the case of 31 D_H which corresponded with the conditions at which the UC Berkeley flow field data had been taken. (In fact, no major differences in the flow or thermal

to p. 2

temp.(

behaviour in the bend itself arose from the variation in the
length of development). Downstream of the bend 40 hydraulic
diameters of instrumented straight ducting allowed the effects of
decaying secondary flow to be studied.

Heating was provided by electrically-heated Intrex
sheeting, a gold film deposited uniformly on a plastic substrate.
The sheets were cut to size and affixed to the inside of the duct
with the gold film on the surface exposed to the airstream.
Variations in resistivity of the Intrex were found to be within $\pm$
8% of the mean provided material from near the edges of the roll
was discarded. In use a certain amount of ageing was evident and
when local non-uniformities became serious the sheets were removed
and replaced by new material.

Thermocouple measurements at up to 9 stations recorded wall
temperatures at 12 positions around one half of the perimeter
(the flow being nominally symmetric about the surface passing
through the centre of the duct and lying in the plane of the
bend). Temperatures were also measured at 3 positions on the
opposite side of the duct to provide symmetry checks. The maximum
wall temperature was limited to $30^{\circ}C$ above ambient to limit the
rate of deterioration of the Intrex sheeting and to keep the
variation in air properties to unimportant levels. A rake
carrying 13 chromel-alumel thermocouples allowed measurements of
the temperature field over the duct cross section at the same
positions as the wall temperatures were recorded.

The ducting was encased in expanded polystyrene insulant to
a thickness of 40 mm.

2.1.2 **Test Program** Measurements of wall and interior
temperatures and heat fluxes were made at a Reynolds number of
56700 corresponding to that of the Berkeley experiment. Moreover,
although Professor Humphrey's group were responsible for

documenting the flow field [6], some limited velocity-field measurements were judged necessary at UMIST to establish that our flow conditions were indeed sensibly the same as at Berkeley (this verification acquired further importance as it was found that the numerical computations exhibited a strikingly different flow pattern midway around the bend from the measurements). Velocity profiles were obtained by hot-wire traverse 5 diameters upstream of the bend and at 90°.

The remaining tests were made with 70 diameters of inlet flow development in order to establish essentially fully-developed conditions at entry to the bend. Limited temperature and velocity-field data were taken at the same Reynolds number as the earlier test; these indicated no significant variations in flow structure. In the limited time available attention was mainly directed at obtaining data on heat transfer coefficients over as wide a range of Reynolds number as possible rather than focusing on a very detailed mapping of the interior temperatures at one Reynolds number. Data were thus obtained at nominal Reynolds numbers of 9×10^3 and 9×10^4.

2.1.3 <u>The Experimental Results</u> Figure 1 compares Berkeley and UMIST measurements of streamwise velocity at 90^σ around the bend. A striking feature of the Berkeley measurements was the double peak in streamwise velocity (a feature that neither their nor our computations reproduce). The velocity data obtained at UMIST confirm this feature of the Berkeley experiments. The small differences between the two sets of readings could well be due to a positioning error in the UMIST data. (Our original intention had been to take only a single bottom-to-top traverse along the mean radius of curvature but, to allow more direct comparison with the Berkeley data, which were obtained from side-to-side traverses, rather rudimentary adaptations were made to allow traverses at other radii). It was concluded therefore that we could assume that the flow-field in the UMIST apparatus was indeed

essentially the same as documented in the geometrically similar half-scale Berkeley apparatus.

Temperature profiles across the duct are shown for 45°, 90° 135° and 180° in figure 2. These mimic closely the corresponding velocity profiles. For example, by 45° the "peak" temperature (actually the coolest point in the stream) has shifted right of centre, while at 90° there is a deep trough in the temperature in just the same position as the trough in velocity shown in figure 1. The remains of these troughs are still clearly present at 135° and are faintly visible even at 180°.

The development of the Nusselt number around the bend is shown in figure 3. Up to entry to the 180° section the Nusselt number is nearly uniform along all walls. By 45°, however, the level of Nu on the inner line of symmetry has fallen by 25% while the average level has risen by about 10%. By 90° there is more than a 2:1 ratio in the Nusselt numbers recorded on the inner and outer symmetry planes. This ratio remains nearly constant over the second half of the bend though the absolute level of Nu diminishes slowly. There remains a significant difference in heat transfer coefficient even 10 diameters downstream of the bend, the heat transfer coefficient on the outer bend wall being 30-50% higher than on the inner wall. Throughout, the heat transfer coefficient on the side wall follows closely that on the outer wall.

2.2 Computational Program

2.2.1 Numerical and Physical Model

The computer program embodying a three-dimensional semi-elliptic solving scheme for the averaged equations of motion was provided by Professor Humphrey. It is based on the discretizational and programming strategy of the TEACH family of computer codes save that convective transport

is here represented by *quadratic* upstream weighting [7] . The code incorporates as alternatives the $k \sim \varepsilon$ Boussinesq viscosity and the algebraic stress models of turbulence, both of which utilize the standard transport equations for the turbulence energy and its dissipation rate ε.

The effort at UMIST initially consisted of a very thorough re-checking of the algebraic and coded forms of the transport equations for the flow-field variables. This exercise proved very useful in establishing confidence that what was inevitably a large and complex code was free from coding error.

Thereafter the computer program was adapted to incorporate a new wall-function treatment for the viscosity-affected zone between the near-wall node and the wall itself [8]. A further adaptation was the inclusion of the streamline-curvature modification to the transport equation for ε [9] proposed on the basis of two-dimensional flows. Further details are given in ref. [1] appended. A solving routine was also included for the thermal energy equation. Since the fluid properties were taken as independent of temperature, this equation was solved only after a converged solution had been obtained to the velocity field.

2.2.2 <u>Comparison of Computed and Measured Behaviour</u> Initial computations were made using a 20 x 12 non-uniform grid to map the cross-section of the duct with 110 streamwise planes, 60 of which were located on the bend itself (i.e. a 3° spacing). The nodal density was subsequently refined to 15 x 28 in the cross-section while over the first 45° of the bend computational planes were spaced at $1\frac{1}{2}^\circ$ intervals. These refinements, while leading to changes up to a maximum of 10% in the secondary flow, had only a very weak effect on the streamwise velocity profiles.

The situation regarding computations can most effectively be conveyed by reference to the 90° plane (ref. [1] in the Appendix shows further details). From figure 4 it is evident that the

large trough in the streamwise velocity shown by the experiments
is not reproduced by the computations. There are unfortunately no
data between the 45° and 90° stations but the computations seem to
indicate that the trough has arisen through the secondary velocity
separating off the inside wall somewhere between these two
stations thus giving a secondary recirculation, figure 5, in the
opposite sense than usual. It must be said however that
measurements at 90° show no sign of such a reversed eddy so this
explanation remains tentative. The behaviour shown in figure 4 is
nearly the same as that obtained at Berkeley by Chang [10] using,
in both cases, the k~ε Boussinesq viscosity model. The relative
insensitivity of the results to grid refinement[†] and to the choice
of wall function suggests that the poor predictions are mainly due
to the turbulence model used in the main flow region. Yet it is
found [1] that very little effect resulted from introducing the
curvature correction to the transport equation or from adopting
the algebraic stress model. Although Mr. Johnson has now
concluded his research, Professor Young Don Choi, an academic
visitor mentioned in the footnote, continues to address the
problem.

3   ROUND SECTIONED DUCT

3.1   Experimental Program

        The experimental work on the round sectioned duct has
greatly benefited from extensive interaction with Professor J.W.
Baughn of the Mechanical Engineering Department, University of
California Davis. We concluded that the attainment of a
uniform-heat-flux boundary condition was impracticable for this
particular geometry and so the apparatus design has been based on
a uniform wall temperature rig. The 180° bend section has been
fabricated in two halves (figure 5) machined from solid blocks of
aluminium. The ratio of bend radius:pipe diameter is the same as

---

† Current work at UMIST by Professor Young Don Choi with twice as many cross-
sectional nodes and 50% more streamwise planes has led to only minor improve-
ments.

for the square sectioned duct, 3.35:1. Inlet and outlet tangent sections each 40 diameters in length made of high-grade aluminium tubing are installed. At the downstream end of this assembly, connection is made to the flow-metering section and fan exhaust used for the square duct experiment.

Heat transfer rates to the duct wall are to be obtained by heat flux meters based on the design of Professor Baughn and one of his students at UC Davis, ref.[11] . The holes into which the meters will be cemented are clearly visible in figure 6. A sketch of the meter is shown in figure 7. The principle of operation is that heat is supplied via resistors to the flat metal cone at a rate that is just sufficient to keep the cone temperature the same as that of the pipe. At present a prototype meter has been built and is undergoing testing.

3.2   Computational Program

3.2.1 Numerical Solution Procedure   In the 1981/82 Annual Report we reported that a semi-elliptic procedure for flow through toroidal ducts had been developed and showed its successful application to one of the laminar flow cases of Agrawal, Talbot and Gong [12] at a Dean number of 183. During 1982/83 the procedure has been applied to duct flows at successively higher Dean numbers and this has pointed the need for further refinements.

An important step has been the replacement of the SIMPLE algorithm by the more recent SIMPLER procedure, Patankar [13] The former approach, while successful enough when curvature terms were moderate, did not succeed in procuring convergence as the Dean number was successively raised. Details of how SIMPLER has been implemented in the present semi-elliptic scheme are given in reference [2] and [3] contained in the Appendix.

A numerical refinement of a different kind has been prompted by the problem of computing turbulent flow. Because of the very strong secondary flow that is generated close to the wall, it was felt strongly desirable to discard the habitually used wall-function approach and instead carry out the integration to the wall itself. However, there was insufficient core available to us to add the further ten or so radial lines needed to resolve the viscous and buffer regions[+]. The problem was removed, however, by recognizing that across the region where viscous effects were significant, the pressure variation would be adequately obtained from assuming radial equilibrium. In a semi-elliptic solver it is the pressure that limits the mesh density because only this variable requires three-dimensional storage. Thus, we put in additional *velocity* nodes across the near-wall sublayer but no corresponding nodes for the pressure. Further details may be found in [4] in the Appendix.

The computations for turbulent flow have so far adopted the standard $k \sim \varepsilon$ Boussinesq viscosity model in the fully turbulent region matched to the Van Driest form of the mixing length hypothesis across approximately the 5% of the flow nearest to the wall. Further details are given in ref. [3] in the Appendix. In solving the thermal energy equation to predict heat transfer coefficients, a uniform turbulent Prandtl number of 0.9 is adopted throughout the pipe.

3.2.2 **Examples of Applications** Although the main interest in the project is in turbulent flow, a thorough testing of the computational scheme for laminar flow was felt desirable in view of the several sets of data available. In continuation (from our 1981/82 report) of the study of the Agrawal data [12], figure 8 compares streamwise velocity profiles at two sections for a Dean number of 563. The computations started at the entry to the bend with a uniform inlet velocity assumed. The grid employed was 20 x 20 x 100. Close agreement is displayed between the computed and measured behaviour. A further case examined was that of

---

[+] In the present work this region is spanned with the mixing length hypothesis. More than 10 nodes would probably be required if a more elaborate closure were adopted.

Enayet et al [14] in a 90° bend with a radius:diameter ratio of only 2.8:1 giving a Dean number of 464. In this case the bend was preceded by a straight entry section and, as a result, at entry the boundary layer thickness was about 0.5 times the pipe radius. The higher Dean number and the presence of relatively thick boundary layers leads to a stronger secondary flow being established. Figure 9 indicates, however, that a satisfactory numerical simulation is nevertheless obtained.

Enayet et al [14] also measured the development of turbulent flow through the same duct and our computations of streamwise velocities in this flow are shown in figure 10. Agreement is now less complete than for the laminar flow case and, in particular, the trough in the velocity profile at 60° and 75° is only qualitatively predicted. Nevertheless, the measured behaviour is simulated far more satisfactorily than for the square sectioned duct discussed in Section 2.

Computations of the heat transfer behaviour are provided in ref. 4 in the Appendix. Comparisons with the experiments of Seban and McLaughlin [15] of fully-developed flow in a coil suggest that our scheme predicts accurately the rise in the circumferentially averaged heat transfer coefficient but that the augmentation on the outside of the bend is underestimated as is likewise the damping around the inside. This is qualitatively the type of behaviour to be expected with a Boussinesq-type model since it does not mimic the great sensitivity to streamline curvature that real turbulence displays. The thermal field computations of the 2.8:1 90° bend of Enayet et al [14] indicate a five-fold variation of local heat transfer coefficient around the bend at 75°. The *experiment* was purely concerned with the flow field - no heat transfer was involved - but, on the basis of the comparison with the Seban-McLaughlin data, it would seem probable that in that geometry as much as a ten-fold variation in heat transfer coefficient may actually occur between the inside and outside of the bend.

4 Future Work

4.1 Experimental Research

The principal experimental work concerns the commissioning of the circular-sectioned tube apparatus. First tests on the assembled rig will begin during April 1984. The initial testing will be concerned with the *in situ* performance of the heat flux meters, tested in the straight entry section against well-established data of developing flow in a circular tube. The pattern of experiments will be similar to that in the square-sectioned duct: a detailed set of measurements of wall flux and a mapping of the temperature field at the same Reynolds number as the Berkeley circular tube experiments. Some limited confirmatory velocity field data will also be gathered. Thereafter wall flux data will be obtained at the extremes of Reynolds number accessible to the fan.

Looking further ahead (further than the period covered by the present grant), we will aim to obtain from the two 180° bend apparatuses several additional sets of experimental data. These will include explorations where the flow entering the bend is essentially at uniform velocity and studies at the low-Reynolds-number end of the turbulent regime where partial laminarization may occur in passage around the bend.

4.2 Computational Work

Our present efforts are directed at incorporating an algebraic stress model into the circular bend code. There is reasonable optimism that useful improvements in the fidelity of the computer simulation will result. The lingering doubt concerns the fact that, when included in the square duct code, the algebraic stress model did not produce better results. Against this discouraging fact, however, may be set many striking

successes (recorded in the literature of the last ten years) from applying algebraic stress models to curved flows. Moreover, in contrast to the fairly satisfactory prediction of the round-sectioned 90° bend with the $k \sim \varepsilon$ Boussinesq viscosity model, the square-sectioned duct predictions with the same turbulence model go completely wrong beyond 45° of arc. Our current view is that the poor accuracy of predictions in the square sectioned duct is mainly due to weaknesses in the dissipation rate equation. Over the remaining period of the grant Professor Choi's efforts will be directed at improving this aspect of the modelling.

References

1   Chang, S.M., Humphrey, J.A.C., Johnson, R.W. and Launder, B.E.
    (1983) Proc. 4th Sympos. Turbulent Shear Flows 6.20
    University of Karlsruhe

2   Humphrey, J.A.C., Iacovides, H. and Launder, B.E. "Some
    numerical experiments on developing laminar flow in 180°
    circular-sectioned bends" UMIST Mech. Eng. Dept. Rep.
    TFD/84/2

3   Iacovides, H. and Launder, B.E. "The computation of momentum
    and heat transport in turbulent flow around pipe bends" 1st
    U.K. National Heat Transfer Conference, Leeds, July 1984
    (Inst. Chem. Engrs. Symposium Series 86)

4   Iacovides, H. and Launder, B.E. "PSL - An economical approach
    to the numerical analysis of near-wall elliptic flow" ASME
    J. Fluids Eng. 106, to appear 1984

5   Launder, B.E., Johnson, R.W. and Iacovides, H. "Convective
    transport in flow around a 180° bend" Annual Rep. 1981/82
    on ONR RG N00D14-80-G-0130, UMIST Mech. Eng. Rep.
    TFD/83/2(R), 1983

6   Chang, S.M., Humphrey, J.A.C. and Modavi, Physico-chemical
      Hydrodynamics, 4, 243-269, 1983

7   Leonard, B.P. Comp. Meth. Appl. Mech. Eng. 19, 59, 1979

8   Johnson, R.W. PhD Thesis, Faculty of Technology, University
      of Manchester, 1984

9   Launder, B.E. Priddin, C.H. and Sharma, B.I. J. Fluids. Eng.,
      99, 231-239, 1977

10 Chang, S.M. PhD Thesis, Department of Mechanical Engineering,
      University of California, Berkeley, 1983

11 Kraabel, J.S., Baughn, J.W. and McKillop, A.A. ASME J. Heat
      Transfer 102, 576, 1980

12 Agrawal, Y., Talbot, L. and Gong, K. J. Fluid Mech. 85, 497,
      1978

13 Patankar, S.V. and Spalding, D.B. Int. J. Heat Mass Transfer
      15, 1787, 1972

14 Enayet, M.M., Gibson, M.M., Taylor, A.M. and Yianneskis, M.
      Int. J. Heat & Fluid Flow 3, 213, 1982

15 Seban, R.A. and McLaughlin, E.F. Int. J. Heat Mass Transfer,
      6, 387
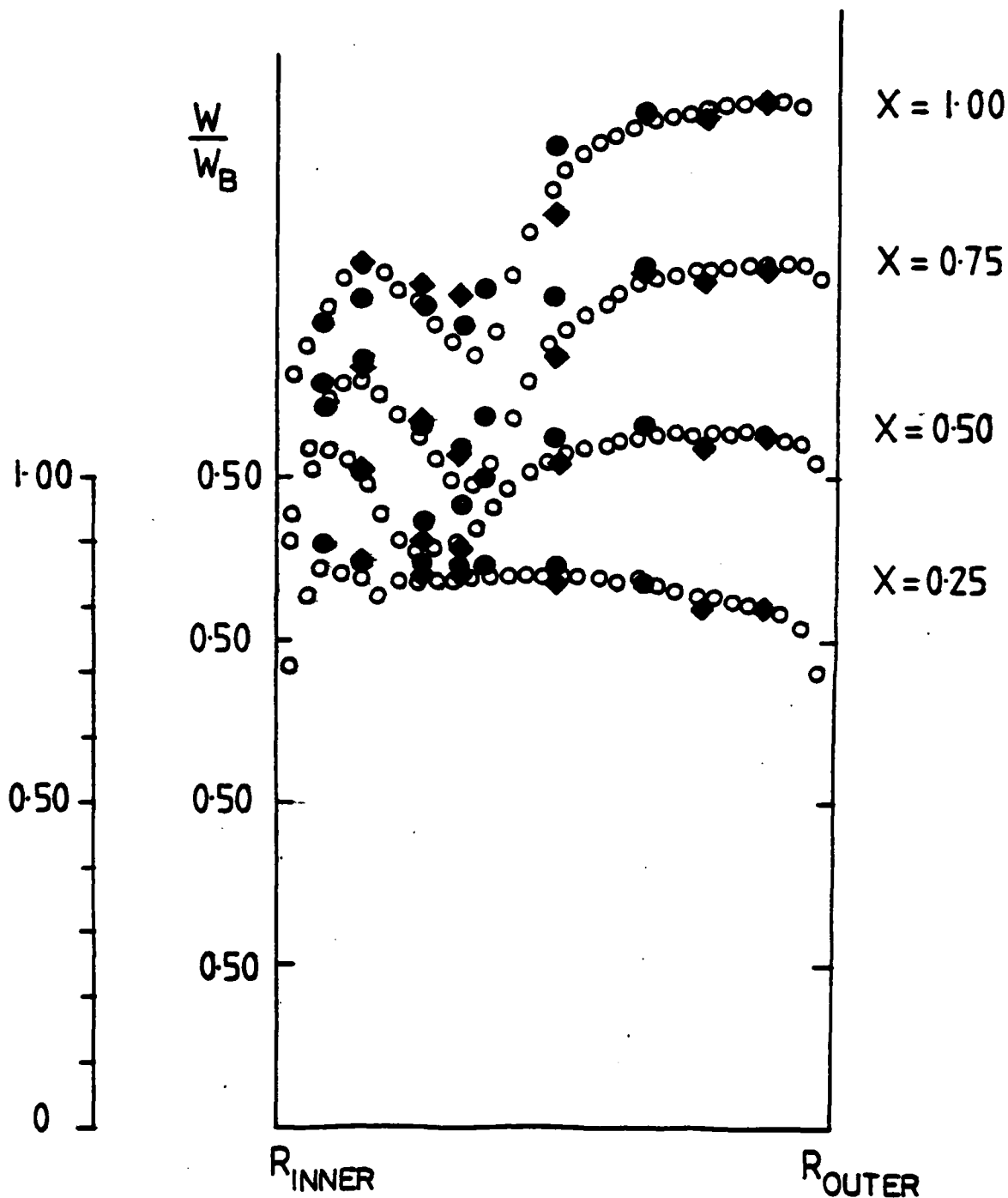
Figure 1   Comparison of normalised mean streamwise velocity at
90° in the bend; ◯ - data Chang et al (1983), 3·1 D_H
inlet, Re = 56,690; ◆ - data present study, 30 D_H
inlet, Re = 57,300; ● - data present study, 72 D_H
inlet, Re = 56,500.
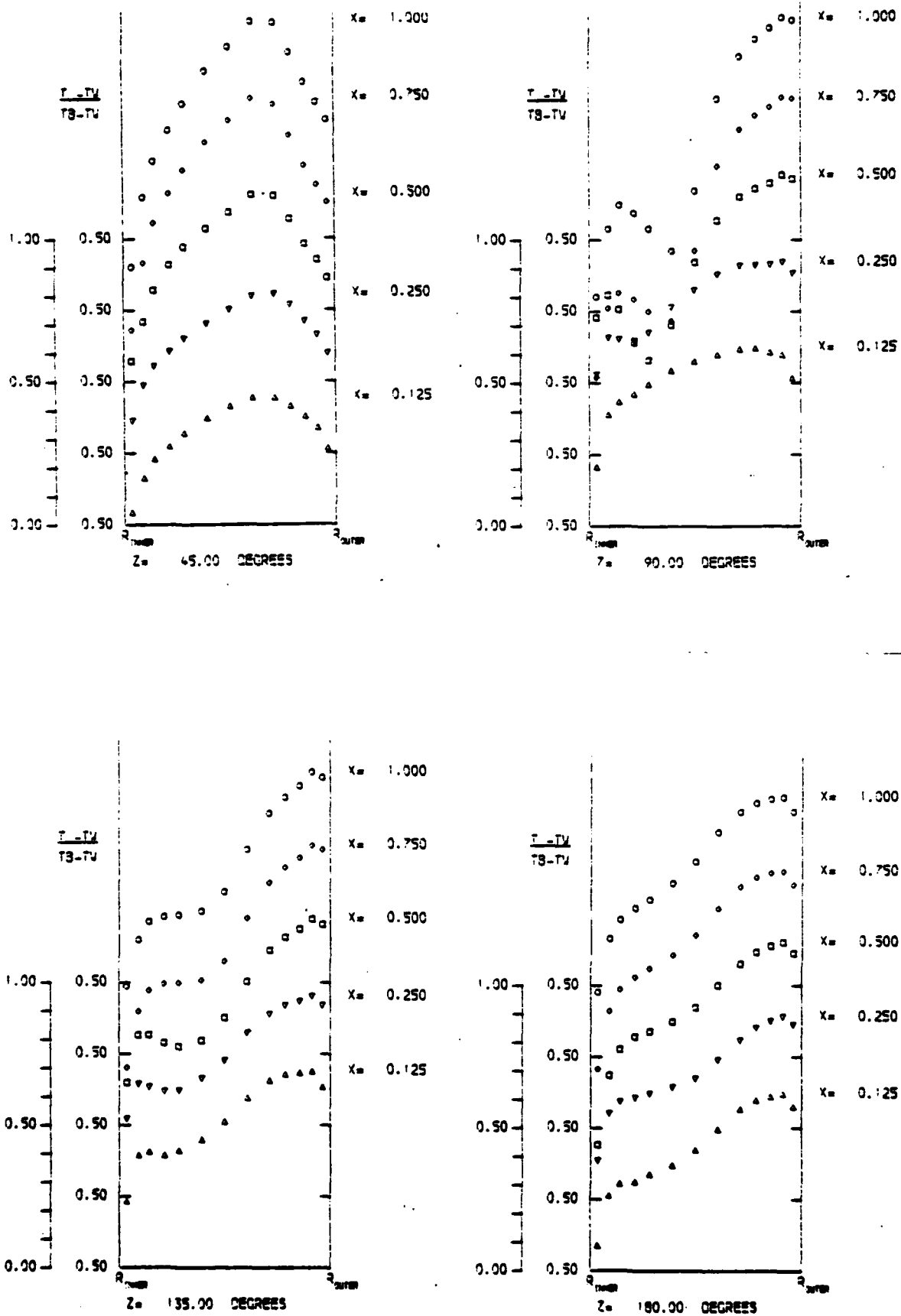
Figure 2   Turbulent flow measurements of mean temperature at
0°, 45°, 135° and 180° in the bend , non-dimensionalised
with respect to the wall temperature (T_W) on the outer
wall at $2x/D_H = 1$ and the bulk temperature (T_B) for
$Re = 55,800$, inlet tangent $30D_H$
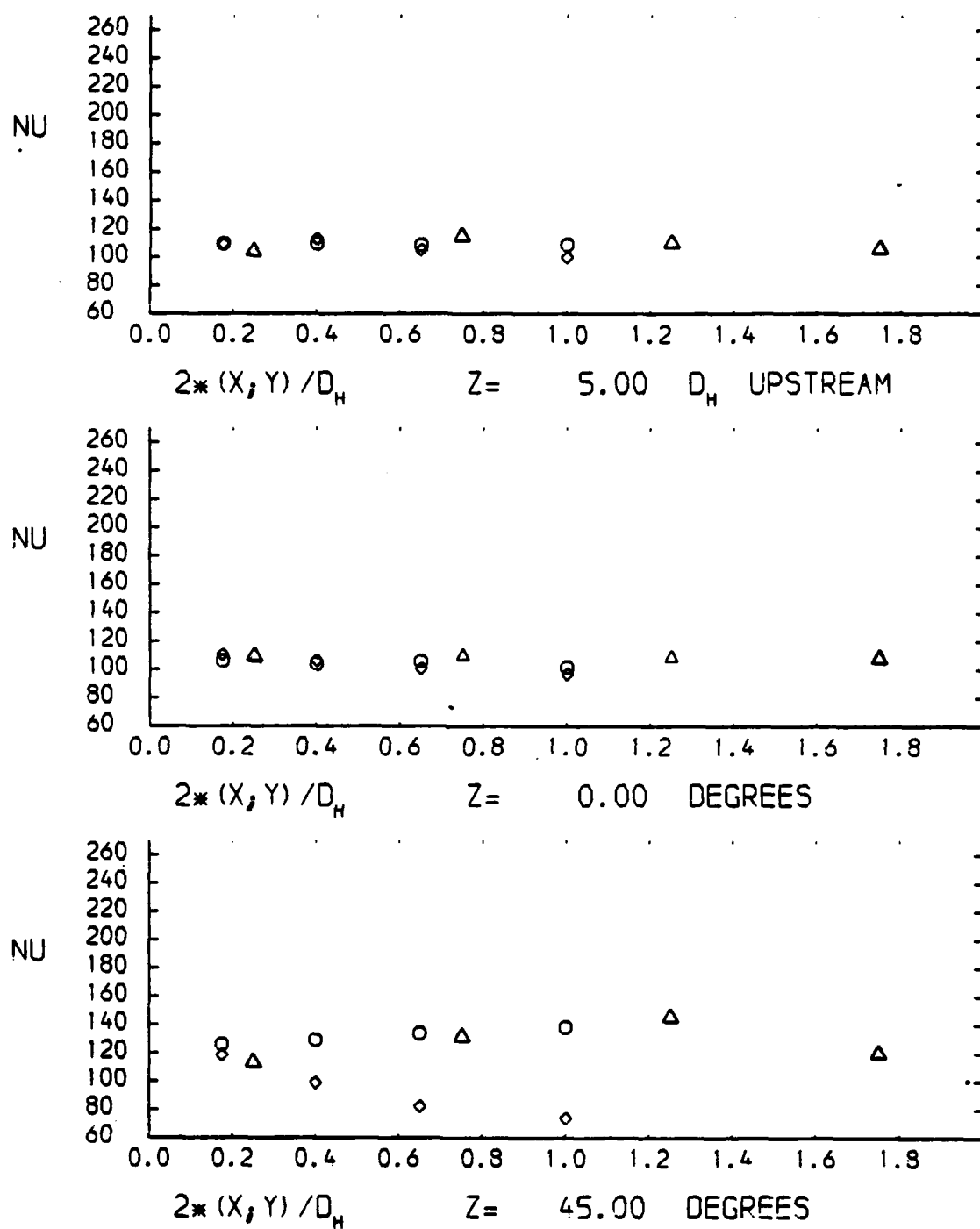
Figure 3(a)   Nusselt number computed from experiment at 5 D_H upstream and 0° and 45° in the bend; O - outer wall, Δ - bottom wall, ◇ - inner wall; inlet tangent 30 D_H; Re = 56,030.
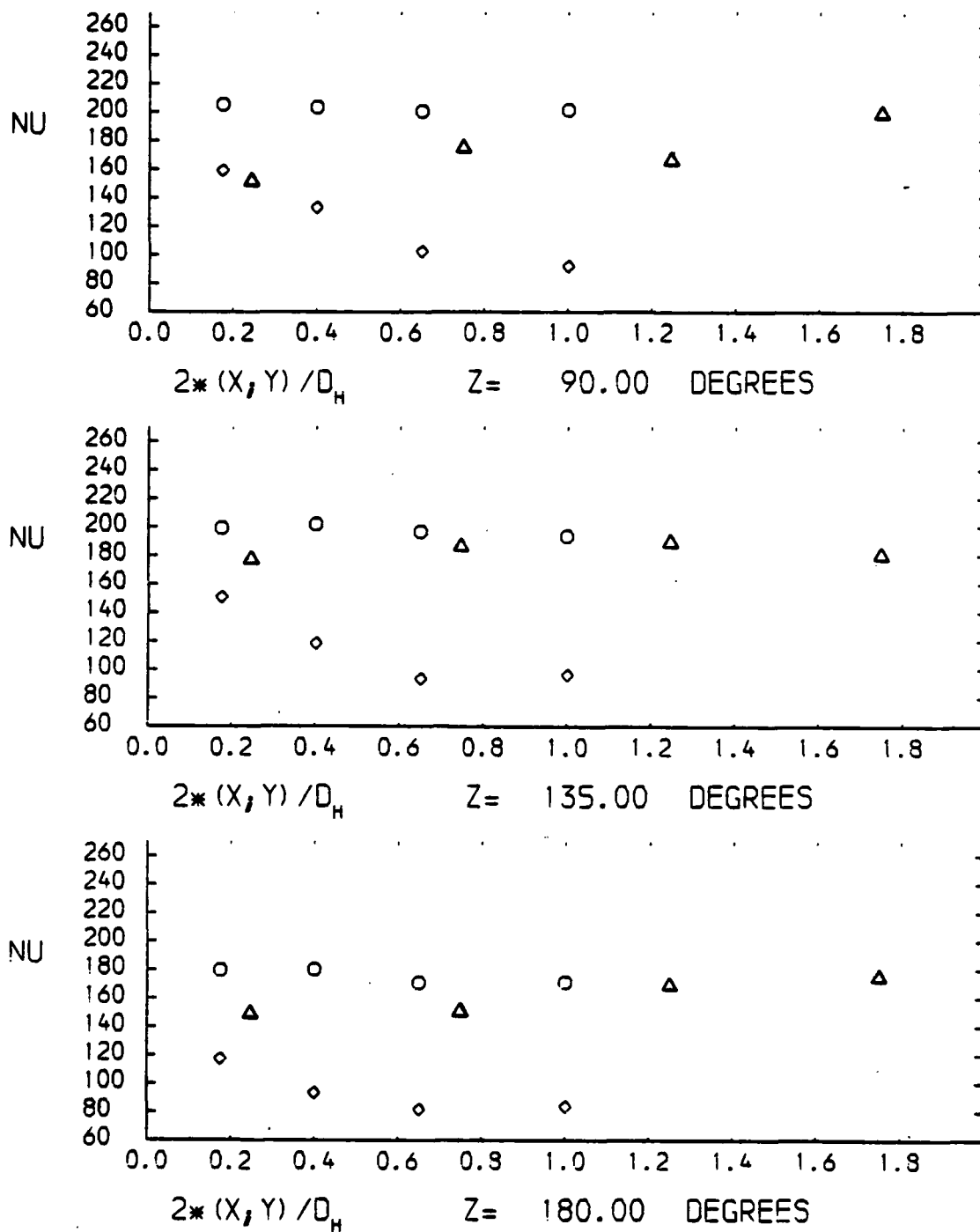
Figure 3(b)   Nusselt number computed from experiment at 90°, 135° and 180° in the bend.
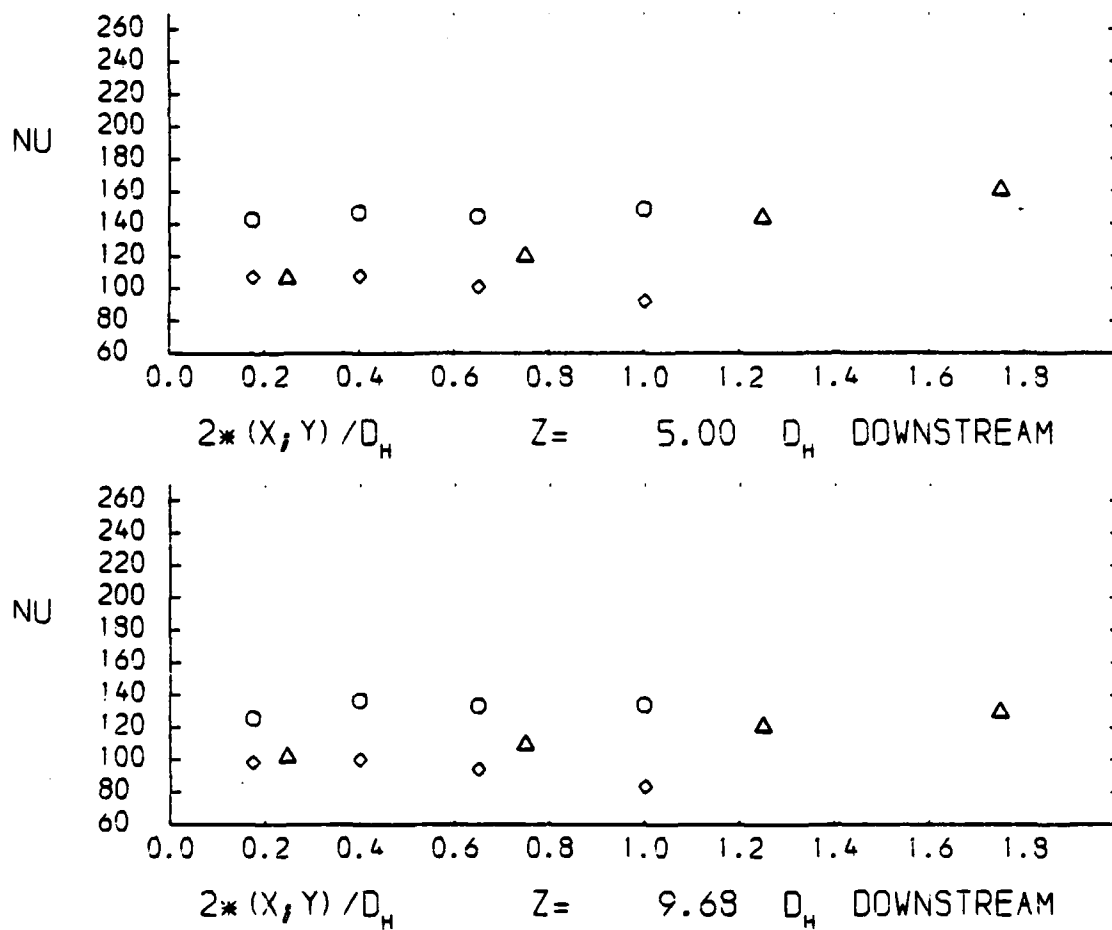
Figure 3(c)   Nusselt number computed from experiment at 5 D_H
and 10 D_H downstream of the bend.
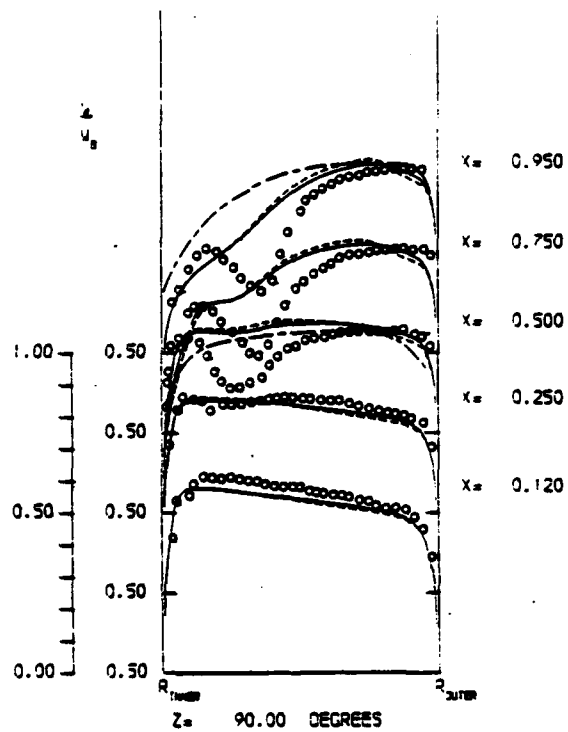
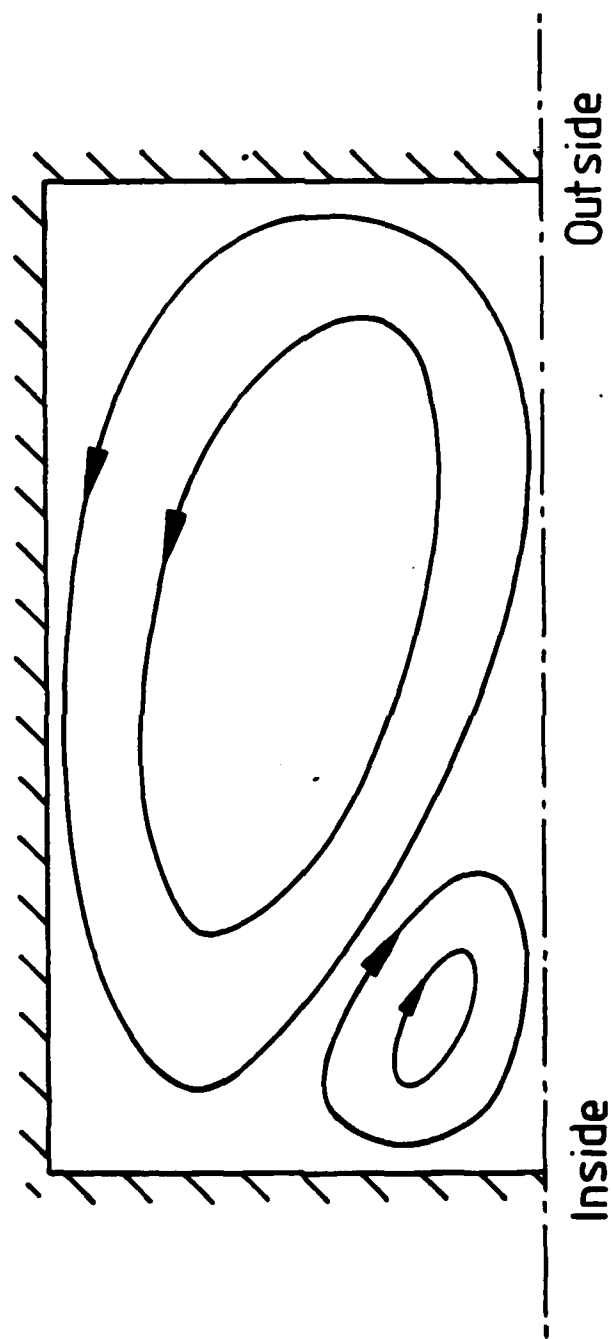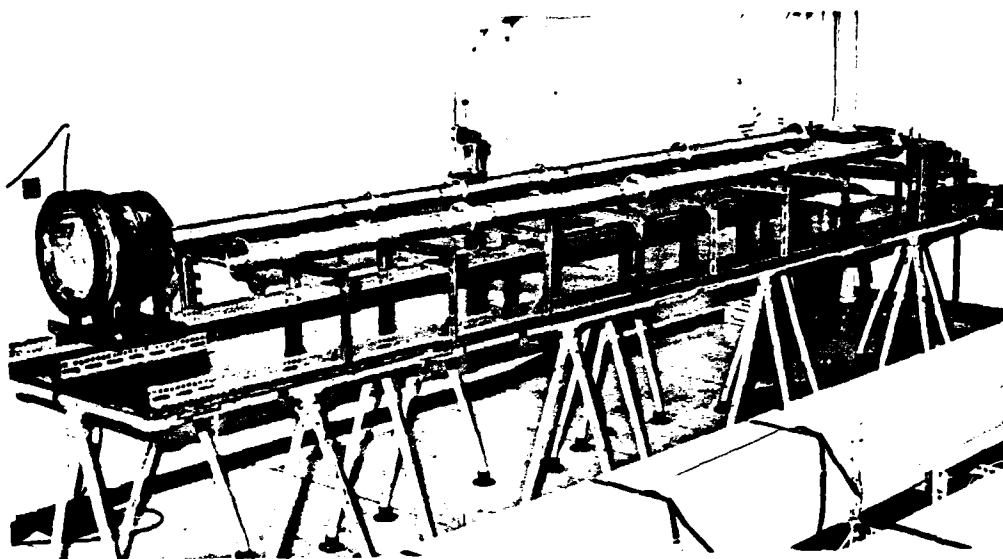Figure 4   Comparison of predictions and experiment
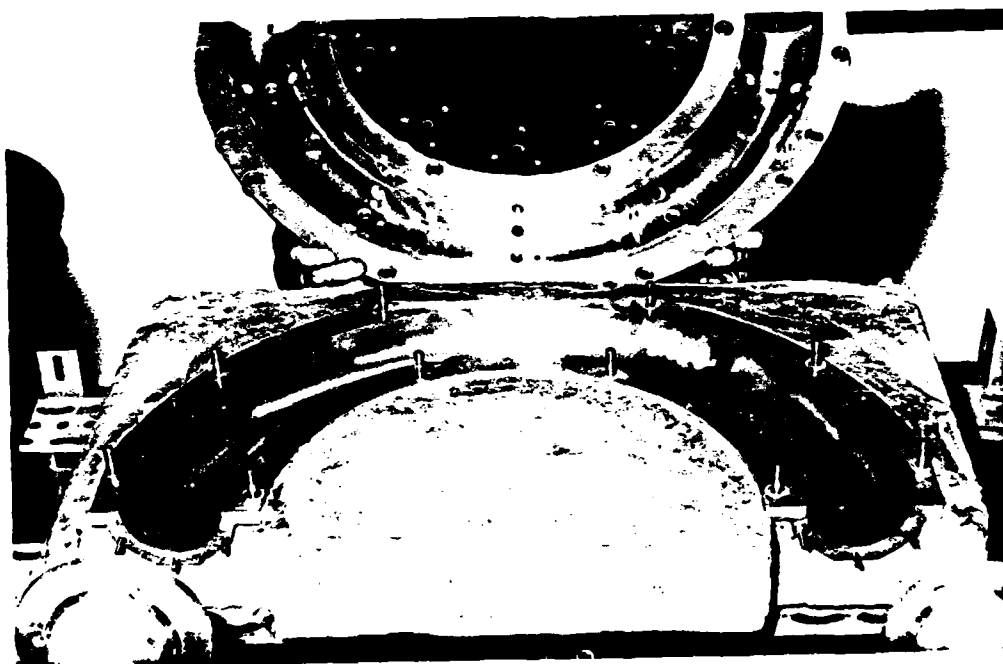   at 90° plane

Outside

Inside

Fig. 5 Possible secondary flow recirculation giving rise to trough in streamwise velocity

a) The complete test section

b) Close-up of 180° bend sections

Figure 6   Photograph of 180°-bend test
            section

Note: Holes in hand-held section are
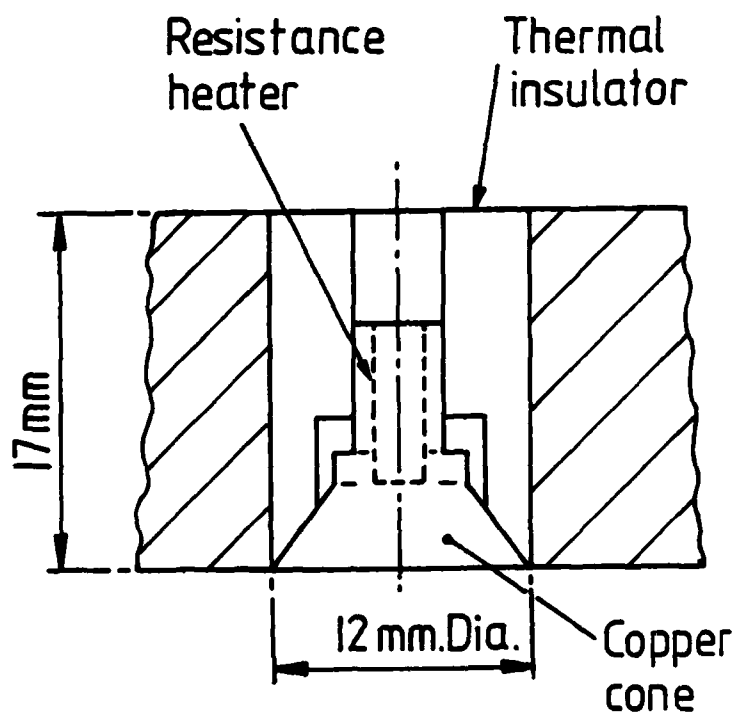   provided for heat flux meters)

Fig. 7   Heat flux meter
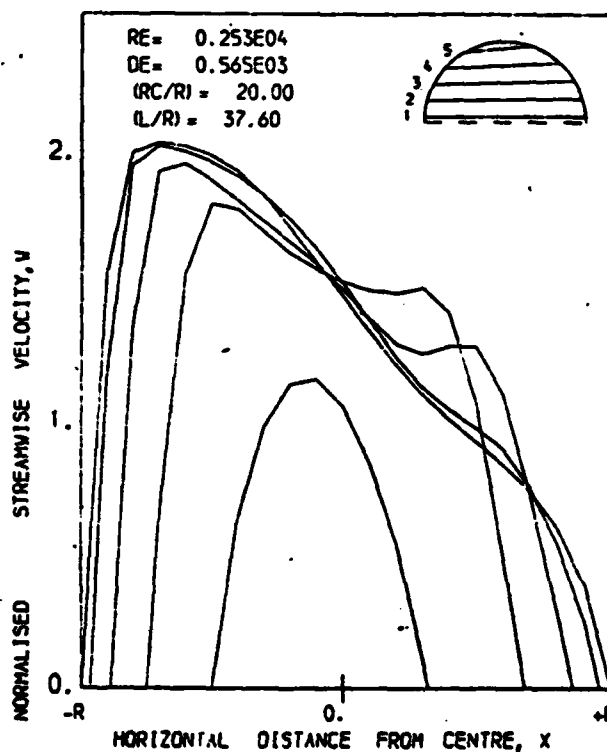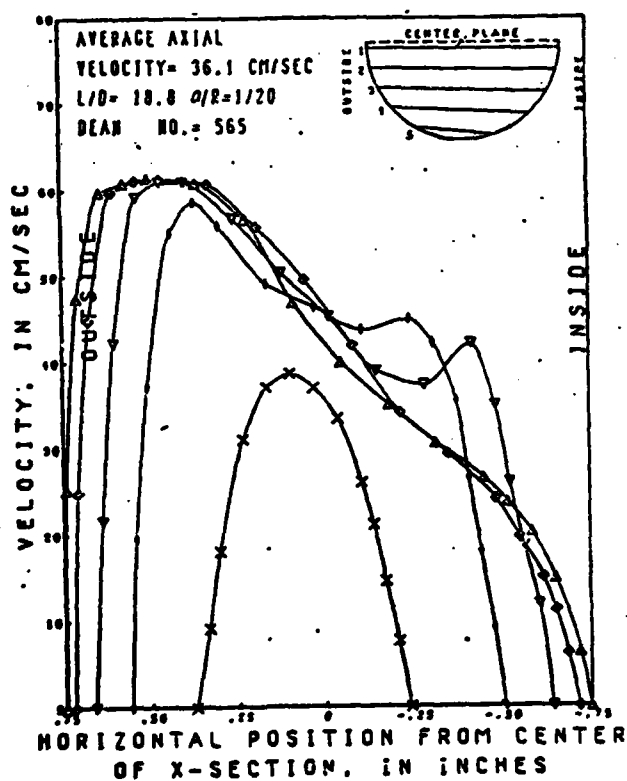
Fig. 8   Comparison of computed and measured streamwise
         velocities in laminar flow around 180° bend

De = 565

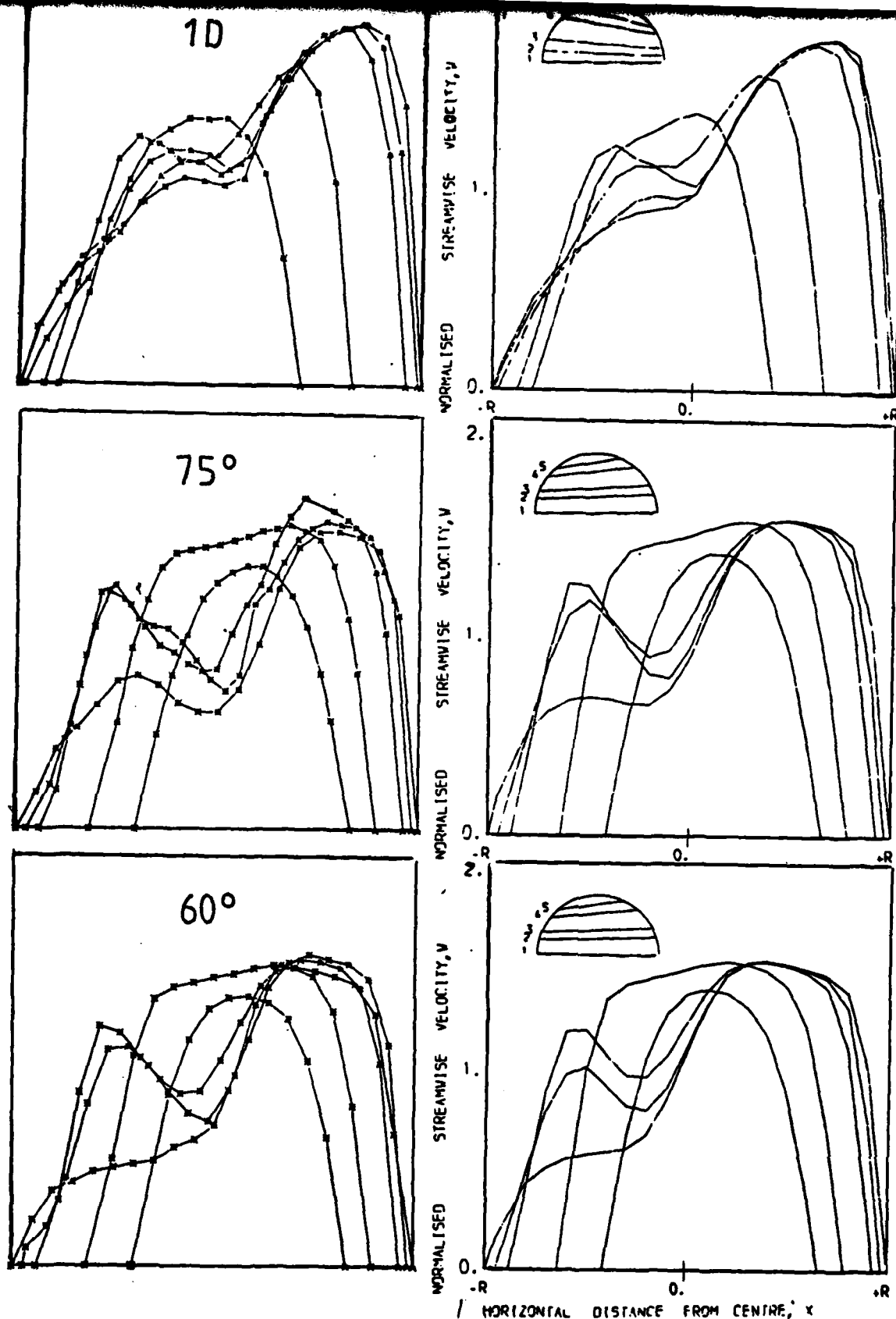a)   Agrawal et al [12]   b)   Iacovides and Launder [3]

Figure 9   Streamwise velocity profiles in laminar flow around 90° bend
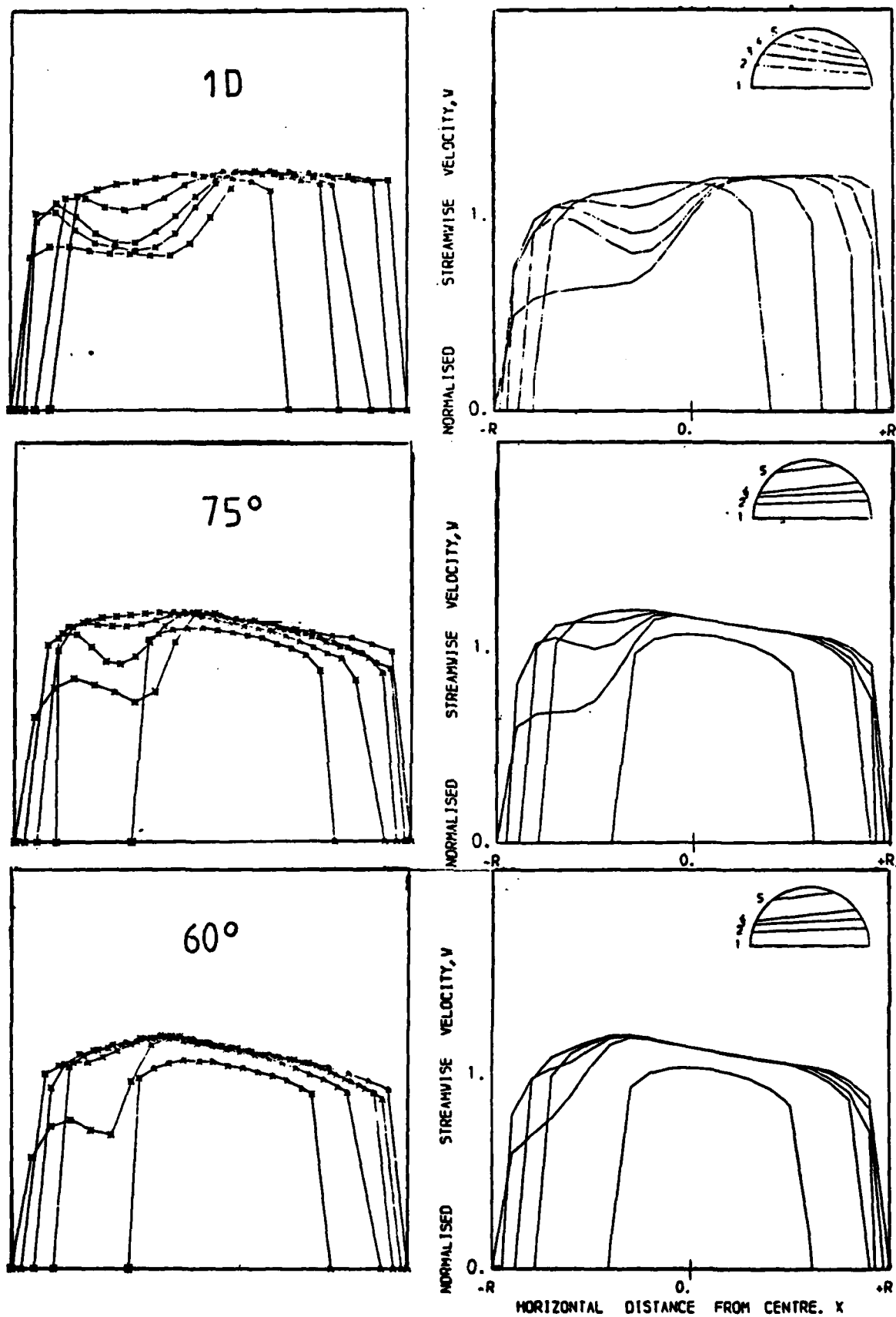Re = 1.09×10^3 —w— Experiment (Enayet et al) ——Present computations

Figure 10 Streamwise velocity profiles in turbulent flow around 90° bend
Re = 4.3 x 10⁴ ← Experiment (Enayet et al) —— Present computations

APPENDIX 1

TURBULENT MOMENTUM AND HEAT TRANSPORT IN

FLOW THROUGH A 180° BEND OF SQUARE CROSS-SECTION

S.M. Chang   J.A.C. Humphrey   R.W. Johnson   B.E. Launder
Department of Mechanical Engineering,   University of Manchester Institute of
University of California, Berkeley,   Science & Technology,
USA.   Manchester, England.

ABSTRACT

The paper reports flow and heat transfer predictions
of turbulent flow in passage around a 180° square-
sectioned bend. The numerical results are obtained from
a finite-volume discretization of the semi-elliptic form
of the Navier Stokes and energy equations. The turbulent
stresses are represented by the k-ε Boussinesq viscosity
model both in its standard form and with a streamline
curvature correction. Serious differences between
experiment and prediction exist for both forms and
suggestions are made for their origin. Heat transfer
computations indicate that from 45° - 180° the secondary
flow provokes at least a 2:1 circumferential variation
in heat transfer coefficient around the duct perimeter
and that differences of 40% between the mean heat
transfer coefficient in each wall persist at least 10
diameters downstream.

1   INTRODUCTION

Computers and flow solution schemes have developed
to a point where serious numerical studies of convective
heat transfer in complex, 3-dimensional flows can now be
made. But, for turbulent flow, what level of accuracy
can one expect from such a simulation? The question is
of great practical interest for if the accuracy can be
relied on within the allowable tolerances the cost of
computation - typically a few hundred dollars per run
- will often be negligible compared with the cost of
getting the information from experiment. This is the
question our research on flow around 180° bends has been
addressing.
The 180°-bend flow has several qualities that make
it well suited as a bench-mark test case. It has very
strong practical connections, especially in heat
exchangers, yet its topography is relatively simple.
This simplicity means that the flow boundary conditions
can be easily and unambiguously reproduced by a computor;
it also means that obtaining tolerably accurate *numerical*.
solutions (whatever may be the frailties of the physics)
is a target within sights - though there may be argument
about whether it is yet within range. It is a more
challenging flow than the 90° bend that provided one of
the test cases at the 1981 Stanford Conference (Kline
et al, 1981, 1982) because turbulent stresses generated
by the strong secondary flow have longer to act on the
mean flow. Moreover, and most importantly, detailed
experimental data are available (Chang et al, 1983) with
which to draw comparison.
Computations of flow around the 90° square-sectioned
bend adopted for the Stanford Conference have been
reported by Humphrey et al (1981, McDonald (1982),
Abdelmeguid et al (1982), Rodi et al (1982), Moore and
Moore (1982) and Chang et al (1982); the first three
employ a discretisation of the full Navier Stokes
equations, the last two adopt a semi-elliptic formulation

in which only the pressure field is stored over the full
domain (Pratap and Spalding, 1975) and, necessarily,
streamwise derivatives in the momentum equations are
discarded. All but McDonald's and Moore's studies
employed the same mathematical model for the turbulent
stress field - the k-ε Boussinesq viscosity model. Yet
the flow patterns predicted by these schemes bear only a
qualitative resemblance to each other or, for that
matter, to the experimental data. The fully three-
dimensional discretizations have of necessity to use a
coarse grid which has severely limited the numerical
accuracy available. The semi-elliptic schemes which have
allowed 80 or more streamwise planes (not all, of
course, in the bend itself) achieve somewhat better
overall agreement with data.
The computations of Moore and Moore (1983) and
McDonald (1983) extend through the viscous sublayer to
the wall allowing a better numerical resolution of the
near-wall region than the k-ε treatments (which apply
"wall functions" to bridge the 5% of the flow nearest
the wall). This fine-grid approach was also followed in
the work of Cousteix et al (1983) for the same conference
though they make only a two-dimensional inviscid
calculation for the pressure field. The numerical
simplification this brings is considerab' .i..'s a three-
dimensional marching scheme may be adopt d; in view of
the poor agreement obtained, however, it remains
questionable whether this basis for obtaining the pressure
is useful in bends of small aspect ratio with substantial
curvature. Of course, more nodes near the wall means
fewer elsewhere; moreover, instead of calculating the
dissipation rate ε from a transport equation these
groups obtained it via a prescribed length scale distrib-
ution - with much uncertainty as to the appropriate
prescription.
In the intervening two years since computations for
the Stanford Conference were made the authors have cont-
inued to give attention to curved ducts but, for reasons
given earlier, to the 180° bend case.
A detailed mapping of the velocity field by laser
anemometry has been made at Berkeley for the curved duct
shown in figure 1. These data and preliminary numerical
computations are to appear in Chang et al (1983). The
present contribution provides a more refined set of
computations of this flow and examines the influence of
wall boundary conditions and turbulence model on the
computed flow pattern. It also reports solutions of the
enthalpy equation thus providing predictions of the
circumferential distribution of Nusselt number around
the duct perimeter.

2.   SUMMARY OF NUMERICAL SCHEME

Describing Differential Equations

The stationary, turbulent, incompressible flow of
fluid through a curved duct of constant rectangular
cross-section is conveniently described through conserv-
ation equations in cylindrical coordinates. With
coordinates x and r mapping the duct cross-section and

θ the angle of progress along the duct, the describing mean flow equations may be written:

x-momentum

$$UU_x + VU_r + (W/r)U_\theta = -\frac{1}{\rho}p_x + (2\nu U_x - \overline{u^2})_x$$
$$+ r^{-1}(r(\nu(U_r + V_x) - \overline{uv})_r \qquad (1)$$

r-momentum

$$UV_x + VV_r - W^2/r + (W/r)V_\theta = -\frac{1}{\rho}p_r + (\nu(U_r + V_x) - \overline{uv})_x$$
$$+ r^{-1}(r(2\nu V_r - \overline{v^2})_r - 2\nu V/r^2 \quad (2)$$

θ-momentum

$$UW_x + VW_r + VW/r + (W/r)W_\theta = -\frac{1}{\rho r}p_\theta + (\nu(W_x + r^{-1}U_\theta) - \overline{uw})_x$$
$$+ r^{-2}(r^2(\nu(r(W/r)_r + r^{-1}V_\theta) - \overline{vw}))_r \quad (3)$$

continuity

$$V_r + V/r + r^{-1}W_\theta + U_x = 0 \qquad (4)$$

enthalpy

$$UT_x + VT_r + (W/r)T_\theta = ((\nu/\sigma)T_x - \overline{ut})_x$$
$$+ r^{-1}(r((\nu/\sigma)T_r - \overline{vt}))_r \qquad (5)$$

Here U, V and W are the mean velocity components in the x, r, θ directions, $\overline{u^2}$, $\overline{uv}$, etc. are the correspondingly defined Reynolds stresses, T is the mean temperature and τ the temperature fluctuation. The quantities ν, ρ and σ are respectively the fluid kinematic viscosity, density and Prandtl number. The subscripts x, r and θ denote partial differentiation with respect to the space coordinate in question.

The turbulent stresses are obtained from the Boussinesq stress-strain formula which, in cylindrical coordinates, implies:

$$-\overline{u^2} = 2\nu_T U_x - \frac{2}{3}k; \quad -\overline{v^2} = 2\nu_T V_r - \frac{2}{3}k$$

$$-\overline{uw} = \nu_T(W_x + r^{-1}U_\theta); \quad -\overline{vw} = \nu_T(r(W/r)_r + r^{-1}V_\theta)$$

$$-\overline{uv} = \nu_T(U_r + V_x) \qquad (6)$$

where, in accordance with the k-ε model

$$\nu_T = c_\mu k^2/\epsilon , \qquad (7)$$

k being the turbulence energy and ε its dissipation rate. These quantities are themselves found from transport equations solved simultaneously with the mean flow variables:

$$Uk_x + Vk_r + (W/r)k_\theta = r^{-1}(r(\frac{\nu + \nu_T}{\sigma_k}k_r))_r + (\frac{\nu + \nu_T}{\sigma_k}k_x)_x$$

$$+ \nu_T(2(U_x^2 + V_y^2 + r^{-2}W_\theta^2 + U_r V_x + r^{-1}U_\theta W_x + r^{-1}V_\theta W_r)$$

$$+ U_r^2 + r^{-2}U_\theta^2 + V_x^2 + r^{-2}V_\theta^2 + W_x^2 + W_r^2$$

$$+ 2r^{-2}V(2W_\theta + V) - r^{-2}W(2V_\theta + 2rW_r - W)) - \epsilon \qquad (8)$$

$$U\epsilon_x + V\epsilon_r + (W/r)\epsilon_\theta = r^{-1}(r(\frac{\nu + \nu_T}{\sigma_\epsilon}\epsilon_r))_r + (\frac{\nu + \nu_T}{\sigma_\epsilon}\epsilon_x)_x$$

$$+ c_{\epsilon 1}\nu_T (2(U_x^2 + V_y^2 + r^{-2}W_\theta^2 + U_r V_x + r^{-1}U_\theta W_x + r^{-1}V_\theta W_r)$$

$$+ U_r^2 + r^{-2}U_\theta^2 + V_x^2 + r^{-2}V_\theta^2 + W_x^2 + W_r^2$$

$$+ 2r^{-2}V (2W_\theta + V) - r^{-2}W(2V_\theta + 2rW_r - W)) - c_{\epsilon 2}\epsilon^2/k \qquad (9)$$

The empirical coefficients are assigned the usual values optimised by Launder et al (1973):

$$c_\mu = 0.09; \; c_{\epsilon 1} = 1.44; \; c_{\epsilon 2} = 1.92; \; q_k = 1.0; \; \sigma_\epsilon = 1.22$$

The semi-elliptic truncation has been applied to all these equations in that terms containing second derivatives on θ are dropped.

The Difference Equations and their Solutions

Finite-difference forms of the transport equations were derived by integration over discretized volumes in the flow domain following broadly Pratap's (1975) guidelines. As is now customary, the velocity components and pressure are stored on a staggered mesh. Streamwise convective transport is approximated by upwind differences. In the cross-sectional plane, however, both upwind and quadratic upwind (QUICK) options are included. The latter scheme devised by Leonard (1979) has been tested by Han et al (1981) for turbulent flow in a driven cavity and found to be distinctly better than an upwind approximation. (In fact, so far as the cross-stream components are concerned, the flow around a bend *is* very like a driven cavity). The method of implementing the scheme in the numerical algorithm is as given by Han et al (1981).

In the course of iteration, the adjustments to the pressure field in response to mass imbalances for the control volumes surrounding each pressure node is essentially as proposed in the SIMPLE algorithm (Patankar and Spalding, 1972) except that, with the velocity field held on only two successive θ planes, reorganization is required (Pratap, 1975). At any x-y plane the U and V velocity components are solved first. The streamwise momentum equation is solved next to obtain the W velocity (displaced half a cell down-stream as a result of the 'staggering') using new values of V and U in the convective terms; finally, perturbations to the pressure field are introduced in conjunction with re-adjustments to the current-plane U-V field. This procedure is applied at all planes beginning at the upstream boundary and stepping downstream, successively overwriting 'upstream' velocities by current values. On completing such a pass over the domain the computation starts over again at the upstream end unless the residual error is small enough that convergence is signalled.

Because the computation as outlined above has had to make extensive use of upstream values (rather than current plane values) of velocity in evaluating convection coefficients and sources, a certain upstream bias is introduced into the solution if a purely marching treatment is followed. For this reason, as the computation approaches its apparent solution, it is necessary to introduce iteration on the velocity components at each step. That is to say, when current plane values have been obtained the equations are resolved using current-values as appropriate in -forming coefficients and source terms. Approximately 45 passes were needed, starting from an assumed uniform pressure field to obtain converged results; this was deemed to have been achieved when the magnitude of the mass errors summed over every cell of the domain fell below 1% of the entering mass flow. (Other studies have typically accepted mass errors of 0.5% per plane which is larger by a factor of 50 than tolerated here).

The flow field generated in the duct is symmetric about the mid-plane of the cross-section lying in the plane of the bend. Computations were thus extended over just one half of the duct, the cross-section being mapped by a 15x25 interior grid for most of the results presented here-under with the mesh expanding mildly from each wall. The computations began seven hydraulic diameters upstream of the bend and extended 11.5 downstream; this region was covered by a total of 117 streamwise planes.

Boundary Conditions

Along the symmetry plane the gradients of all but one of the dependent variables were set to zero; the value of U, the velocity normal to this plane, was made zero. On the three sides bounded by the duct wall, wall functions were employed to supply appropriate near-wall sources and sinks to the various dependent variables. Besides the 'standard' wall treatment habitually employed in codes developed by those associated with the Imperial College school (Launder and Spalding, 1974) a more elaborate version originating in the present work has been used. It is an extension of the schemes of Chieng and Launder (1980) and Johnson and Launder (1982). In relation to the present study its most significant feature is that the wall friction opposing the secondary motion is obtained independently of the streamwise velocity by performing the integration $V = \int (\tau_{yx}/\mu_{eff})dx$ between the wall and the first node. By contrast, the IC wall treatment assumes that the resultant near-wall velocity parallel to the wall obeys the usual logarithmic law (the streamwise and cross-stream wall stress components are then obtained by resolving appropriately).

Flow inlet conditions are detailed in the next section.

3. COMPUTATIONS AND EXPERIMENT COMPARED

The experimental data providing the basis for this comparison are those reported by Chang et al (1983) for a duct in which the mean radius of the bend was 3.35 hydraulic diameters. The flow entering the bend had developed through a straight entry section of 31 D_H after being passed through a series of screens to promote shear layer development. Thus, while the flow had not become fully developed there was no inviscid core remaining when the flow encountered the bend. The experiments were taken at a bulk Reynolds number of 56700.

A parallel experiment at UMIST is underway which reproduces, so far as we are able to, the Berkeley test conditions. The apparatus dimensions are twice those of the Berkeley rig and since air rather than water is employed, velocities need to be increased by a factor of 8 to maintain the same Reynolds number. While the main output from the UMIST study will be convective heat transfer data it has served to provide checks on an unexpected feature of the Berkeley measurements. At 90° around the bend their streamwise velocity profile along a radial line had exhibited a pronounced double maximum. This feature while most strongly present on the plane of symmetry was still evident along the line midway between the symmetry plane and the end wall. Figure 2 compares the laser anemometer profiles reported by Chang et al (1983) with those obtained with a pair of slant hot wires at UMIST. It is seen that the double-peak feature is present in both sets of data; indeed, there is very satisfactory agreement between the two realisations of this flow.

Computations were started, as noted, seven hydraulic diameters upstream of the bend using, as initial conditions the velocity and turbulence energy profiles of Melling and Whitelaw (1976). The turbulence energy dissipation rate was assigned as: $\varepsilon = k^{3/2}/\ell$ where the length scale was assigned as the smaller of $\kappa/c_\mu^{3/4}$ times the distance to the nearest wall or $.375D_H$. The former is consistent with a mixing length varying as κ times the wall distance; the latter imposes a uniform length scale at distances greater than $0.15D_H$ from any wall. It is our view that the uncertainties in initial conditions make no significant contribution to differences between experiment and computation in the bend itself. In support of this view, experiments at UMIST with a virtually fully developed flow at entry to the bend produced streamwise velocity profiles at 90° only slightly different from those shown in fig. 2.

The computed development of the streamwise and radial velocity components around the bend is shown in figures 3 and 4. Serious discrepancies between computation and measurement quickly develop. At 45° the predicted radial velocity on the centreline is somewhat too low and, as a result, the streamwise calculated profile at this position is biased towards the inside of

the bend while in the experiment the velocity peak is displaced somewhat towards the outer radius. (It appears that the experimental measurement of W_B, the bulk mean streamwise velocity, may be too low at this position causing all the measured profiles to lie above the prediction; the differences in shape that are present are not affected by this, however). At 90° the differences are more pronounced including the very strong double peak in the measured streamwise profile and its complete absence in the predictions. The radial velocity profiles likewise display a sharp peak near the inner boundary radius that is not reproduced in the computation. Similar anomalies are present at 135° (the experimental data are at 130°) but by 180° (177° for measurements) the streamwise profiles, at any rate, are showing closer agreement; the secondary flow is still seriously in error, however.

Clearly something starts to go quite seriously wrong with the simulation fairly early on in the bend and a substantially different flow pattern is computed at 90° from that measured. In search of the cause of the differences a number of adaptations have been considered. The most recent calculations have benefitted from significant mesh refinement in the near-wall region compared with an earlier set (Johnson and Launder 1983) yet the differences in the calculations are small compared with the differences between measurement and calculation. The procedure for finding the secondary wall shear stress seems a particular area of weakness and so a test was made where the wall stresses in the x-y plane were set to zero. This is clearly an incorrect hypothesis but it served to indicate whether wall stress errors could conceivably account for the large differences. The largest difference between the two practices occurs at 135° for which the primary velocity profiles are shown in figure 5. The changes produced by this step slightly improve agreement with experiment and along $2X/D_H = 0.5$ a peak in W near the inner wall is present. Nevertheless large differences remain.

It is well known that the k-ε model does not correctly capture the great sensitivity of real turbulence to small amounts of streamline curvature. Although this weakness is intrinsic to the use of the Boussinesq stress-strain relation, for two-dimensional curved flows it has been found possible to imitate the effect of curvature on turbulent shear stresses fairly well by introducing the following term in place of the sink $-c_{\varepsilon 2}\varepsilon^2/k$ in the ε transport equation:

$$-c_{\varepsilon 2} \frac{\varepsilon^2}{k}(1-0.2\ Ri)$$

where $Ri \equiv (k/\varepsilon R)^2 W(RW)_R$ is a curvature Richardson number and R is the local radius of curvature of a streamline. This is given by

$$R^{-1} = ((UV_t - VU_t)^2 + (UW_t - WU_t)^2 + (VW_t - WV_t)^2)^{1/2}/K^{3/2} \quad (10)$$

where $U_t \equiv UU_x + VU_y + WU_z$ and $K \equiv (U^2 + V^2 + W^2)^{3/2}$

In places the secondary velocity field resulting from this modification was changed by 20%; the effect on the streamwise velocity, however, was nowhere more than 3% and is thus insignificant compared with the differences here in question. This result could have been anticipated for one could not expect an empirical 'fix' on one stress component in a two-dimensional shear to be satisfactory for all the stress components in a complex three-dimensional flow.

The logical next step in improving the representation of the Reynolds stress is the introduction of an algebraic stress model of turbulence (ASM) in place of the Boussinesq stress-strain relation. Models of this type have been conspicuously successful in mimicking the effects of curvature in two-dimensional shears *without* the introduction of specially tuned empirical terms (e.g. Rodi et al, 1982). Unfortunately, switching from a model based on a turbulent viscosity to one where the turbulent stresses enter the calculation as sources and sinks is a severely de-stabilizing departure. At the time of writing no converged results have been obtained with the QUICK treatment of convection. With the upwind scheme, however, convergence has been achieved though largely, we believe, because this approach brings

its own *false* diffusion to assist stability.
Streamwise velocity profiles drawn from these results
appear on figure 4 for the 90° position. The
particular form of ASM adopted is that which results
from applying Rodi's (1976) algebraic transport
hypothesis to Gibson and Launder's (1978) second-moment
closure proposals. The Gibson-Launder study which
considered the case of flow past a single plane wall
included terms representing the effects of pressure
reflection from the rigid boundary. Here there are four
walls present and their effect is assumed to be accounted
for by applying a linear superposition; this extends to
three-dimensions the usual two-dimensional practice.
It is clear from fig. 3 that the introduction of the
ASM scheme has brought no improvement in accuracy,
somewhat the reverse. Based on earlier experiences
with the k-ε Boussinesq model artificial diffusion
introduced by upwind differencing modifies the
streamwise velocity typically by amounts similar to the
difference between the curves representing ASM and k-ε
predictions in fig. 4 (and in the same direction). That
no improvements are recorded from adopting this higher-
level closure can only be said to be extremely perplex-
ing. It is hoped that by the time of the meeting at
which this work is formally presented an explanation
will have emerged.

The heat transfer behaviour considered in figure 6
is that arising from using the Boussinesq k-ε model.
The greatest difference between heat transfer rates on
the inside and outside of the bend initially occurs at
the centre plane. The secondary flow driving cold
fluid towards the outer wall on this plane produces
higher heat transfer levels as is typical of impinge-
ment conditions. Conversely, on the inside of the bend,
the fluid adjacent to the wall has arrived there after
travelling relatively slowly over a slightly greater
length (due to the secondary motion). This fluid has
thus been heated considerably more than that near the
outer wall and heat transfer coefficients are thus
lower. At 45° the ratio of the Nusselt number on the
two sides is 3:1. This difference diminishes with
passage around the bend as the secondary and primary
flow patterns become more complex; even at 180° however
the mean level of Nusselt number is 60% greater on the
outer than the inner wall associated with the fact that
the faster moving fluid is located near the outer wall
(see fig. 3): this produces higher velocity gradients
which in turn produce higher kinetic energy level.

Downstream of the bend the secondary flow decays
(the maximum radial velocity is only .02 W_B at ten
diameters) though the Nusselt number distribution
around the duct perimeter remains strongly non-uniform.
The mean level of Nusselt in the bend is some 30% higher
than is found in a straight tube at the same Nusselt
number.

4. CONCLUDING REMARKS

Experiments under identical flow conditions in our
two institutions using different methods of measurement
have confirmed that at the 90° position in a square-
sectioned U-bend the streamwise velocity displays a
secondary peak near the inner wall. None of our numeri-
cal simulations using relatively fine meshes and the
QUICK treatment of convection has succeeded in mimick-
ing this important flow feature. For the present we
cannot offer a convincing explanation for this failure:
grid refinement in the cross-sectional plane has had
little influence while introducing an ASM apparently
brings no benefit. There are two steps we propose to
take that may bring about a marked improvement. The
first is to concentrate a far greater proportion of the
streamwise calculational planes in the first 90° of the
bend. (The present distribution provides a virtually
uniform spacing around the bend and only modest
variations in the upstream and downstream tangents).
The second will be to abandon, on the flat walls of the
bend, the wall-function treatment. Instead, a fine
mesh will be introduced, to allow computations to be
carried into the viscous sublayer. In this way uncert-
ainties as to the appropriate wall boundary condition
are removed. We have found from parallel work in the
round-sectioned U-bend that by assuming a radial
equilibrium pressure distribution across the viscous

and buffer regions the introduction of a very fine
near-wall grid has negligible effect on either convergence
rates or storage requirements.

With the velocity field in such relatively poor
agreement with data over most of the bend no very defin-
itive conclusions can be drawn from the detailed heat
transfer behaviour. However, results very probably give,
in their overall pattern, a correct indication of the
effects on heat transfer levels: i.e. at least a 2:1 ratio
of heat transfer coefficients on the outer and inner
curved walls of the bend; a mean level some 30% higher
than in a straight duct and a strong non-uniformity in
Nusselt number persisting at least 10 diameters down-
stream.

REFERENCES

Abdelmeguid, A.M., Goh, S.Y., Ilegbusi, J. and
Spalding, D.B. 1982 Proc. AFOSR-HTTM-Stanford
Conf. on Complex Turbulent Flows, vol. III, 1521.
Chang, S.M., Han, T. and Humphrey, J.A.C. 1982.
Proc. AFOSR-HTTM-Stanford Conf. on Complex
Turbulent Flows, vol. III, 1375.
Chang, S.M., Humphrey, J.A.C. and Modavi, A. 1983.
Int.J. Physico Chemical Hydrodynamics (to appear).
Chieng, C.C. and Launder, B.E. 1980.
Num. Heat Transfer 3, 189.
Cousteix, J. et al. Proc. AFOSR-HTTM-Stanford
Conf. on Complex Turbulent Flows, vol. III, 1326.
Gibson, M.M. and Launder, B.E. 1978.
J.Fluid Mech. 86, 491.
Han, T.Y., Humphrey, J.A.C. and Launder, B.E. 1981.
Comp.Math.Appl.Engrg. 29, 81.
Humphrey, J.A.C., Whitelaw, J.H. and Yee, G. 1981.
J.Fluid Mech. 103, 433.
Johnson, R.W. and Launder, B.E. 1983. Dept. Rep.
TFD/83/2LR).
Johnson, R.W. and Launder, B.E. 1982. Num.Heat
Transfer 5, 493.
Kline, S.J., Cantwell, B. and Lilley, G.K. 1981, 1982
(editors) Proc. 1980-81 AFOSR-HTTM-Stanford
Conf. on Complex Turbulent Flows, Thermosciences
Division, Stanford University.
Launder, B.E., Morse, A., Rodi, W. and Spalding, D.B.
1973. Proc. 1972 Langley Free Shear Flows Conf.
NASA SP321.
Launder, B.E., Priddin, C.H. and Sharma, B.I. 1977.
J.Fluids Engrg. 98, 763.
Launder, B.E. and Spalding, D.B. 1974. Comp.Math.
Appl.Mech.Eng. 3, 269.
Leonard, B.P. 1979. Comp.Math.Appl.Mech.Engrg. 19,
59.
McDonald, H. 1982. Proc. AFOSR-HTTM-Stanford
Conference on Complex Turbulent Flows, vol. III,
1424.
Melling, A. and Whitelaw, J.H. 1976. J.Fluid Mech.
78, 289.
Moore, J. and Moore, J.G. 1982. Proc. AFOSR-HTTM-
Stanford Conf. on Complex Turbulent Flows, vol. III,
1453.
Pratap, S.V. and Spalding, D.B. 1975.
Aero.Quart. 26, 219.
Rodi, W. 1976. ZAMM 56, 219.
Rodi, W. et al. 1982. Proc. AFOSR-HTTM-Stanford
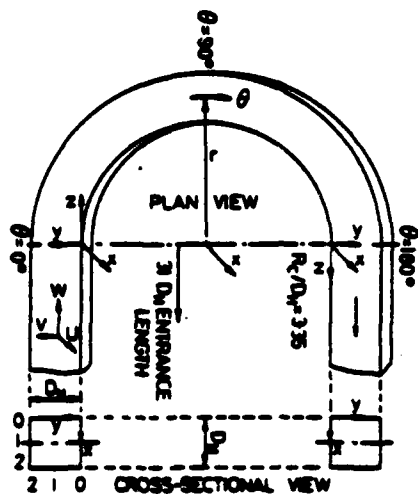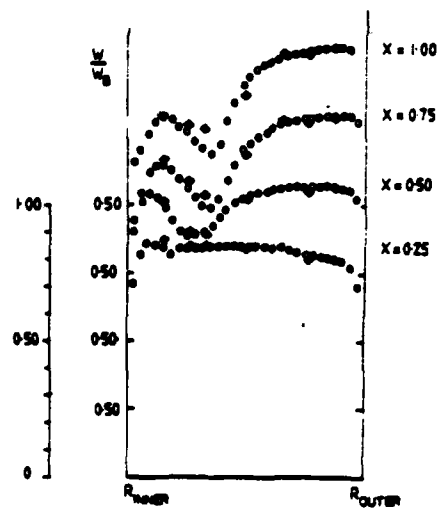Conf. on Complex Turbulent Flows, vol. II, 1495.

Fig. 1   The flow considered

Fig. 2   Comparison of streamwise velocity profiles at 90°.
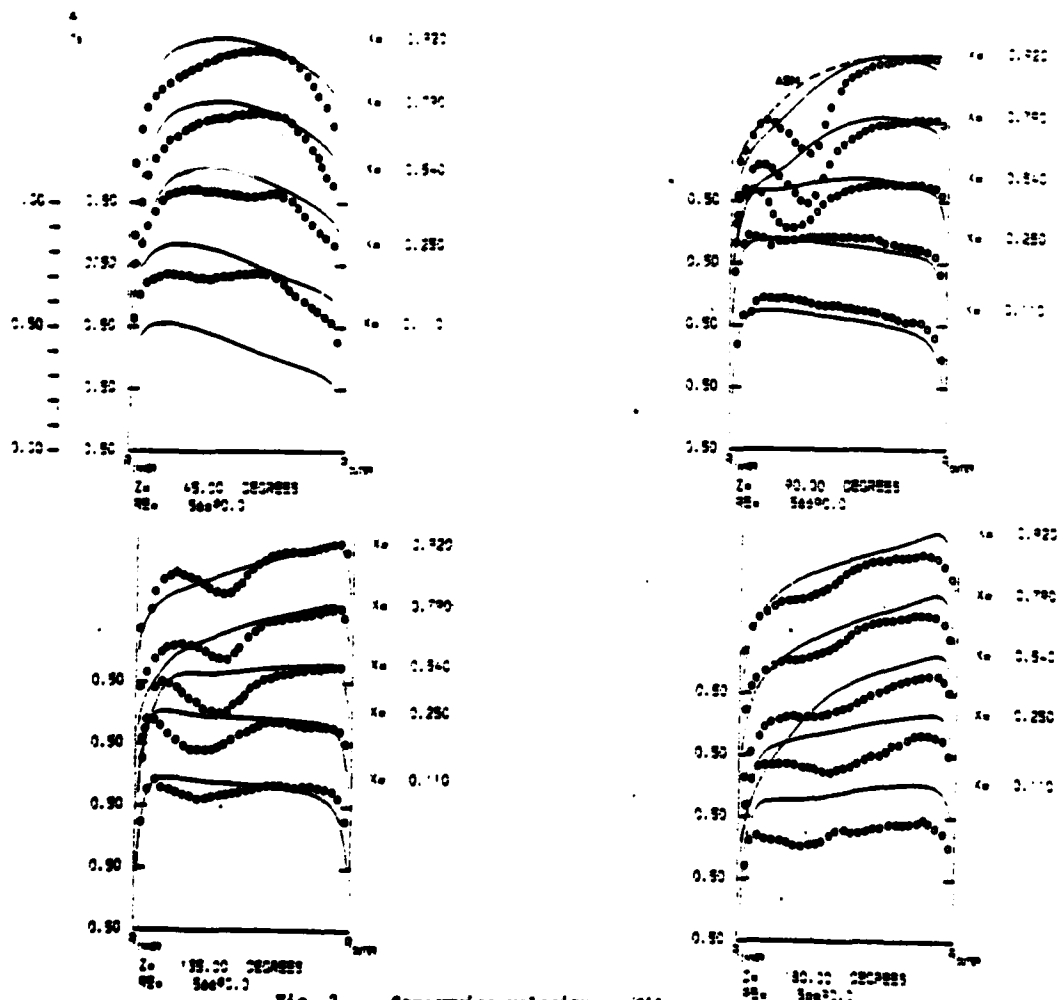o – Berkeley data   ◆ UMIST data

Fig. 3   Streamwise velocity profiles at 45°, 90°, 135° and 180° around the bend

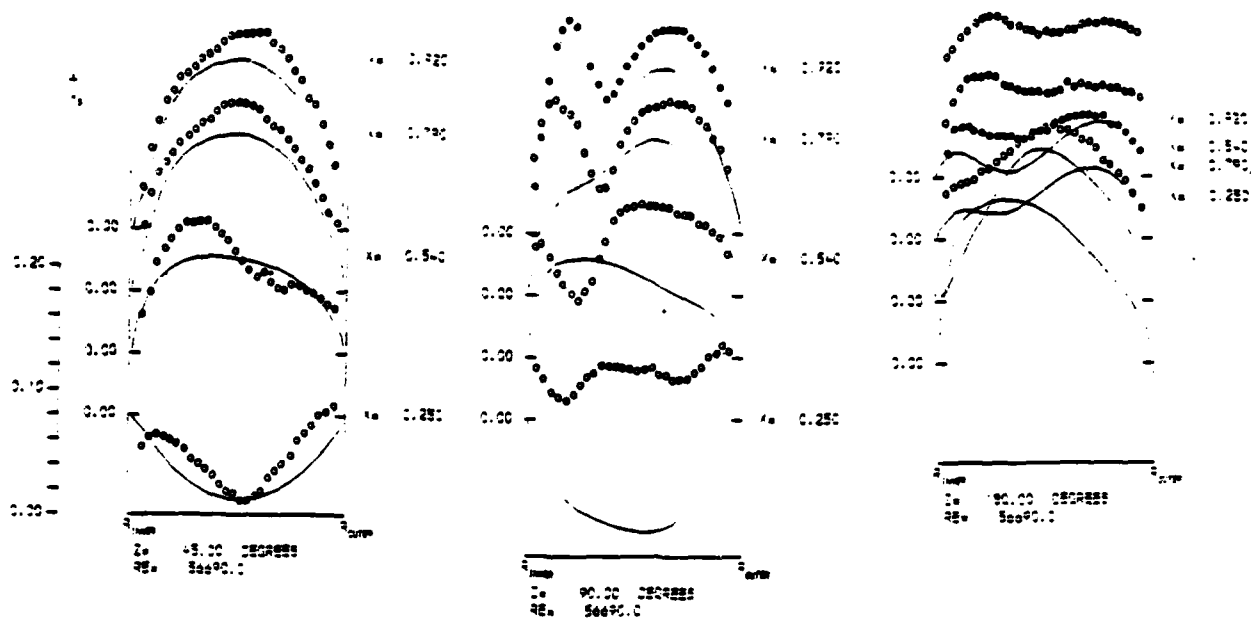o o   Experiment (Chang et al 1983)

——   Present predictions

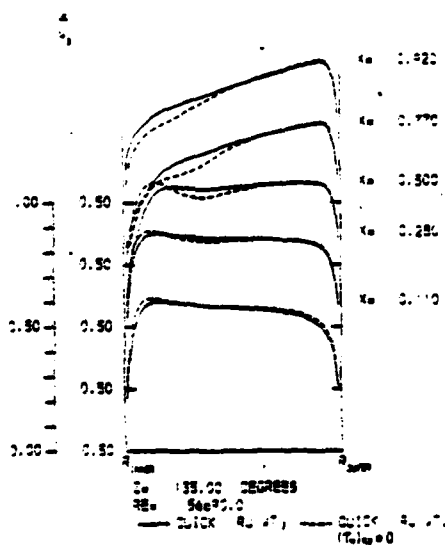Fig. 4   Radial velocity profiles at 45°,
          90° and 180° around bend

Fig. 5   Effect of removing wall shear
          stress opposing secondary motion

          —— standard results;

          —— secondary wall
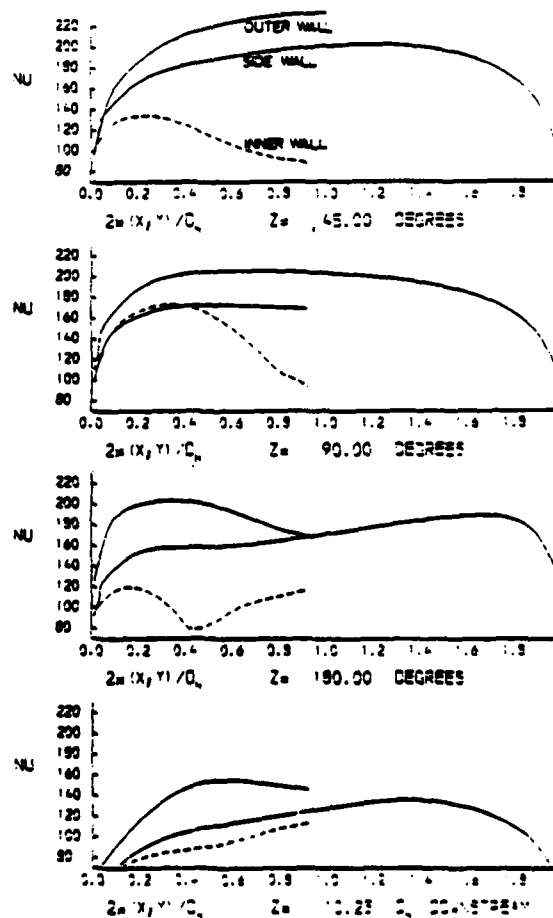   stress = 0

Fig. 6   Development of computed heat
          transfer coefficient around and
          downstream of bend

APPENDIX 2

UNIVERSITY OF MANCHESTER INSTITUTE OF SCIENCE AND TECHNOLOGY

Department of Mechanical Engineering

Thermodynamics and Fluid Mechanics Division

SOME NUMERICAL EXPERIMENTS ON

DEVELOPING LAMINAR FLOW IN

CIRCULAR SECTIONED BENDS

by

J.A.C. Humphrey*, H. Iacovides and B.E. Launder

* Department of Mechanical Engineering,
  University of California, Berkeley

INTRODUCTION

The movement of fluid through curved pipes and bends is of considerable practical and fundamental interest. It is well known that in such flows secondary motions arise in the cross-stream planes producing a streamwise flow pattern which may be far removed from that found in a straight pipe. The secondary motions can be explained qualitatively in terms of the response of a viscous fluid element to an imbalance between the centripetal acceleration and the cross-stream pressure gradient induced by lateral curvature of the main flow; see, for example, Cuming (1957) and Johnston (1978). In a curved pipe, the result is a cross-stream or secondary motion carrying fluid symmetrically along the pipe walls from the outer to the inner line of symmetry and along the symmetry plane of the pipe from the inner to the outer line of symmetry as shown in Figure 1.

Analysis of the equations describing laminar flow through curved pipes shows that two parameters characterize the flow: the radius ratio $\delta = a/R$ and the Dean number De $= \delta^{\frac{1}{2}}$ Re, Berger et al (1983). In the above definitions, a is the radius of the pipe cross-section, R is the pipe mean radius of curvature, and Re is the flow Reynolds number $\bar{W}$ 2a/ν where $\bar{W}$ is the bulk average velocity through the pipe and ν is the fluid kinematic viscosity. Since the Dean number is equal to the ratio of the square root of the product of the inertia and centrifugal forces to the viscous force, it provides a measure of the intensity of the secondary flow. The radius ratio δ is a more direct measure of the influence of pipe geometry on the flow. It affects the balance of inertia, viscous and centrifugal forces. Berger et al (1983) point out that the influence of δ on the flow through curved pipes is not as well understood as that of the Dean number.

Fully developed flow in curved pipes has been the subject of extensive research, a review of the subject having recently been made by Berger et (1983). The more complex entry flow into a curved pipe has been studied far less completely. Theoretical attempts to solve the problem have been seriously handicapped by a lack of sureness in the simplifying assumptions underlying the various analytical approaches. In addition, for fixed δ and De, the flow developing in a curved pipe is a function of the inlet plane boundary conditions and these present some difficulties for general values of Re; see Stewartson et al (1980) and Berger et al (1983).

Yao and Berger (1975) and Stewartson et al (1980) have investigated the entry flow development problem theoretically for De >>1. In the former case, two sets of equations were derived, one for the inviscid core flow and the other for the three-dimensional boundary layer. At the inlet plane zero cross-stream velocity components and a uniform axial velocity were prescribed. Along the pipe wall zero-slip, impermeable conditions were specified. A development of the Karman-Pohlhausen integral

method was used to solve the boundary layer equations.

A set of boundary layer equations, equivalent to that of Yao and Berger, was solved numerically by Stewartson et al, but core-flow/boundary-layer interactions were neglected. They also prescribed zero cross-stream velocity components at the inlet plane, but they followed Singh (1974) in imposing a potential-vortex condition for the streamwise velocity component. At any fixed streamwise location, $R\theta$, the calculation sequence always advanced from $\phi = 0$ at the outer line of symmetry to $\phi = 180°$ at the inner line of symmetry. Use was made of preliminary solutions of the flow field for all ϕ when $R\theta = 0$ and all $R\theta$ when $\phi = 0$. The Keller box scheme was used to solve partial differential equations for the leading terms in a power series expansion. The coefficients in the series were obtained seriatum and the series summed to yield the preliminary solutions.

Yao and Berger's solution of the boundary layer flow in a curved pipe predicts that separation of the secondary flow or circumferential boundary layer will take place at a streamwise location from the inlet plane of about $0.01a(De/\delta)^{\frac{1}{2}}$. The width of the separation zone, i.e. the distance between $\phi = 180°$ and the point of separation, was found to increase with streamwise location, tending asymptotically to a maximum value of $54°$. This finding is in qualitative agreement with the integral solution for fully-developed flow obtained by Barua (1963) who predicts a secondary boundary layer separation at $\phi = 153°$, but does not accord with either the fully-developed integral solution of Ito (1969) or the numerical studies of Collins and Dennis (1975) who do not predict separation. In contrast, and for the first time, Stewartson et al predict a vanishing of the streamwise component of skin friction on the inner line of symmetry, $\phi = \pi$, at $R\theta = 0.943 \, a/\delta^2$. The position of zero shear stress represents a singularity in their calculations since the shear stress increases again immediately past the zero point on the inner line of symmetry. From their study, the authors concluded that the secondary boundary layers "collide" at $\phi = 180°$ forming a radial jet which takes fluid from the inner to the outer pipe wall region along the symmetry plane.

Experimental measurements obtained by Agrawal et al (1978) using the laser-Doppler velocimeter technique in a transparent curved pipe with $\delta = 1/7$ suggest that separation of the circumferential boundary layer, in the sense predicted by Yao and Berger, for example, may have occurred by $R\theta = 3.46 \, a/\delta^2$ for De $= 138$ and by $R\theta = 6.23 \, a/\delta^2$ for De $= 678$. The values 3.46 and 6.23 are considerably larger than those suggested by either Yao and Berger's analysis (0.12 and 0.26) or the constant 0.943 predicted by Stewartson et al for the position of zero streamwise shear stress. However, it is interesting to note that for their higher Dean number Agrawal et al observed a striking modification of the secondary flow profiles measured in the region of the inside of the bend at two stations: $R\theta = 1.39 \, a/\delta^2$ and $R\theta = 2.31 a/\delta^2$.

Although the authors found it difficult to interpret their results, they associated the phenomenon with some form of separation.

In an effort to verify the finding of Stewartson et al, Talbot and Wong (1982) used an electrochemical technique to obtain the wall shear stress along the inner line of symmetry in a curved pipe with $\delta = 1/7$. Measurements were made over the range $188 \leqslant De \leqslant 1622$. They found that the wall shear decreased to a minimum value with increasing De, the minimum being located at $R\theta \approx 0.96 \ a/\delta^2$, in close agreement with the value predicted by Stewartson et al. Upstream of the minimum the measured wall shear stress was also in agreement with the predictions by Stewartson et al, but on the downstream side substantial discrepancies were found between measurements and predictions. Berger et al point out that the calculations of Stewartson et al are inaccurate beyond the singularity on the inner line of symmetry and must be discounted; further discussion of this point is given by Talbot and Wong (1982).

From the above it is clear that several important aspects of developing curved pipe flow have not yet been resolved. Analytical methods seeking to model the flow as an inviscid core interacting with a three-dimensional boundary-layer lead to asymptotic results that are at variance with numerical calculations of the fully-developed form of the Navier-Stokes equations. Analytical models do not yet exist which include the effect of boundary-layer separation on the inviscid-core flow and, more importantly, the very existence of separation is still an unresolved issue.

The arrival of large core digital computers has made feasible the numerical solution of either the full or some truncated version of the Navier-Stokes equation. Predictions of developing laminar flows in curved pipes by three-dimensional finite-difference procedures have been reported by Patankar et al (1974), Rushmore (1975), Liu (1976, 1977), Humphrey (1977) and Levy, Briley and McDonald (1983). The procedure of Patankar et al is based on the boundary-layer equations (with a uniform streamwise pressure gradient applied over each cross-sectional plane) and is thus applicable only to pipes with very large radius ratios. Levy et al also adopt a marching scheme by taking the pressure field from a potential solution with a bulk correction applied plane-by-plane to maintain the same mass flow at any section. While this appears a powerful and economical approach to apply in the early stages of development, the laminar flow entry problem was not that of principal interest to these workers and consequently no extensive investigation was reported. Moreover, the approach becomes less accurate when there is strong interaction between the viscous and non-viscous regions at high Dean number. The other numerical studies noted above have been based on discretizations of the full Navier-Stokes equations and share in common the problem of false diffusion arising from the use (for stability) of upwind differencing with an inevitably

coarse mesh. As a result flow details, such as small secondary eddies, tend to be smeared out; none of the studies, for example, has reported separation of the secondary flow.

The present contribution is aimed at throwing some light on the various unresolved phenomena discussed above associated with developing flows in pipe bends. Efforts have been made to reduce numerical errors to unimportant levels by following Pratap and Spalding (1975) in using a semi-elliptic rather than a fully-elliptic treatment (thus permitting considerably finer meshes than earlier studies), by adopting the third-order *quadratic* upwind differencing of Leonard (1978) (rather than the usual first-order upwinding) and by removing the numerical singularity at the pipe axis. Although numerical resolution is gradually lost as the Dean number is raised, the results provide evidence of secondary flow separation - albeit very weak - for De greater than 500. They also show the occurrence of a minimum streamwise wall shear stress on the inner line of symmetry. As the Dean number is successively raised, the minimum value decreases and occurs at progressively smaller values of $R\theta\delta^2/a$ though, even at the highest value of De considered, this dimensionless position is still approximately twice as far downstream as predicted by Stewartson's analysis.

During the documentation stage of the present study, the very recent thesis of Soh (1983) came to our attention. As in several earlier studies he has used a fully-elliptic discretization. Despite the resultant coarseness of his numerical mesh, by using central differencing for convective transport and by carefully arranging the mesh non-uniformly over the domain, his results reproduce at least qualitatively a secondary separation. Comparisons are drawn with Soh's work wherever possible; the impression is that the differences between his results and ours are attributable to the finer meshes that have been possible in the present work.

SUMMARY OF THE NUMERICAL SOLUTION PROCEDURE AND BOUNDARY CONDITIONS

The equations describing the development of a viscous fluid in a toroidal duct such as shown in Figure 1 may be written

Continuity

$$\frac{\partial}{\partial\phi} r_c U + \frac{\partial}{\partial r} rr_c V + \frac{\partial}{\partial\theta} rW = 0$$

(1)

Momentum

$$\rho(C(\psi) + S_C(\psi)) = D(\psi) + S_D(\psi) + S_p(\psi)$$

(2)

In equation (1) U, V and W denote velocity components in the circumferential (ϕ), radial (r) and streamwise directions (θ) respectively, $r_c = R + a\cos\phi$ is the local radius from the centre of the bend, while in equation (2), ψ stands for any of the velocity components, the associated source and sink terms being given in Table 2.1. The operators $C(\psi)$ and $D(\psi)$ are defined by

$$C(\psi) \equiv (rr_c)^{-1}\left[\frac{\partial}{\partial\phi}(r_c U\psi) + \frac{\partial}{\partial r}(rr_c V\psi) + \frac{\partial}{\partial\theta}(rW\psi)\right]$$

(3)

$$D(\psi) \equiv (rr_c)^{-1}\left[\frac{1}{r}\frac{\partial}{\partial\phi}\left(r_c\mu\frac{\partial\psi}{\partial\phi}\right) + \frac{\partial}{\partial r}\left(rr_c\mu\frac{\partial\psi}{\partial r}\right)\right]$$

(4)

We note from eq (4) that second-derivatives with respect to θ are omitted. In consonance with this form of the describing equations a 'semi-elliptic' finite-volume discretization is adopted, a description applied to a solution where only the pressure field is treated as elliptic. The pressure thus requires storing over the whole domain. In contrast, the velocity components are solved in a marching fashion and thus require values to be held only on two adjacent r-ϕ planes of nodes. This type of solution procedure, first introduced by Pratap and Spalding (1975), is particularly attractive in three-dimensional flows for then the savings in memory required for the velocity components (compared with a fully elliptic solution) may allow a sufficiently fine mesh to be used for the pressure field to reduce numerical errors to unimportant levels. The present numerical procedure has broadly followed the strategy of Pratap and Spalding, but several differences in discretization and organization have been introduced to improve the numerical accuracy of the results. Quadratic upstream interpolation (Leonard, 1979) is used to approximate convective transport in the cross-sectional plane of the duct following the conclusions of Huang et al (1983) that this was overall the most accurate of the simple treatments of convection (see also Han et al, 1980). The pressure/continuity connection is applied by way of Patankar's (1980) SIMPLER algorithm; in preliminary tests this was found to give convergence rates an order of magnitude faster than the earlier and very widely used pressure-correction scheme SIMPLE, Patankar and Spalding (1972).

In the original semi-elliptic scheme of Pratap and Spalding (1975) no in-plane iterations were made on the velocity field and thus, of necessity, coefficients of the difference equations were based entirely on upstream information. Although economical, this practice proved to be inadequate in the present study which has included tighter bends than those examined by Pratap and Spalding [†] and where, as a result, streamwise variations are more rapid. As the pressure field, which was iterated by repeated streamwise sweeps over the solution domain, approached convergence, first one and finally two in-plane iterations on the velocity field were made with all coefficients being re-evaluated

---

[†] The Pratap-Spalding study was confined to square sectioned bends

ψ	$S_C(\psi)$	$S_p(\psi)$	$S_D(\psi)$
U	$\dfrac{VU}{r} + \{\dfrac{W^2\sin\phi}{r_c}\}$	$-\dfrac{1}{r}\dfrac{\partial p}{\partial\phi}$	$\dfrac{1}{r_c}\dfrac{\partial}{\partial\phi}\{r_c\mu(\dfrac{\partial U}{\partial\phi}+2V)\} + \dfrac{1}{rr_c}\dfrac{\partial}{\partial r}\{r_c\mu(\dfrac{\partial V}{\partial\phi}-U)\}$ $+\mu\dfrac{\partial}{\partial r}\{\dfrac{U}{r}\} + \dfrac{\mu}{r^2}\dfrac{\partial V}{\partial\phi} + \dfrac{1}{r}\dfrac{\partial}{\partial\theta}\{\mu\dfrac{\partial}{\partial\phi}(\dfrac{W}{r_c})\}$ $-\dfrac{2\mu\sin\phi}{r_c^2}\{U\sin\phi - V\cos\phi - \dfrac{\partial W}{\partial\theta}\}$
V	$-\{\dfrac{\cos\phi W^2}{r}\}$ $-\{\dfrac{U^2}{r}\}$	$-\dfrac{\partial p}{\partial r}$	$\dfrac{1}{r_c}\dfrac{\partial}{\partial\phi}\{r_c\mu\dfrac{\partial}{\partial r}(\dfrac{U}{r})\} + \dfrac{1}{rr_c}\dfrac{\partial}{\partial r}\{rr_c\mu\dfrac{\partial V}{\partial r}\}$ $-\dfrac{2\mu}{r^2}\{\dfrac{\partial U}{\partial\phi}+V\} + \dfrac{1}{r}\dfrac{\partial}{\partial\theta}\{r\mu\dfrac{\partial}{\partial r}(\dfrac{W}{r_c})\}$ $+\dfrac{2\mu\cos\phi}{r_c^2}\{U\sin\phi + V\cos\phi - \dfrac{\partial W}{\partial\theta}\}$
W	$-\{\dfrac{\sin\phi UW}{r_c}\}$ $+\{\dfrac{\cos\phi VW}{r_c}\}$	$-\dfrac{1}{r_c}\dfrac{\partial p}{\partial\theta}$	$\dfrac{1}{rr_c}\dfrac{\partial}{\partial\phi}\{\mu(\dfrac{\partial U}{\partial\theta}+W\sin\phi)\}$ $+\dfrac{1}{rr_c}\dfrac{\partial}{\partial r}\{2\mu(\dfrac{\partial V}{\partial\theta}-W\cos\phi)\}$ $+\dfrac{1}{r_c^2}\dfrac{\partial}{\partial\theta}\{\mu(\dfrac{\partial W}{\partial\theta}-2U\sin\theta+2V\cos\phi)\}$ $-\dfrac{\mu\sin\phi}{r}\dfrac{\partial}{\partial\phi}(\dfrac{W}{r_c}) + \mu\cos\phi\dfrac{\partial}{\partial r}(\dfrac{W}{r_c})$ $-\dfrac{\mu r\sin\phi}{r_c^2}\dfrac{\partial}{\partial\theta}(\dfrac{U}{r}) - \dfrac{\mu\cos\phi}{r_c^2}(\dfrac{\partial V}{\partial\theta})$

Table 2.1   Source terms for dependent variables

using the current plane information.

At the highest Dean numbers a significant economy in the memory required at any cross-sectional plane was achieved by assuming that the static pressure within a thin annular ring adjacent to the pipe wall was obtainable from radial momentum equilibrium. Within this sub-region, which extended from the wall to 0.9a, the pressure was obtained from the following degenerate form of the radial momentum equation:

$$\frac{1}{\rho}\frac{\partial p}{\partial r} = \frac{W^2 \cos\phi}{r} + \frac{U^2}{r} \qquad (5)$$

while the radial velocity V was obtained from the continuity equation, (4). This parabolic sublayer treatment (PSL) was originally developed to facilitate the study of complex *turbulent* flows (Iacovides and Launder, 1984) but it has also proved helpful for the flows examined here since, at entry to the solution domain, the boundary layer is extremely thin and a fine near-wall mesh is inevitably required.

There is no intrinsic need for a particularly fine mesh at the pipe centre. Most earlier numerical treatments, however, have put radial gradients of all dependent variables to zero at $r = 0$ and to keep the harmful consequences of this clearly incorrect prescription to unimportant levels, a refined grid has been needed in the vicinity of $r = 0$. The central difficulty is that at $r = 0$ ($J = 1$) there are many coincident nodes each corresponding to a different circumferential angle ϕ (I). In the present study, to improve the pattern of node distribution, the following reformulation has been adopted. For the streamwise velocity component, W, the same value has been assigned to all these coincident centre nodes ($W(I,1)$), this value being the average value of W over the surrounding nodes:

$$W(I,1) = \sum_{I=2}^{NI-1} W(I,2)/(NI-2)$$

where $I=2$ and $I=(NI-1)$ correspond with 0 and π radians respectively. The U and V components, however, cannot take the same value at the centre. Instead, it is required that the resultant of $U(I,1)$ and $V(I,1)$ should produce the same velocity vector irrespective of the circumferential location. Now this resultant velocity must lie on the symmetry axis: its value V_{res} is obtained as the mean of the radial velocity components on $\phi = 0$ and $\phi = \pi$ on either side of the centre node[†]. The U and V velocity components for other values of ϕ are then obtained as

---

[†] In fact, V_{res} is the average of V on $\phi = 0$ and the *negative* of that on $\phi = \pi$

$$U(I,1) = V_{res} \sin\phi \; ; \quad V(I,1) = V_{res} \cos\phi$$

At the tube wall all three velocity components are set to zero. At the inlet plane the streamwise velocity and pressure are assigned as uniform over the plane while the other velocity components are set to zero. At the $\theta = 180^{o}$ plane no constraints are required on the velocity components (which are treated in a boundary-layer fashion) while the streamwise pressure gradient has been set uniform over the section at a level needed to satisfy continuity. This latter condition, while not in accord with the actual pressure gradient at 180° (which is affected by bend-exit effects) has been found to affect the flow pattern only within 20° of the exit (for $\delta = 1/7$). None of the comparisons drawn below relates to a position in the bend greater than 160° from the entry.

A number of computations reported below have been repeated several times with different distributions of nodes in the three co-ordinate directions and with a progressive mesh refinement. The standard mesh density employed was 20 (radial) x 20 (circumferential,ϕ) x 150 (axial, θ) for the pressure p, and for the velocities 28 x 20 x 2. The difference in the number of radial nodes for the velocity and pressure fields arises from the fact that in the 'parabolic sublayer' pressure nodes are not required but velocity nodes are.

The computations have been made on a CDC7600 computer at the University of Manchester Regional Computing Centre. Central processor time required to proceed from a uniform guessed initial pressure field to a final converged state where residual mass errors summed over the entire domain were below 0.1% of the entering mass flow ranged from 10000s. for De = 138 to 25000s. for De = 2712 for $\delta = 1/7$.

PRESENTATION AND DISCUSSION OF RESULTS

Comparison is drawn first with two experiments reported by Agrawal et al (1978), one in a bend with $\delta = 1/7$ at a Dean number of 183 (Re = 484) and the other with $\delta = 1/20$ and De = 565 (Re = 2530). In the experiments, the bend was preceded by a bell-mouth entry; the computer simulation began with a uniform streamwise velocity and zero secondary velocities at the entry plane to the bend (0°). It will be seen later from a comparison with wall stresses that the unavoidable mismatch between the experimental and computational starting profiles leads to a lag in the computation by approximately 5° of arc in the case of $\delta = 1/7$. Streamwise velocity profiles at representative

stations are shown for these two flows in Figures 2 and 3. Due
to the difference in refractive index between the perspex pipe
and the glycerin-water mixture which provided the working fluid,
experimental velocity traverses were made along the non-parallel
lines indicated in the figures. The numerical data were
interpolated to extract velocities along the same lines.

Near the bend entry the potential vortex is clearly evident
in each case. For the lower Reynolds number there is some
indication that the measured boundary layer is a little thicker
than the computed, in part due to neglect in the computations of
any boundary layer at the entry plane. As the shear flow
develops around the bend, the secondary motion displaces the
velocity maximum to the outside of the bend and, in the case of
the higher Dean number, producing double velocity maxima along
some lines. The computations and the experiments generally
produce a strikingly similar behaviour. The somewhat smaller
distortion of the computed profiles at $De = 183$ and $L/R = 7.34$
(where L is the distance from the bend entry measured along the
circular path through the pipe centre) compared with experiment
is, we believe, probably due to the thinner computational inlet
boundary layer. Other small differences that a close examination
reveals are probably attributable to the uncertainty in the
measured Reynolds number of $\pm 8\%$.

The secondary flow data reported by Agrawal et al (1978)
were in fact obtained later than the streamwise velocities and at
different Dean numbers, 138 and 678. Figures 4 and 5 draw
comparisons between the measured profiles and the corresponding
numerical results. In each case, the secondary flow carries
fluid from the outside to the inside of the bend near the wall
with a slow return flow over the remainder of the cross-section.
At the higher Dean number (or rather, Reynolds number) the
near-wall current is confined closer to the wall due to the
thinner streamwise boundary layer and the return flow pattern is
noticeably more complex near the inside of the bend. The
numerical computations mirror the experimental data reasonably
well but not, it must be acknowledged, as well as in the case of
the streamwise profiles discussed above. The predicted near-wall
outer-to-inner flow is thicker than that measured. This
superficially might appear to arise from numerical diffusion but
the QUICK scheme adopted for convection is accurate up to third
order and does not suffer from the severe numerical smearing to
which upwind differencing is prone. Moreover, grid refinement
produced negligible changes in the results at these Dean numbers.
The question thus arose whether the experimental Dean number
could have been different from that reported. Without claiming
to answer that question it is at least of interest to notice that
in Figure 5 the computed secondary flows at a Dean number twice
that reported experimentally are in significantly closer accord
with the experiment than the reported value of 678. At this
higher Dean number the secondary profiles reflect the weakening
of fluid viscosity through the appearance of secondary maxima and
minima along a number of traverse lines near the inside of the

bend. Indeed, the computations at De = 1356 indicate in Figure 5c a reversal of the direction of secondary flow on the symmetry plane implying the formation of a counter rotating eddy[†]. In the experiments the secondary velocity on the axis is reduced almost to zero along two traverse lines in Figure 5c but does not actually reverse. It may be noted, however, that the measured secondary velocities appear to suffer from a 'rightward' bias. That is to say, the secondary flow profiles indicate a mass flow rate to the right that is from 2 to 6 times larger than that to the left. If the flow were fully developed in the axial direction, continuity would require precisely the same rightward and leftward flow rates along every line drawn from the boundary to the symmetric plane. Now, the fact that the predicted secondary profiles *do* indicate, rather closely, such a balance suggests that the effects of changes of W in the axial direction do not make a major contribution. It is thus difficult not to conclude that the experiments, for whatever reason, have given a spurious augmentation of the secondary velocity towards the outside of the bend. Thus it seems probable that the actual flow does indeed exhibit a secondary flow reversal on the axis. Although the computations - even those at De = 1356 - do not quite show the roller-coaster appearance of the experimental profiles, in view of the above discussion the agreement is probably satisfactory. Agrawal et al (1978) speculated that 'separation' of the secondary flow may have occurred at their data collection point closest to the inside of the bend. In fact, though one cannot distinguish it in the figure, the computed wall-adjacent velocities at this position do take very small negative values as may be inferred from the variation of circumferential shear stress in Figure 12.

A clearer impression of the secondary flow pattern is perhaps conveyed in Figures 6 and 7 which show secondary flow 'vectors' at different axial stations for two values of De. At a Dean number of 138 the *pattern* of the secondary flow streamlines changes little as the flow develops around the bend but the magnitude of the secondary velocities in different regions changes considerably, the maximum levels being reached at about 6 radii into the bend (50°). At De = 678 the initial simple cellular pattern evolves into a kidney shape by 12.8 radii downstream with very rapid spatial variations in magnitude and direction of the secondary flow. In marked contrast with the situation in Figure 7b, the secondary velocities on the centreplane are nearly zero. Soh (1983) reports a qualitatively similar behavious at this Dean number. The behaviour for a Dean number of 1356 (not shown) is similar to that at 678 except that the principal return flow is squeezed somewhat closer to the pipe

---

[†] It is interesting to note that Azzola and Humphrey (1984) have measured such a counter rotating eddy near the symmetry plane for *turbulent* flow in a 180° bend

boundary leaving a larger core with virtually no secondary
motion.

It is of interest to return briefly to the streamwise
velocity component to observe how its isovels are distorted by
the secondary flow field. Figure 8 presents measured and
predicted contours for a Dean number of 565 at 83° from the bend
entry. Soh (1983) provides computed results for this flow
condition at the same location and his predictions are included
in the figure. The contour plots convey a clear impression of
how the secondary flow (similar to that shown in Figure 6c) pulls
out the axial contours as fluid flows along the walls from the
outside to the inside of the bend. Because the bulk of the
return flow also takes place along the periphery of the pipe,
however, the profiles are folded back on themselves forming
hook-like contours or "fingers". The present numerical results
mimic closely the measurements save that the computed fingers are
a little wider. Soh's coarse grid calculations yield contours
for $W/\bar{W}$ equal to 1.2 and 1.4 enclosing smaller regions of the
flow than either the measurements or the present calculations;
the main features of the flow are nevertheless quite well
predicted.

Figures 9-12 relate to the distributions of wall shear
stress around the inside of the bend, a topic that has been the
main concern in the papers by Stewartson et al (1980) and Talbot
and Wong (1982). Figure 9 shows the development of the axial
wall shear stress along the inner line of symmetry at four Dean
numbers; also included is the behaviour predicted by Stewartson
et al. As discussed in the Introduction, the analysis developed
by these workers gives a vanishing shear stress at $Z \equiv \theta(R/a)^{\frac{1}{2}} =$
0.943 which represents a point of singularity in the solution
since immediately downstream therefrom the shear stress rises
sharply then approaches monotonically an asymptotic value.
Stewartson et al comment that their analysis is strictly
applicable only for very small values of δ and for De >> 1.
Certainly, as the Dean number is successively raised the present
numerical results shift *in the direction of* that limit, i.e. the
minimum dimensionless wall shear rate falls as De increases and
the minimum value occurs at progressively smaller values of Z
(though even at De = 2712 the minimum is reached about twice as
far downstream as the predicted singular point). Downstream of
the minimum, the numerical solutions display a damped oscillatory
behaviour, the amplitude growing as the Dean number is raised.
This behaviour is evidently in striking contrast with
Stewartson's result, yet is at least in qualitative agreement
with the inviscid analysis of Hawthorne (1951).

It would have been interesting to extend the numerical
results to higher Dean numbers but this was not feasible since to
achieve sensible grid independence for larger De than those
reported would have required finer meshes - and thus more
in-core storage than was available to us. It is of interest to

note the effect of grid refinement on the present solutions.
Figure 10 shows results obtained for the three highest Dean
numbers with the standard 20 x 28 x 150 grid and with a coarser
version: 20 x 20 x 100. At Dean numbers of 678 and 1356 the
changes in shear stress arising from grid refinement are rather
small and the trend is generally to raise the shear stress
slightly. The change is more substantial at the highest Dean
number, the minimum shear stress being raised by a factor of 3.
It is ironic that for this last case the coarser grid gives a
behaviour up to the position of minimum shear stress much closer
to that predicted by the analysis of Stewartson et al.
Nevertheless, the finer grid solution brings the behaviour at
this highest Dean number much more into line with the numerical
results at lower values of De.

The conclusion that the solution of Stewartson et al did not
adequately describe the flow downstream of the singularity was
originally drawn by Talbot and Wong (1982) on the basis of
experimental shear stress data obtained by an electrolytic
method. Comparisons with these measurements are shown in Figure
11 where the present computational curves are all displaced to
the left a dimensionless distance 0.2 (corresponding to 4.3° of
arc), an arbitrary adjustment to try and account for the effects
of the inlet contraction. For De = 678 the computed curve
corresponding to the streamwise wall stress at $8\pi/9$ is also
included to allow comparison with the resultant stress along this
line measured by Choi et al (1979)[+]. Agreement between the
experimental and numerical results is somewhat mixed. At a Dean
number of 183 the computed values are some 20% below the data,
while at the higher Dean numbers the cluster of data points
around $Z = 1.0$ give substantially lower values than predicted.
It is hard to ascribe a level of accuracy to the experiments:
the calibration curve from Talbot and Wong suggests that the
stress levels are systematically low by an amount ranging from
15-25% depending on the surface strain rate, though no estimates
of other uncertainties are provided. Apart from the case of the
lowest Dean number the impression conveyed by the data seems to
be that they scatter about the numerical predictions rather than
display conclusive differences. Talbot and Wong inferred from a
comparison of their measurement with those at $8\pi/9$ from Choi et
al (1979) that the circumferential wall shear stress at this
position was much smaller than the streamwise stress - a
conclusion which conflicted with the predicted behaviour of
Stewartson et al. The present study provides strong support for
Talbot and Wong's conclusion. The circumferential stress along
$8\pi/9$, shown in Figure 12, is an order of magnitude smaller than
the streamwise component except in the vicinity of its maximum

---

[+] Because the circumferential stress at this position is small compared with
the axial stress, the resultant stress does not differ from the axial value
by more than 1%

value. We note that the streamwise variation of this component is essentially independent of Dean number as far as $Z = 1.5$. Moreover, weakly negative values of circumferential shear stress occur for De = 678 in the range $2.7 \leq Z \leq 4.8$ and for De = 1356 in the range $3.7 \leq Z \leq 5.4$. At the highest Dean number the secondary shear stress remains positive, though close to zero for $Z > 4$. It ought to be said that this last result is not conclusively established since it is possible that a further major grid refinement, while producing negligible changes to the streamwise or secondary velocity field, could nevertheless change the circumferential stress from a very weak negative value to an equally weak positive value - or vice versa.

CONCLUSIONS

Careful numerical solutions have been obtained of several laminar flows developing in 180° bends of circular cross-section that have been the subject of laser Doppler studies by Talbot and his colleagues. Given the small but unquantifiable mismatch between the computational and the experimental entry conditions, agreement between computed and measured streamwise profiles for Dean numbers of 183 and 565 are in extremely close agreement. There is less complete agreement with the secondary velocity profiles and one possibility, that would be consistent with the present results, would be that the experimental data (which were obtained in a separate study from the streamwise profiles) were at a higher Dean number than reported.

The present computational results indicate a gradual approach towards the initial-region behaviour predicted by Stewartson et al (1980) as the Dean number is raised. Even at a Dean number of 2712, however, there are still marked differences from Stewartson's solution. Downstream of the point of minimum shear stress on the inside wall the numerical results indicate an oscillatory development of the streamwise wall stress, the overshoot increasing as the Dean number is raised. This behaviour, which is at least in qualitative agreement with the data of Talbot and Wong (1982), and inviscid flow calculations of the secondary flow by Hawthorne (1951), is in striking contrast with the predictions of Stewartson et al (1980) which show a monotonic approach to steady state conditions.

ACKNOWLEDGEMENTS

REFERENCES

1. Agrawal, Y., Talbot, L. and Gong, K. 1978. "Laser anemometer study of flow development in curved pipes" J. Fluid Mech., 85, pp. 497-518

2. Azzola, J. and Humphrey, J.A.C. 1984. "Developing turbulent flow in a 180° curved pipe and its downstream tangent" Second International Symposium on Applications of Laser Anemometry to Fluid Mechanics, Lisbon

3. Barua, S.N. 1963. "On secondary flow in stationary curved pipes" O. J. Mech. Appl. Math., 16, pp. 61-77

4. Berger, S.A., Talbot, L. and Yao, L-S. 1983. "Flow in curved pipes" Ann. Rev. Fluid Mech., 15, pp. 461-512

5. Choi, U.S., Talbot, L. and Cornet, I. 1979. "Experimental study of wall shear rates in the entry region of a curved tube" J. Fluid Mech., 93, pp. 465-489

6. Chorin, A.J. 1967. "A numerical method for solving incompressible viscous flow problems" J. Comp. Physics, 2, p. 12

7. Collins, W. and Dennis, S.C.R. 1975. "The steady motion of a viscous fluid in a curved tube" Q. J. Mech. Appl. Math., 28, pp. 133-156

8. Cuming, H.G. 1952. "The secondary flow in curved pipes" Aeronaut. Res. Counc. Rep. Mem. No. 2880

9. Han, T.Y., Humphrey, J.A.C. and Launder, B.E. 1981. "A comparison of hybrid and quadratic-upstream differencing in high Reynolds number elliptic flows" Comp. Meths. Appl. Mech. Eng., 29, p. 81

10. Hawthorne, W.R. 1951. "Secondary circulation in fluid flow" Proc. Roy. Soc. A 206, pp. 374-387

11. Huang, P.G., Launder, B.E. and Leschziner, M.A. 1983.
    "Discretization of non-linear convection processes: A broad
    range comparison of four schemes" Submitted to Comp. Meth.
    Appl. Mech. and Engrg.

12. Humphrey, J.A.C. 1977. "Numerical calculation of developing
    laminar flow in pipes of arbitrary curvature radius" Can.
    J. Chem. Eng., $\underline{56}$, pp. 151-164

13. Iacovides, H. and Launder, B.E. 1984. "PSL - An economical
    approach to the numerical analysis of near-wall elliptic
    flow" ASME J. Fluids Eng., $\underline{106}$

14. Ito, H. 1969. "Laminar flow in curved pipes" Z. Angew.
    Math. Mech., $\underline{49}$, pp. 653-663

15. Johnston, J.P. 1978. Chapter 3, Internal Flows, in
    Turbulence (Editor Bradshaw, P.) Topics in Applied
    Physics, $\underline{12}$, Springer-Verlag, New York

16. Leonard, B.P. 1979. "A stable and accurate convective
    modelling procedure based on quadratic upstream
    interpolation" Comp. Meth. Appl. Mech. Eng., $\underline{19}$, 59

17. Levy, R., Briley, W.R. and McDonald, H. 1983. AIAA Paper
    83-056

18. Liu, N-S. 1977. "Developing flow in a curved pipe" INSERM-
    Euromech, 92 71:53-64

19. Patankar, S.V. 1980. Numerical Heat Transfer and Fluid Flow,
    Hemisphere Publishing Corp. - McGraw Hill

20. Patankar, S.V. and Spalding, D.B. 1972. "A calculation
    procedure for heat, mass and momentum transfer in three-
    dimensional parabolic flows" Int. J. Heat Mass Transfer,
    $\underline{15}$, p. 1787

21. Patankar, S.V., Pratap, V.S. and Spalding, D.B. 1974.
    "Prediction of laminar flow and heat transfer in helically
    coiled pipes" J. Fluid Mech., $\underline{62}$, pp. 539-551

22. Pratap, V.S. and Spalding, D.B. 1975. "Numerical
    computations of the flow in curved ducts" Aero. Quart.,
    $\underline{26}$, pp. 219-228

23. Rushmore, W.L. 1975. "Theoretical investigation of curved
    pipe flows" PhD Thesis, State Univ. N.Y. at Buffalo,
    160 pp.

24. Singh, M.P. 1974. "Entry flow in a curved pipe" J. Fluid
    Mech., $\underline{65}$, pp. 517-539

25. Soh, W.Y. 1983. "Laminar entrance flow in a curved pipe" PhD
     Thesis, Univ. of California, Berkeley, 91 pp.

26. Stewartson, K., Cebeci, T. and Chang, K.C. 1980. "A
     boundary-layer collision in a curved duct" Q.J. Mech.
     Appl. Math., 33, pp. 59-75

27. Talbot, L. and Wong, S.J. 1982. "A note on boundary layer
     collision in a curved pipe" J. Fluid Mech., 122, pp.
     505-510

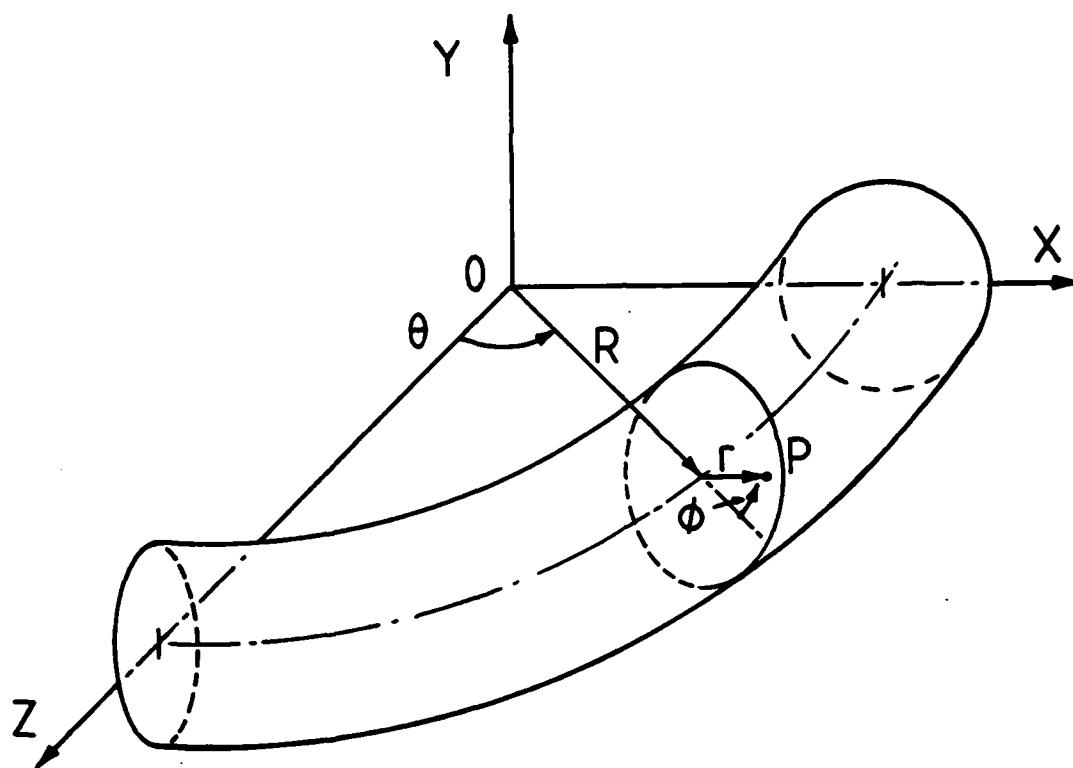28. Yao, L-S. and Berger, S.A. 1975. "Entry flow in a curved
     pipe" J. Fluid Mech., 67, pp. 177-196

Figure 1   The configuration considered and the describing coordinates
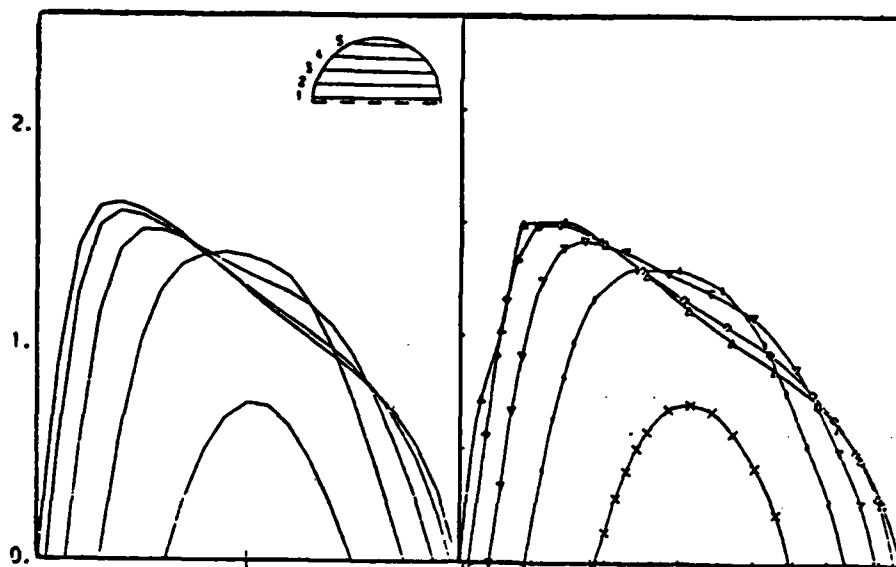
Fig. 2 c   L/a = 19.54
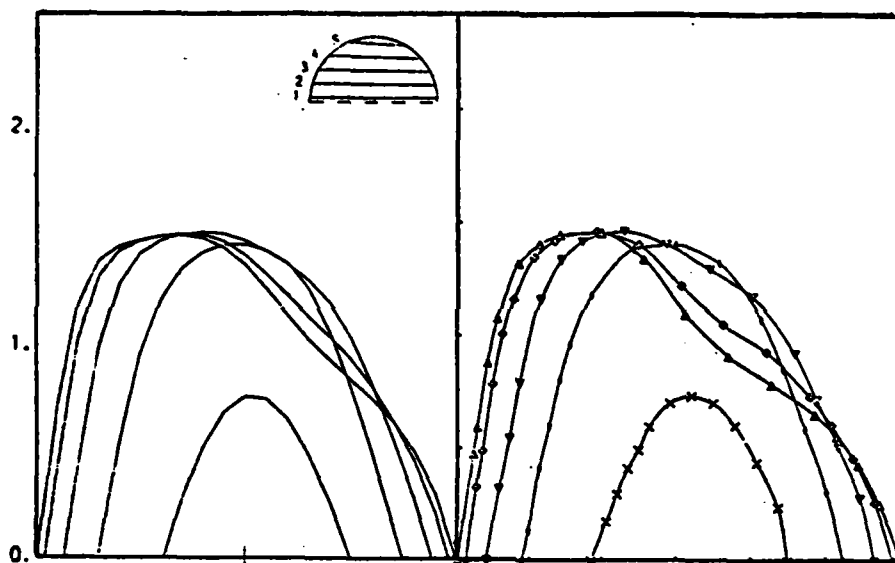
Fig. 2b   L/a = 7.34
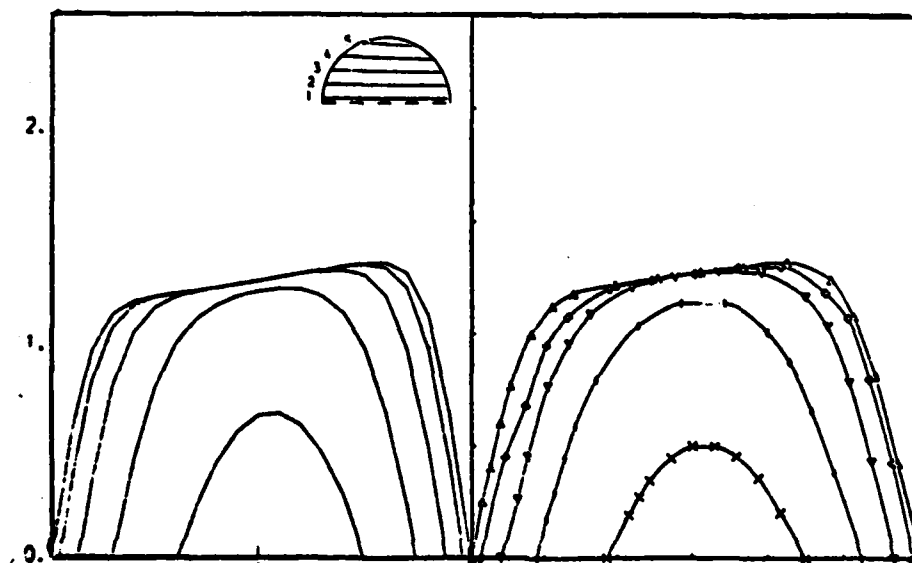
Fig. 2.a   L/a = 1.84

Figure 2   Streamwise velocity profiles along lines 1-5

Right hand figures: experiments Agrawal et al (1978)
Left hand figures: present computations

Fig. 3c   L/a = 57.6

Fig. 3b   L/a = 29.4

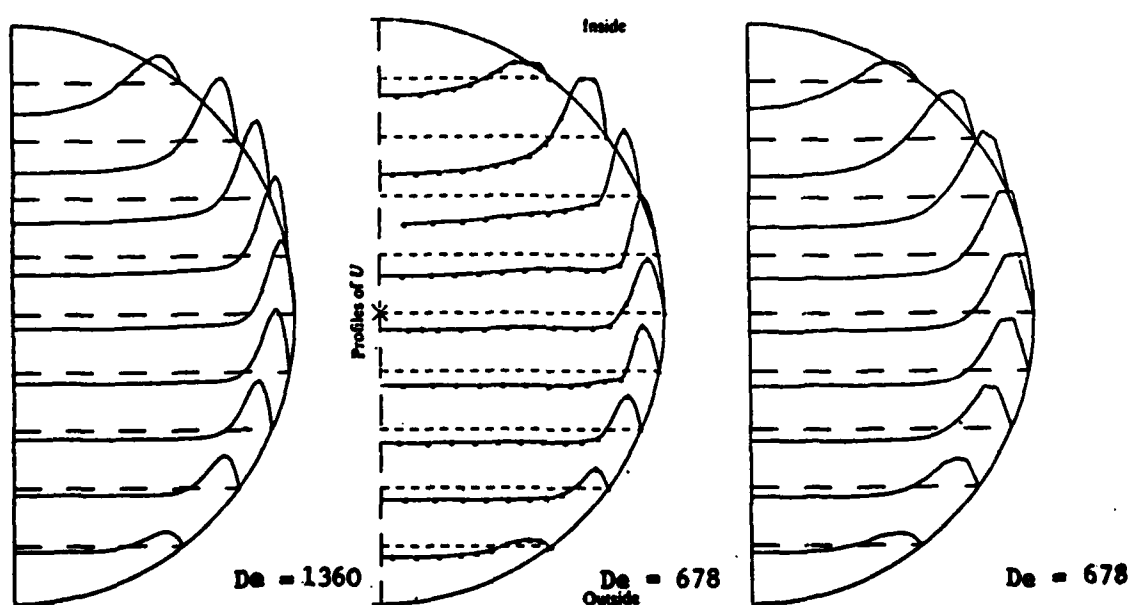Fig. 3a   L/a = 2.4
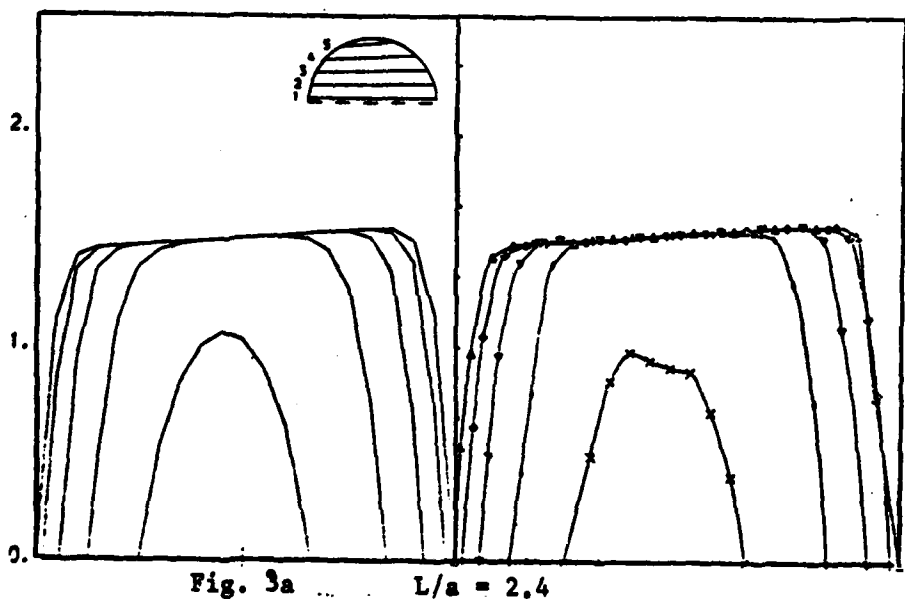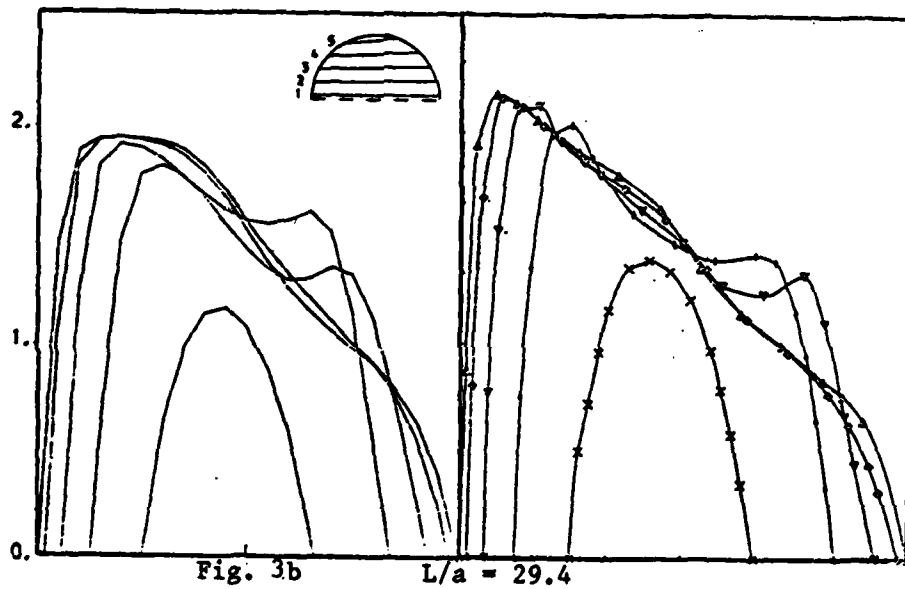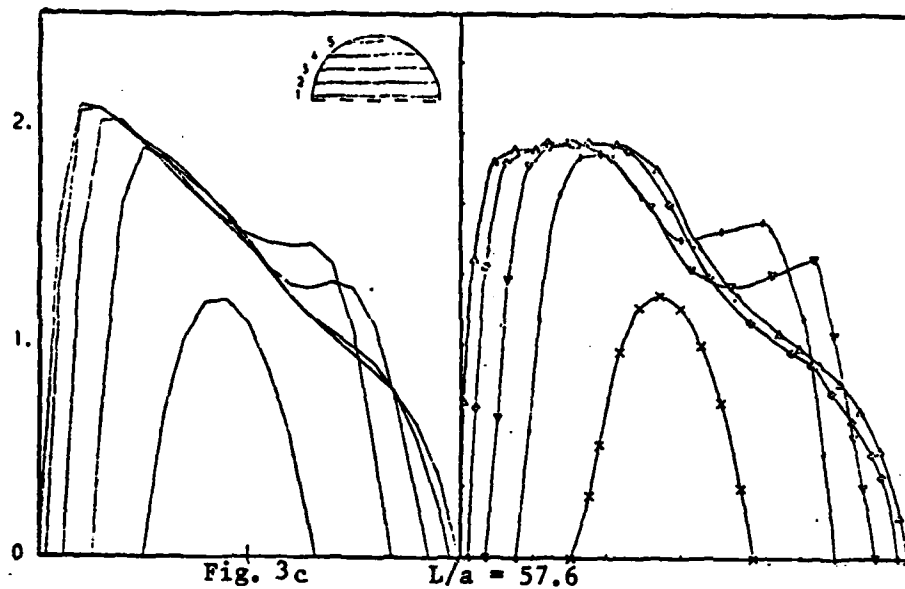
Figure 3   Streamwise velocity profiles along lines 1-5
              Right hand figures: experiments Agrawal et al (1978)
              Left hand figures: present computations
                      De = 683;   R/a = 20
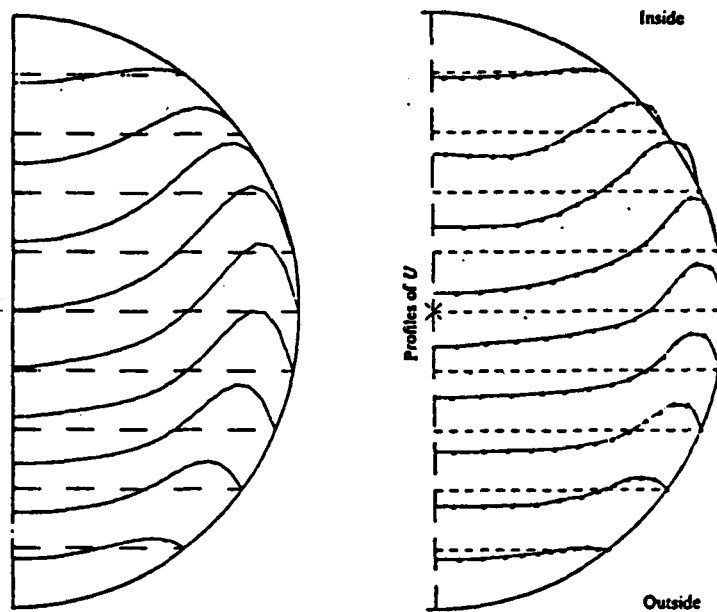
Fig. 4b   L/a = 6.11
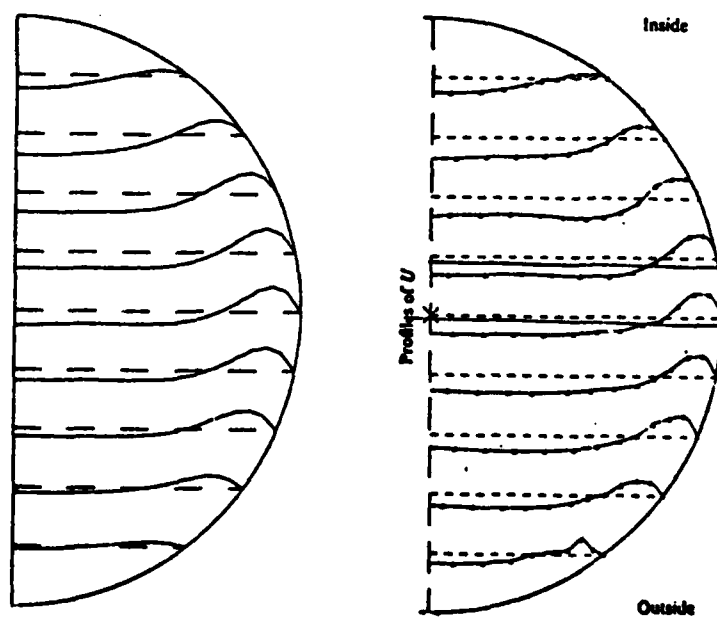
Fig. 4a   L/a = 1.83

Fig. 4   Secondary velocity profiles

Right hand figures: experiments Agrawal et al (1978)
Left hand figures: present computations
De = 138   R/a = 7
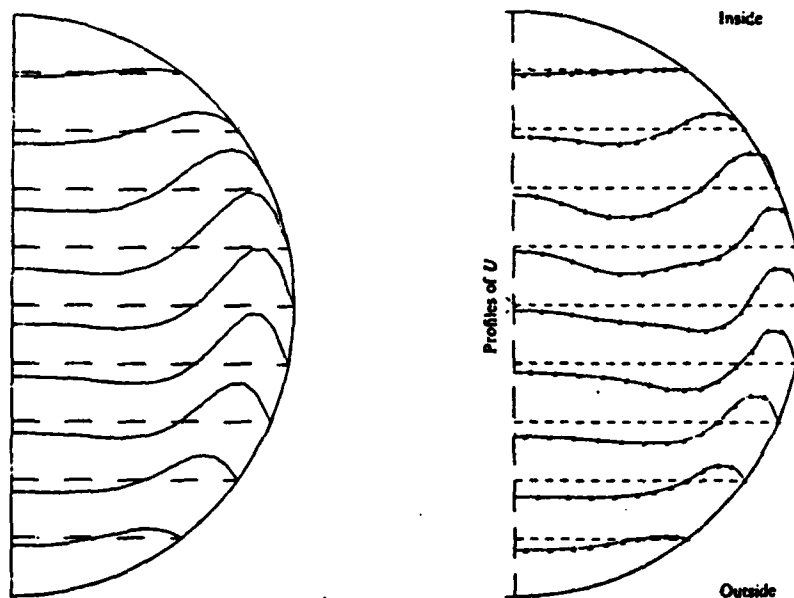
Fig. 4 c   L/a = 12.83
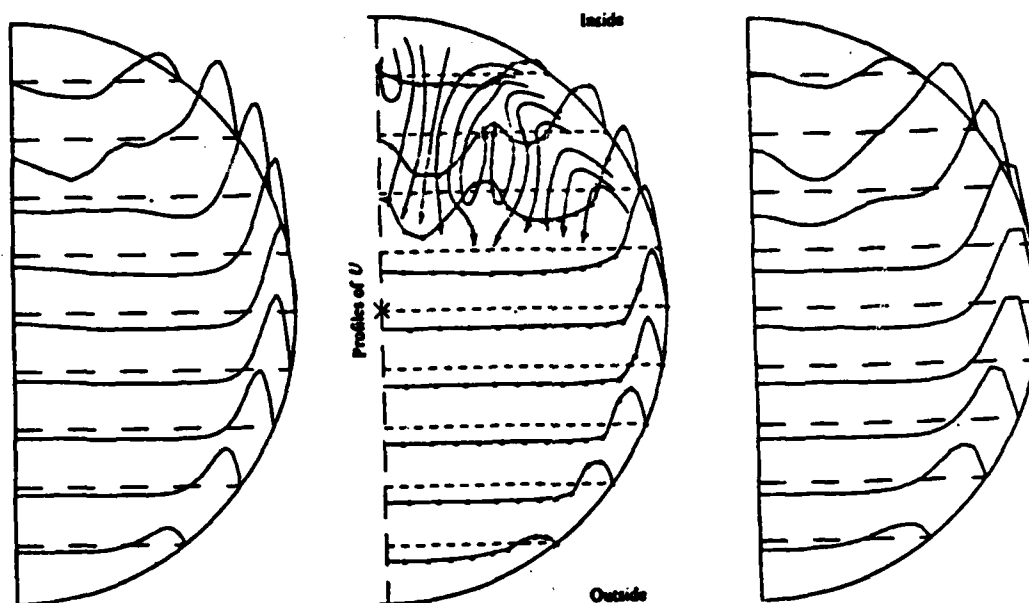
Fig. 5b   L/a = 9.16

Fig. 5a   L/a = 3.67

Figure 5   Secondary velocity profiles

Centre figures: experiments Agrawal et al (1978), De = 678
Right hand figures: present computations, De = 678
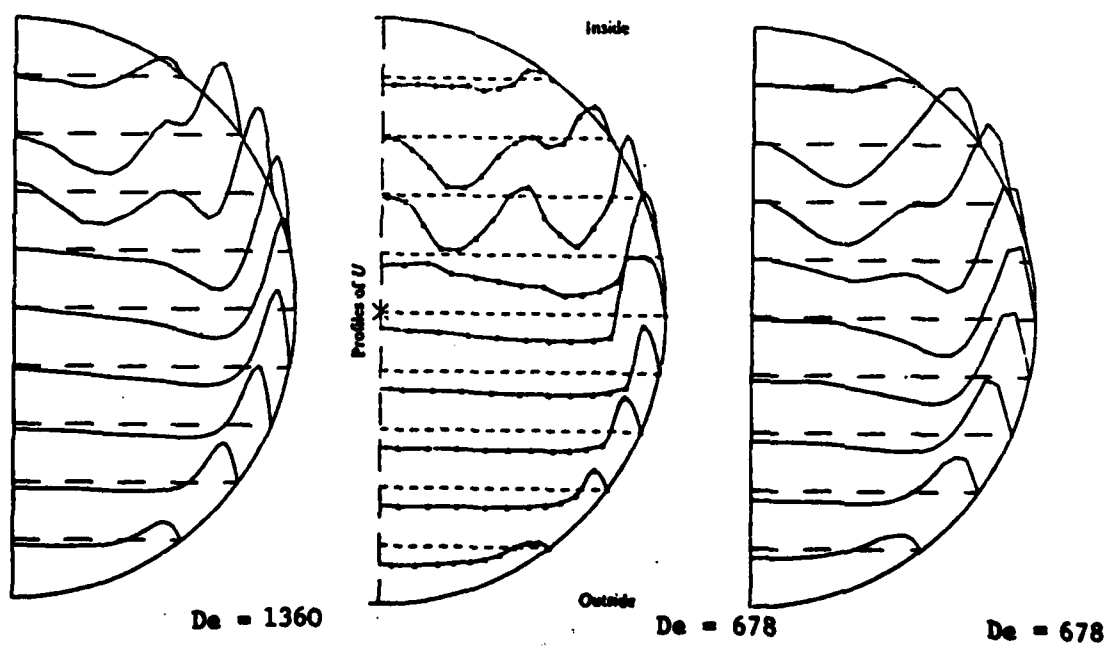Left hand figures: present computations, De = 1360
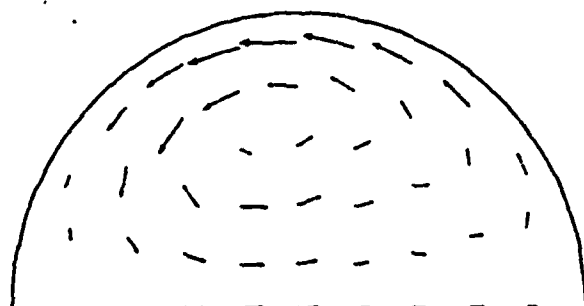
Fig. 5d   L/a = 16.49

De = 1360   De = 678   De = 678
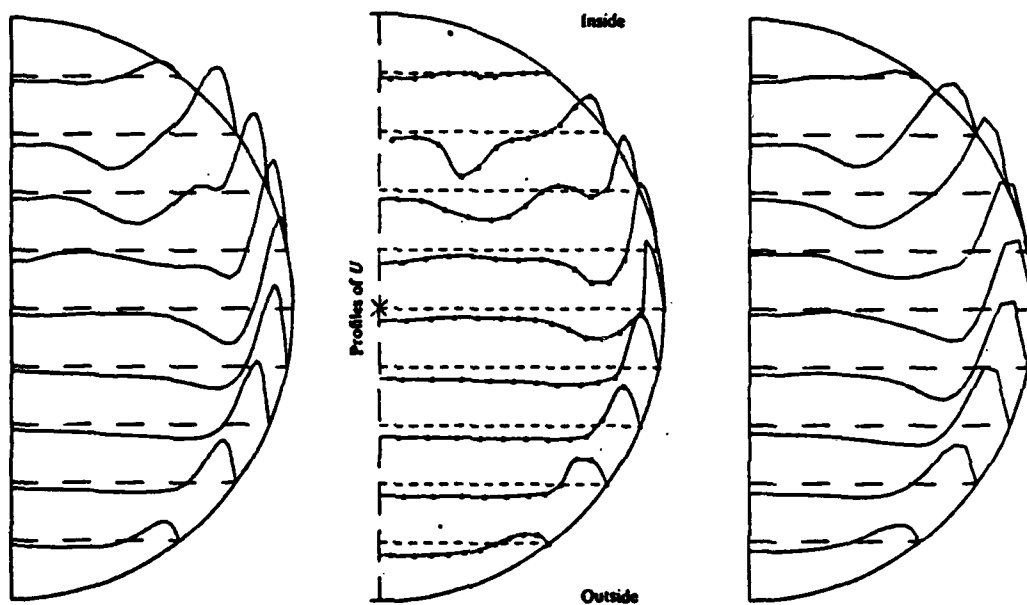
Fig. 5c   L/a = 12.89

Fig. 6c   L/a = 12.83
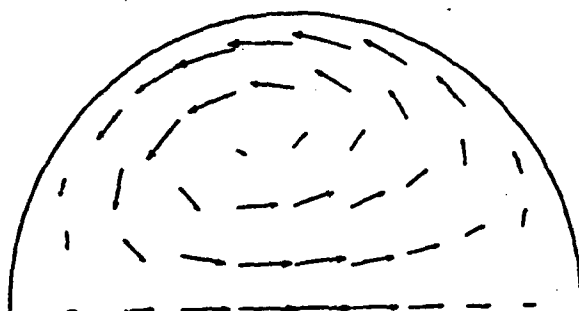
Fig. 6b   L/a = 6.11
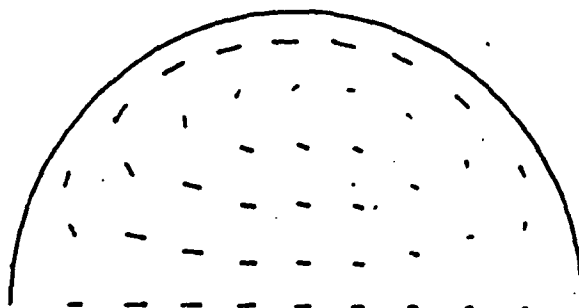
Fig. 6.a   L/a = 1.83

Fig. 6   Secondary velocity vector plots
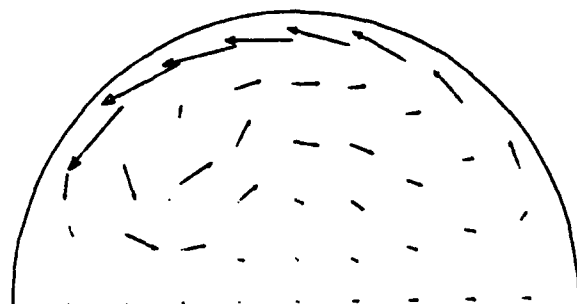
De = 138   RC/a = 7.0
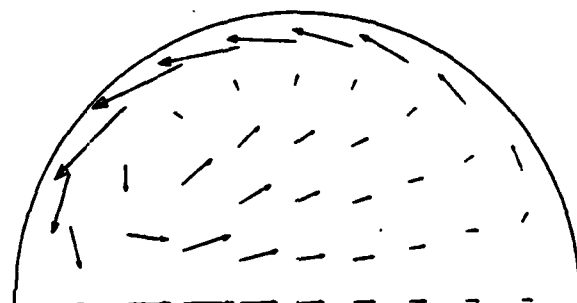
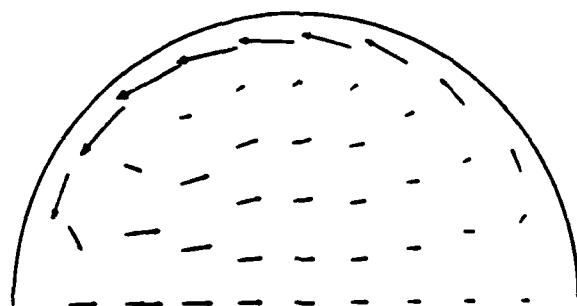Fig. 7c   L/a = 12.81

Fig. 7b   L/a = 6.11

Fig. 7a   L/a = 3.67

Fig. 7   Secondary velocity vector plots

De = 678   RC/a = 7.0
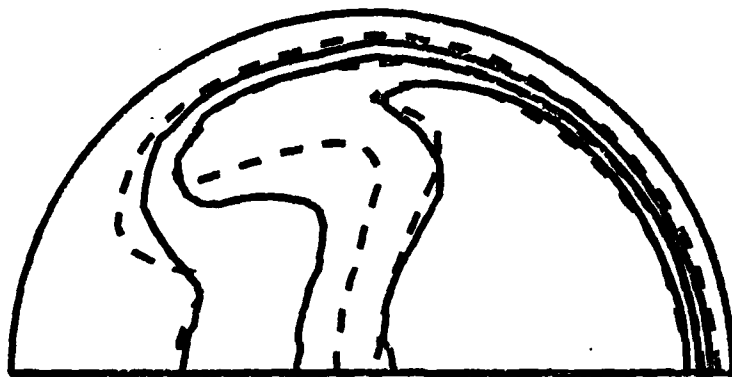
Fig. 8b ———— Present predictions
- - - - Talbot et al (experiment)

Fig. 8a ———— Soh (predictions)
- - - - Talbot et al (experiment)

Fig. 8   Streamwise velocity contours

De = 565   R/a = 20.0

L/a = 29.4
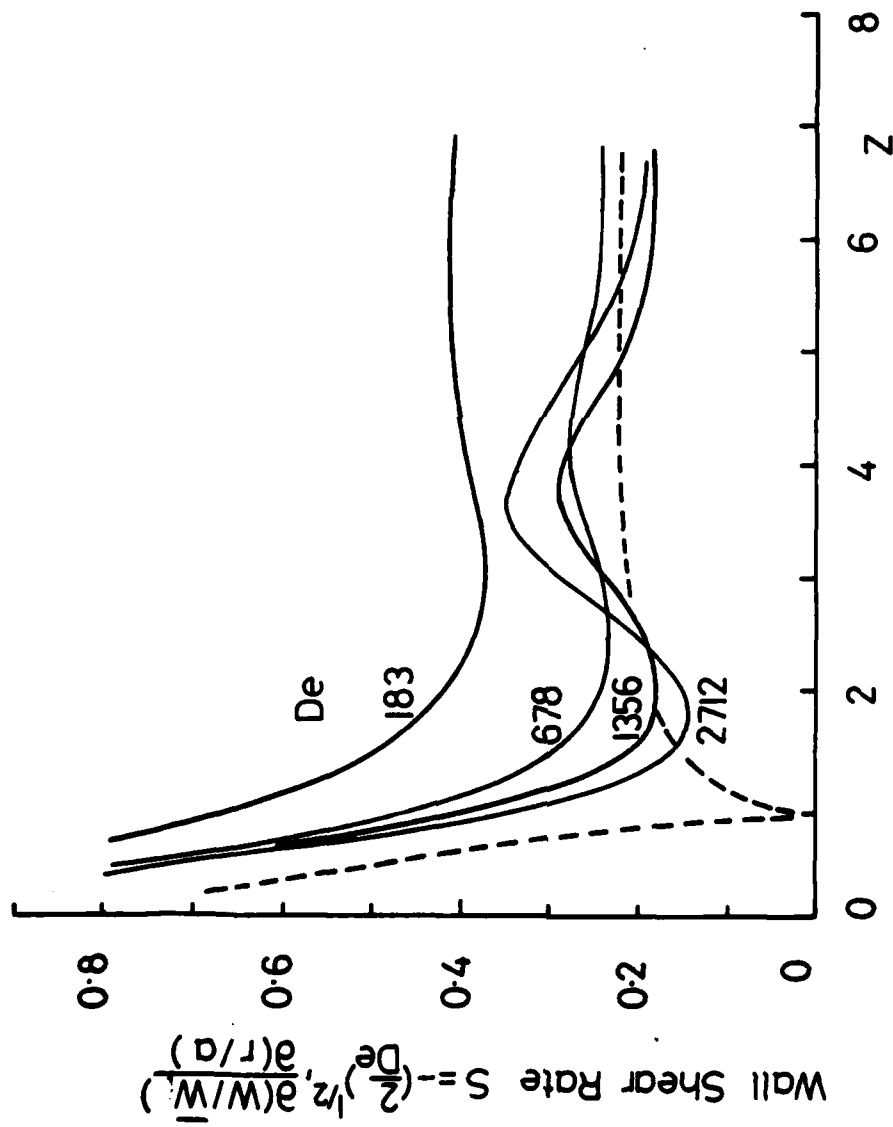
Figure 9 Distribution of dimensionless wall shear stress along inner line of symmetry

Wall Shear Rate $S = -\left(\frac{2}{De}\right)^{1/2}, \dfrac{\partial(w/\overline{w})}{\partial(r/a)}$

De

183

678

1356

2712

—— Present computations

--- Stewartson et al (1980)

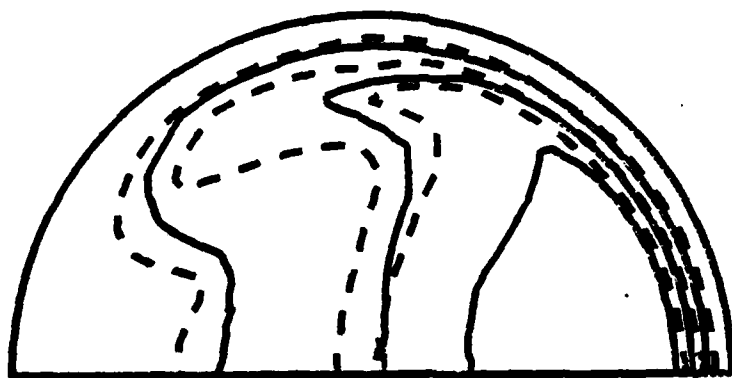Figure 10   Distribution of dimensionless wall shear stress along inner line of symmetry.   Sensitivity of results to grid refinement.
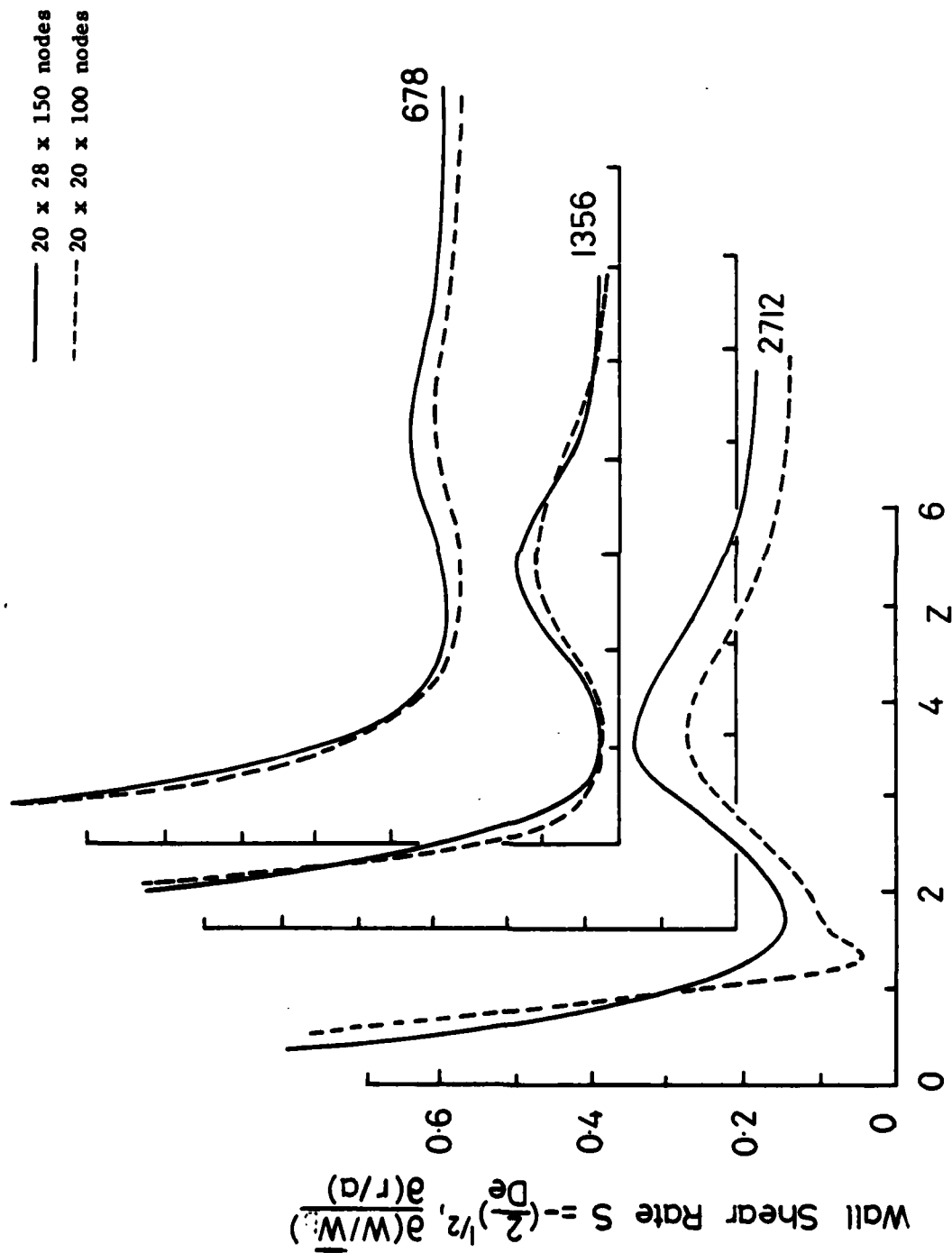
20 x 28 x 150 nodes

20 x 20 x 100 nodes

678

1356

2712

$$\text{Wall Shear Rate } S = -\left(\frac{2}{De}\right)^{1/2} \frac{\partial(W/\overline{W})}{\partial(r/a)}$$

Figure 11 Comparisons of experimental and measured wall shear stresses

Figure 12   Dimensionless circumferential shear stress along $\phi = 8\pi/9$

APPENDIX 3

The Computation of Momentum and Heat Transport in

Turbulent Flow around Pipe Bends

H. Iacovides and B.E. Launder

A numerical solving procedure is described based on a semi-
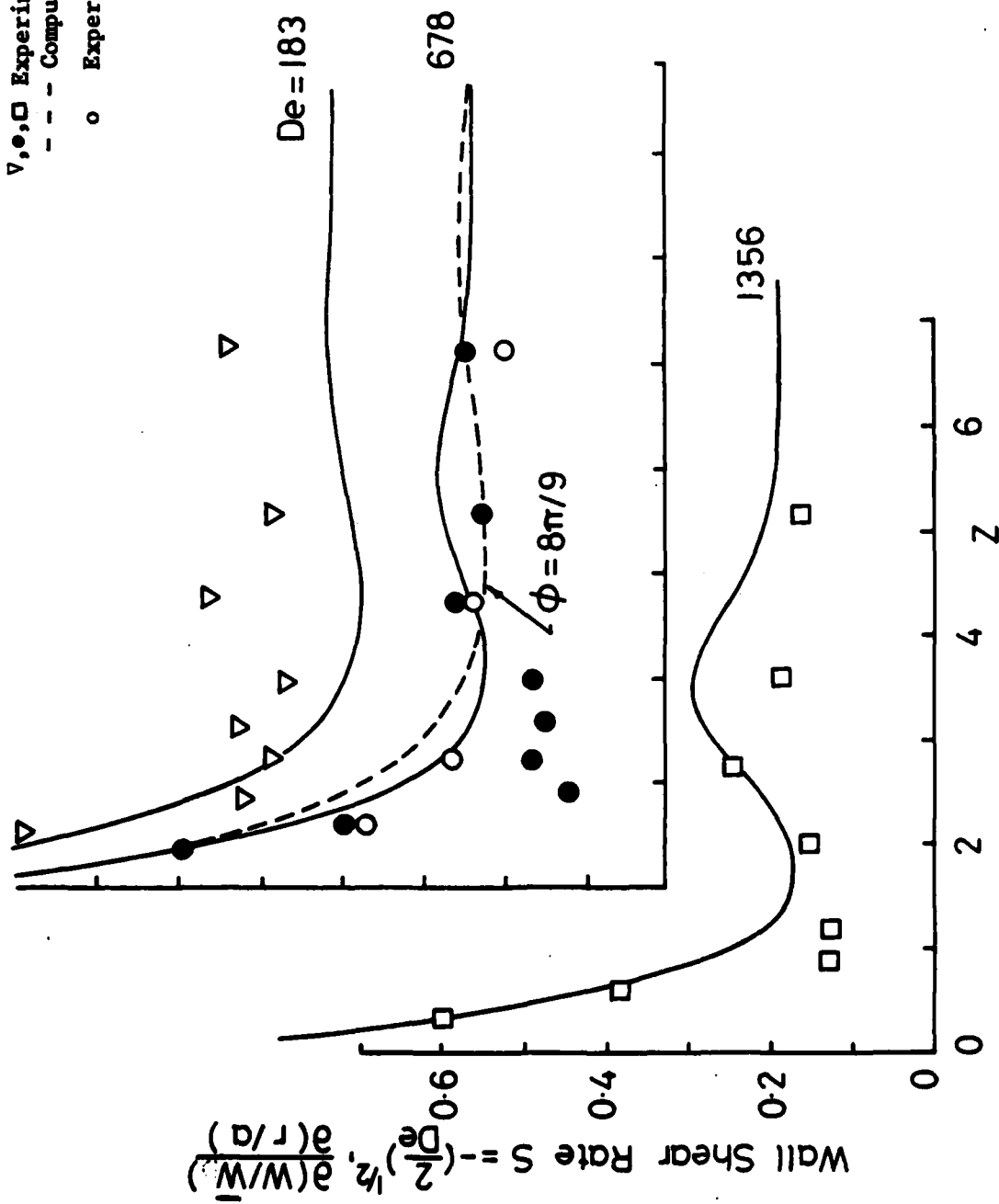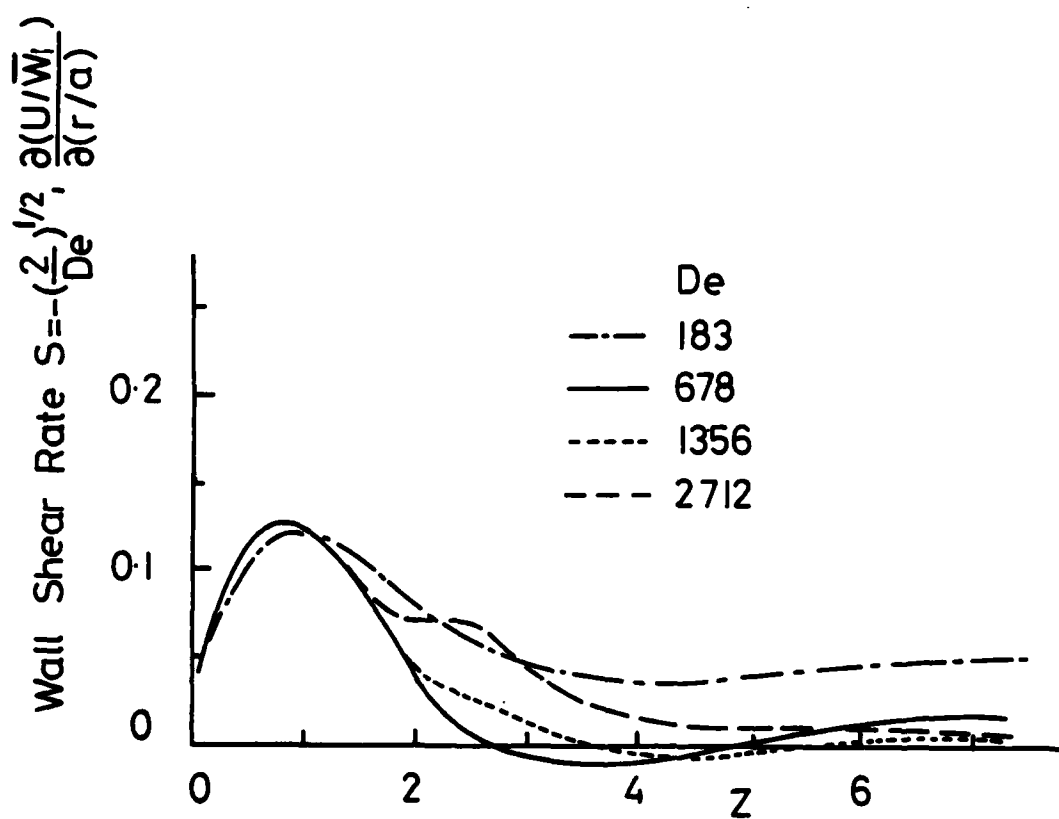elliptic discretization of the averaged equations of motion
describing turbulent flow through curved circular-sectioned
tubes. It adopts Leonard's QUICK treatment of convection
and Patankar's SIMPLER algorithm for handling the pressure-
velocity connection. Applications are reported of laminar
and turbulent flow in a 90° bend (adopting, in the latter
case, the standard k-ε Boussinesq viscosity model for the
Reynolds stresses). Solutions of the thermal energy
equation for this case indicate a marked rise in the average
heat transfer coefficient at any section but with a five-
fold variation in Nu between the inside and outside of the
tube.

1. Introduction

Turbulent flow around pipe bends is a common feature of heat
exchangers, condensers, boilers and other heat-transfer equipment.
Such flows also arise in the internal cooling passages of various
components of power generation equipment from gas turbine blades
to the rotating cores of electrical generators. Besides the very
complex three-dimensional flow that occurs in the bend itself, the
secondary flow generated in the bend can carry over to have an
appreciable effect on the velocity and temperature fields many
diameters downstream.

Despite the importance of the flow, little is known of the
detailed structure in the turbulent flow regime. For the most
part, studies have reported overall pressure-loss coefficients for
bends of different angles and different ratios of pipe diameter to
bend radius. Exceptions are the measurements of mean velocity by
Rowe (1970) in a rather gentle 180° bend and the recent experiment
of Enayet, Gibson, Taylor and Yianneskis (1982) which reports the
development of the mean and rms turbulent streamwise velocities
around a 'tight' 90° bend (pipe diameter: mean radius of curvature
= 2.8:1). There are no local heat transfer data available, so far
as we know, in the development region of a circular sectioned
pipe, though a joint programme of experiments on both the flow and
thermal fields is now in progress at UMIST and the University of
California, Berkeley (Professor J.A.C. Humphrey).

The advance in speed and core capacity of computers, coupled
with improvements in numerical methods for solving the fluid flow
equations, make it feasible to undertake computer simulations of
three-dimensional flows; these can provide far more detail of the
velocity and thermal fields than could any experimental

realization of the same flow. Whether or not the resulting calculations provide a close approximation of the real flow depends on how small the computor has been able to keep his numerical error and on how well the unknown turbulent momentum and heat fluxes are represented by the 'turbulence model' adopted. In the case of developing turbulent flow around pipe bends, the first computations were reported by Pratap and Spalding (1975). The paper introduced a novel simplification of the full three-dimensional Navier Stokes equations in that, while the fully elliptic form of the pressure equation was retained, a parabolic truncation was adopted for the velocity field wherein streamwise momentum diffusion was omitted. This simplification allowed the velocity field to be stored on only two adjacent streamwise planes instead of over the whole domain. The savings in core that such semi-elliptic schemes allow enables a far finer mesh to be employed for the pressure field (which must be stored over the full domain) than would otherwise be possible. Pratap and Spalding (1975) achieved moderately good agreement in their simulation of Rowe's (1970) experiment, though some of the features of their original calculation method are unsuitable for computing the practically far more important case of flow around sharp bends with R/d in the range 2-4.

Perhaps the most serious limitation of the Pratap-Spalding scheme for such flows is their use of "wall functions" (c.f. Launder and Spalding, 1974), based on experimental data for plane two-dimensional turbulent flows, to provide the near-wall boundary conditions on the velocity field. This approach provides an unreliable basis for fixing the secondary velocity parallel to the wall and it is difficult to conclude other than that the only satisfactory treatment is to carry the integration to the wall. This approach has been adopted by McDonald's group (McDonald, 1982) in computing turbulent flow around a 90° bend of square cross section as part of their contribution to the 1981 Stanford Conference on Complex Turbulent Flows (Kline et al, 1982). The results of this computation, while, overall, not superior to those of other submissions, did nevertheless give a more accurate account of the development in the first 30° of the bend where there is a strong secondary flow confined very close to the wall carrying fluid from the outside to the inside of the bend. The numerical procedure developed by McDonald's group obtains the pressure distribution as a one-dimensional correction to a potential flow. This simple approach works very well when the boundary layers are thin but appears to be a major factor in the deterioration in their predictions of the square bend experiment beyond 45°. A further potential source of error is the use of the very simple mixing-length hypothesis to compute the Reynolds stresses. The scheme entirely neglects transport effects on turbulence; moreover, as Levy et al (1983) comment, the prescription of a boundary-layer thickness – required to fix the mixing length – becomes arbitrary in such a three-dimensional flow.

The present contribution reports our attempts at achieving a more satisfactory numerical and physical computational model of turbulent flow around bends than has hitherto been reported. We adopt, following Pratap and Spalding (1975), a semi-elliptic approach though, like Levy et al (1983), we eschew the use of wall

functions and instead extend the computations to the pipe wall using, in the low-Reynolds-number sub-layer, the Van Driest (1956) version of the mixing length hypothesis. In the main flow, however, the $k\sim\varepsilon$ Boussinesq viscosity model is adopted to allow some account to be taken of transport effects on turbulence.

Extensive comparisons are drawn with the laminar and turbulent flow data of Enayet et al (1982) in a 90° bend. We report also the computed behaviour for the thermal field for this geometry. Finally, comparisons are drawn with the Seban and McLaughlin (1963) measurements of local Nusselt number in fully developed flow through coiled tubes.

2. Summary of the Computational Procedure

2.1 The Describing Equations and Boundary Conditions

The flow is analysed in the toroidal, r, ∅, θ system shown in figure 1. If we adopt the Boussinesq turbulent viscosity concept to represent the momentum and heat fluxes due to the turbulent motion, the describing continuity, momentum and energy equations may be written as follows:-

Continuity

$$\frac{\partial}{\partial\emptyset} r_c U + \frac{\partial}{\partial r} r r_c V + \frac{\partial}{\partial\theta} rW = 0$$

(2.1)

Momentum and Energy

$$\rho(C(\psi) + S_c(\psi)) = D(\psi) + S_d(\psi) + S_p(\psi)$$

(2.2)

In equation (2.1) U, V and W denote the velocity components in the ∅, r, θ directions, r_c is the local radius from the centre of the bend (R + rcosθ), while in equation (2.2) ψ stands for any of the velocity components or the temperature. The associated source and sink terms are given in Table 2.1 and the operators C(ψ) and D (ψ) denote:

$$C(\psi) \equiv (rr_c)^{-1}\left[\frac{\partial}{\partial\emptyset}(r_c U\psi) + \frac{\partial}{\partial r}(rr_c V\psi) + \frac{\partial}{\partial\theta} (rW\psi)\right]$$

$$D(\psi) \equiv (rr_c)\left[\frac{1}{r}\frac{\partial}{\partial\emptyset}(r_c (\frac{\mu}{\sigma\psi} + \frac{\mu}{\sigma_\psi}t)\frac{\partial\psi}{\partial\emptyset} + \frac{\partial}{\partial r}(rr_c(\frac{\mu}{\sigma\psi} + \frac{\mu}{\sigma_\psi} t)\frac{\partial\psi}{\partial r})\right]$$

The quantity σ^ψ is unity in all but the energy equation where it denotes the molecular Prandtl number of the fluid. Notice that second derivatives with respect to θ are dropped, an essential feature of semi-elliptic treatments. Where computations are to be made in straight approach sections of the pipe or in downstream tangents, the mean radius of curvature R is set to some suitably large value in these regions.

ψ	$S_c(\psi)$	$S_p(\psi)$	$S_D(\psi)$
U	$\dfrac{VU}{r} + \{\dfrac{W^2\sin\phi}{r_c}\}$	$-\dfrac{1}{r}\dfrac{\partial p}{\partial\phi}$	$\dfrac{1}{r_c}\dfrac{\partial}{\partial\phi}\{r_c\mu_{eff}(\dfrac{\partial U}{\partial\phi}+2V)\} + \dfrac{1}{rr_c}\dfrac{\partial}{\partial r}\{r_c\mu_{eff}(\dfrac{\partial V}{\partial\phi}-U)\}$ $+ \mu_{eff}\dfrac{\partial}{\partial r}\{\dfrac{U}{r}\} + \dfrac{\mu_{eff}}{r^2}\dfrac{\partial V}{\partial\phi} + \dfrac{1}{r}\dfrac{\partial}{\partial\theta}\{\mu_{eff}\dfrac{\partial}{\partial\phi}(\dfrac{W}{r_c})\}$ $- \dfrac{2\mu_{eff}\sin\phi}{r_c^2}\{U\sin\phi - V\cos\phi - \dfrac{\partial W}{\partial\theta}\}$
V	$-\{\dfrac{\cos\phi W^2}{r^2}\}$ $-\{\dfrac{U^2}{r}\}$	$-\dfrac{\partial p}{\partial r}$	$\dfrac{1}{r_c}\dfrac{\partial}{\partial\phi}\{r_c\mu_{eff}\dfrac{\partial}{\partial r}(\dfrac{U}{r})\} + \dfrac{1}{rr_c}\dfrac{\partial}{\partial r}\{rr_c\mu_{eff}\dfrac{\partial V}{\partial r}\}$ $-\dfrac{2\mu_{eff}}{r^2}\{\dfrac{\partial U}{\partial\phi}+V\} + \dfrac{1}{r}\dfrac{\partial}{\partial\theta}\{r\mu_{eff}\dfrac{\partial}{\partial r}(\dfrac{W}{r_c})\}$ $+\dfrac{2\mu_{eff}\cos\phi}{r_c^2}\{U\sin\phi + V\cos\phi - \dfrac{\partial W}{\partial\theta}\}$
W	$-\{\dfrac{\sin\phi UW}{r_c}\}$ $+\{\dfrac{\cos\phi VW}{r_c}\}$	$-\dfrac{1}{r_c}\dfrac{\partial p}{\partial\theta}$	$\dfrac{1}{rr_c}\dfrac{\partial}{\partial\phi}\{\mu_{eff}(\dfrac{\partial U}{\partial\theta}+W\sin\phi)\}$ $+\dfrac{1}{rr_c}\dfrac{\partial}{\partial r}\{2\mu_{eff}(\dfrac{\partial V}{\partial\theta}-W\cos\phi)\}$ $+\dfrac{1}{r_c^2}\dfrac{\partial}{\partial\theta}\{\mu_{eff}(\dfrac{\partial W}{\partial\theta}-2U\sin\theta+2V\cos\phi)\}$ $-\dfrac{\mu_{eff}\sin\phi}{r}\dfrac{\partial}{\partial\phi}(\dfrac{W}{r_c}) + \mu_{eff}\cos\phi\dfrac{\partial}{\partial r}(\dfrac{W}{r_c})$ $-\dfrac{\mu_{eff}\,r\sin\phi}{r_c^2}\dfrac{\partial}{\partial\theta}(\dfrac{U}{r}) - \dfrac{\mu_{eff}\cos\phi}{r_c^2}(\dfrac{\partial V}{\partial\theta})$
T	0	0	0

$$\mu_{eff} = \mu_t + \mu$$

Table 2.1 Source and diffusion terms in mean flow equations

Calculations are made over the semi-circular half cross section bounded by the diametral plane of symmetry passing through the centre of the pipe bend. The velocity normal to that plane is set to zero, while the *gradients* of W and V normal to the plane are zero. Along the pipe wall no-slip conditions are applied. The velocity components and pressure are all prescribed at entry to the flow domain while at exit the second derivative of the static pressure in the streamwise direction is set to zero; the velocity and energy equations are only first order in θ and no outlet boundary condition is required.

As described in detail elsewhere (Launder, Johnson and Iacovides, 1983; Humphrey, Iacovides and Launder, 1984) a new treatment of the U and V boundary condition at the tube axis has been evolved in this work that removes the usual singularity problem. The need for special care arises because the axis coincides with the location of *many* U and V nodes each corresponding to different values of the co-ordinate ∅. Now, since the nodes in question lie at the symmetry plane, we know that for every such node the *resultant* velocity in the plane of the cross section must be the same and directed *along* the symmetry plane – since as noted in §2.1. there can be no velocity component normal to this plane. We thus conclude that:

$$U(I,1) = V_{res} \sin \varnothing(I)$$
$$V(I,1) = V_{res} \cos \varnothing(I)$$

(2.5)

where V_{res} is the average radially directed velocity at the axis, $\frac{1}{2}(V|_{\phi=0} - V|_{\phi=\pi})$.

Application of these conditions has removed the need for a very small near-axis cell adopted in earlier treatments (e.g. Levy et al, 1983).

2.2 The Turbulence Model

Although in the future the authors aim to include a model of turbulence based on closure of the stress and heat-flux transport equations, the present computations all adopt the Boussinesq concept of an isotropic turbulent viscosity μ_t; in the momentum equations σ_ψ is unity, while in the energy equation it represents the turbulent Prandtl number and is assigned the uniform value 0.9.

It cannot be said in advance how serious the undoubted conceptual weakness of such an approach will in fact prove to be. It seemed desirable to us to adopt this simple hypothesis initially since its use facilitates the numerical solution of the describing equations; moreoever, it will be desirable to have a 'baseline' prediction available against which to judge computations to be obtained later with more elaborate models of the turbulence field.

From the wall extending to a radius of $0.94a - 0.95a$, where a is the pipe radius, the turbulent viscosity is given by the mixing length hypothesis (Prandtl, 1926) extended to three-dimensional

flows by requiring consistency with the local equilibrium form of the turbulent kinetic energy equation. In the near-wall zone, gradients with respect to r far outweigh other terms and so:

$$\mu_t = \rho \ell_m^2 \left[\left(\frac{\partial W^2}{\partial r} \right) + \left(\frac{\partial U}{\partial r} - \frac{U}{r} \right)^2 \right]^{\frac{1}{2}}$$

(2.6)

The mixing length ℓ_m is given by Van Driest's (1956) proposal that

$$\ell = \kappa y (\ell - \exp - y U_\tau / 26 \nu)$$

(2.7)

where y is the distance from the wall $(a-r)$ and U_τ is the friction velocity based on the *resultant* wall shear stress. The von Karman constant κ takes the value of 0.419.

Over the main region of flow the turbulent viscosity is obtained from the standard high Reynolds number version of the k~ε Boussinesq viscosity model (Jones and Launder, 1972, Launder and Spalding, 1974) wherein

$$\mu_t = c_\mu \rho \kappa^2 / \varepsilon$$

(2.8)

and the turbulent kinetic energy k and its rate of dissipation are found from the solution of transport equations of the same type as equation (2.2) in which the source/sink terms take the following form:

ψ	$S_c(\psi)$	$S_d(\psi)$	$S_p(\psi)$
k	0	$\mu_t G$	$- \rho\varepsilon$
ε	0	$c_1 \frac{\varepsilon}{k} \mu_t G$	$- c_2 \frac{\rho\varepsilon^2}{k}$

where G $\equiv 2\left(\frac{\partial V}{\partial r}\right)^2 + 2\left(\frac{1}{r_c}\frac{\partial W}{\partial \theta} + \frac{V\cos\theta - U\sin\phi}{r_c}\right)^2 + 2\left(\frac{1}{r}\frac{\partial U}{\partial \phi} + \frac{V}{r}\right)^2$

$+ \left(\frac{\partial W}{\partial r} - \frac{W\cos\phi}{r_c} + \frac{1}{r_c}\frac{\partial V}{\partial \theta}\right)^2 + \left(\frac{1}{r}\frac{\partial V}{\partial \phi} + \frac{\partial U}{\partial r} - \frac{U}{r}\right)^2$

$+ \left(\frac{1}{r}\frac{\partial W}{\partial \phi} + \frac{1}{r_c}\frac{\partial U}{\partial \theta} + \frac{W\sin\phi}{r_c}\right)^2$

The empirical coefficients appearing in the k and ε equations take the following standard values:

$C_\mu = .09; \quad C_1 = 1.44; \quad C_2 = 1.90; \quad \sigma_k = 1.0; \quad \sigma_\varepsilon = 1.22$

At the interface with the mixing length hypothesis, the values of k and ε are fixed by requiring that the viscosity given by equations (2.6) and (2.8) should be the same and by taking the turbulent length scale $\ell(\equiv k^{3/2}/\varepsilon)$ equal to $\ell_m/c_\mu^{3/4}$ as in a simply sheared, equilibrium, near-wall flow. The resultant expressions are

$$k = \mu_t^2 / c_\mu^{1/2} \, \ell_m^2 \; ; \qquad \varepsilon = c_\mu k^2 / \mu_t$$

where μ_t is the value of turbulent viscosity given by eq (2.6).

2.3 Discretization

The present computational procedure has taken as its starting point a code for solving the fully-elliptic laminar flow equations in toroidal co-ordinates kindly provided by Professor J.A.C. Humphrey (Humphrey, 1977). This had been developed within the framework of the well-known TEACH family of computer programs. Like other finite-volume, primitive variable procedures, the differential equations presented in §2.1 and §2.2 are discretized by integrating them over small contiguous control volumes which together cover the whole flow domain. To each control value is attached a discrete value of the dependent variable. A staggered arrangement of grid nodes is adopted with velocity components located at the boundaries of the control volumes for the scalar variables (p,T,k and ε). We retain the usual TEACH practice of assuming a linear variation of dependent variable between nodes in evaluating diffusion processes while treating source and sink terms as uniform over each control volume with a value equal to that at the node.

In the treatment of convection, the upwind/central hybrid differencing normally incorporated in TEACH is retained only for the streamwise velocity component W. For the components in the plane of the cross section, the more accurate quadratic upwind interpolation (Leonard, 1979) has been incorporated. (See Han et al, 1981 and Huang et al, 1983 for a comparison of the performance of quadratic and hybrid differencing).

Pratap and Spalding (1975) adopted the SIMPLE procedure (Patankar and Spalding, 1972) for use in their semi-elliptic computations. We have found, however, that the newer scheme SIMPLER (Patankar, 1980) produced rates of convergence an order of magnitude faster. The original pressure-velocity iteration sequence has had to be modified somewhat to allow it to fit compatibly within the present semi-elliptic treatment with only the pressure available in three-dimensional storage: (i) The solution begins with a guessed initial pressure field starting from the initial (upstream) plane and marching plane by plane downstream. At each step with the pressure field fixed, the U and V momentum equations are first solved on a plane followed by that for the W velocity (located one half cell downstream). (ii) The velocity field is next corrected by way of the standard pressure-correction equation in order to satisfy continuity. (iii) The current plane pressure field is then updated by solving the Poisson equation for pressure over the plane using the updated

velocities.   (iv) The current plane velocity field is
re-calculated using the updated pressure field.   (v) The current
plane velocities and the pressure field on all downstream planes
are   adjusted   by   way   of   the   Pratap-Spalding   bulk   pressure
correction to ensure that the prescribed mass flow rate is passing
that section.   (vi) The current plane velocity field is
re-corrected via the pressure-correction equation.   (vii) For
turbulent flow, the turbulent kinetic energy and dissipation rate
are solved and the turbulent viscosity is updated.

The above steps are repeated at each succeeding plane and,
when a complete downstream sweep has been completed, the sequence
begins over again at the upstream plane unless the solution has
fully converged.

As the calculation approaches convergence, first one and
later two iterations are introduced at each plane in solving the
momentum equations in order to re-form coefficients and source
terms in terms of current plane values.   (When marching without
iteration, one necessarily has to evaluate these quantities from
upstream values).   Although, apparently, Pratap and Spalding
(1975)   did   not   incorporate   such   iterations   into   their
computations, the bend flows considered in their study were far
milder than those of the present study and thus streamwise
variations were less rapid.

Within a thin annular ring extending from the wall to 0.05a
a much simpler and economical numerical procedure has been adopted
in our most recent calculations.   The region is treated as a
parabolic sublayer (PSL), Iacovides and Launder (1984) in which,
for a given ϕ and θ, the pressure at any point in the sublayer
above that at the first node <u>outside</u> the sublayer is obtained by
assuming radial equilibrium.   Thus, no pressure nodes are required
in the PSL, a feature that allows the use of a fine near-wall mesh
for the velocity field without prohibitive core demands (the
pressure, it will be recalled, is the only variable for which
three-dimensional storage is needed).   A further simplification is
that the radial momentum equation is not solved, the V velocities
being obtained directly by application of continuity to the
control volume surrounding the pressure node.

3.   Numerical Results

The computations reported below have been obtained on UMRCC's
CDC7600 computer with meshes sufficiently fine that purely
numerical errors are believed to be of minor importance.   There
is little scope for establishing grid-independence of three-
dimensional flows by successive mesh refinement with a computer of
this size and accordingly our attention is directed first at the
laminar flow results of Enayet et al (1983) for R/D = 2.8 at a
Reynolds number of 1093.   The computed results have been obtained
with 20 nodes in the radial (r) and circumferential (θ) directions
and with 100 streamwise planes, 70 of which are in the 90° bend
itself and the remainder in the approach and downstream tangents.
A preliminary run was made of developing flow in a straight pipe,
the flow being allowed to develop until best agreement was
obtained with the 90° bend data at the station 0.58 diameters

upstream of the bend. The computed profiles obtained in that run 2.4 diameters upstream of that position were then used as the starting profiles in the calculation proper (i.e. at a position 3 diameters ahead of the 90° bend).

The development of the measured and computed axial velocity profiles is shown in figure 2 at three stations. Due to differences in the refractive index of the perspex tube walls and the fluid, the LDA measurements were made along the non-parallel lines shown in the inset; the corresponding computed velocities along the same lines have been obtained by interpolation. Agreement between measurement and calculation is generally very close. This set of data has previously been predicted by Levy et al (1983) using their scheme for correcting, in a one-dimensional marching manner, the potential flow pressure distribution. Agreement between their results and the present computations is close over the first half of the bend, but deteriorates somewhat towards the flow-exit, presumably because their rather simple pressure treatment gradually loses accuracy as the shear flow becomes more tangled. In fact, Levy et al (1983) report two regions of flow separation in their computations, one on the outside of the bend from 0-15° of arc and the other on the inside from about 80° to the downstream limit of computations (the location of this final plane was not reported). There seems no suggestion in the experimental data that separation occurred and in the present computations the minimum value of friction factor was 57% of that in fully developed flow in a straight tube at the same Reynolds number and occurred just beyond the 90° position.

The corresponding turbulent flow calculations are shown in figures 3-5, the experimental data again being due to Enayet et al (1982) obtained in the same curved duct but now at a Reynolds number of 4.3×10^4. Computations of the velocities were made on a 20 x 27 mesh in the cross-sectional plane, the additional seven nodes being placed in the 'parabolic sublayer'. At the node adjacent to the wall, a typical value of the normal distance yU_τ/ν was 3; thus turbulent stresses were entirely negligible compared with those due to viscous shear. As with the laminar flow tests, a preliminary run was made in a straight duct to develop the boundary layer by the same amount as the experiments indicate. Streamwise velocity profiles are shown in figure 3. For this flow, agreement beyond 30° is not as complete as for laminar flow. Although the general character of the development is reproduced, with the accumulation of low momentum fluid on the inside of the bend, the detailed behaviour, particularly the double peak in the streamwise velocity on the plane of symmetry at 60° and 75°, is not correctly predicted. (In this region the present computations give nearly the same behaviour as those of Levy et al (1983) who have also examined this flow). At one diameter downstream of the bend, agreement is significantly improved. Indeed, while the remarks above have emphasized *differences* between experiment and computation, it may be noted that the level of agreement achieved is far superior to that obtained by Chang et al (1983) in a *square* sectioned 180° bend with the same turbulence model in the main flow but where wall functions were used to apply near-wall boundary conditions.

Typical secondary velocity profiles are shown in figure 4.

The most striking feature is the fact that the maximum secondary velocity occurs very close to the wall, well within the region of substantial viscous influence. It is this feature that makes the wall-function approach inappropriate to this type of flow. The streamwise wall shear stress around the inner line of symmetry is shown in figure 5. Due to the combined effect of secondary flow and the adverse pressure gradient encountered on exit from the bend, the shear stress falls to zero (indeed becomes marginally negative) in the exit region. The present semi-elliptic scheme can strictly not cope with streamwise separations but the reverse flow velocities were very weak and confined within the viscous region so that no special measures were needed since the troublesome convective terms were negligible. That the turbulent flow should separate but the corresponding laminar flow should not is of course entirely contrary to experiences in two-dimensional flow.

The thermal energy equation has also been solved in this case for a molecular Prandtl number of 0.7. A uniform heat flux is applied starting 3 diameters upstream of the bend, the flow entering at uniform temperature. As the flow develops around the bend there is a moderate increase in the average level of the Nusselt number. Figure 6 indicates that the circumferential variation is small over most of the perimeter, but by 60° a strong decrease in heat transfer coefficient develops on the inside of the bend due to the fact that the fluid arriving there has been passing close to the pipe wall as it moves from the outside to the inside of the bend (cf. figure 4). There is also a small peak in Nu at the outer line of symmetry, in this case due to the impingement of relatively cool high velocity fluid. The ratio of maximum:minimum Nusselt number grows to nearly 5:1 by 75°. These large variations diminish rather slowly on entry to the straight downstream tangent, the ratio of outer to inner heat transfer coefficients having fallen only to 4:1 at one diameter beyond the end of the bend.

An even stronger impression of the acrobatic variation of heat transfer coefficient is conveyed by figure 7 which shows the Nusselt number variation around the inner line of symmetry. (The values are normalized by the maximum value in the field which occurs at the initial station. Since the entering fluid temperature is uniform, the actual value of Nusselt number is of no physical significance - it depends simply on the distance from the pipe wall of the near-wall node). The modest rise in Nu at entry to the bend arises from the initial flow acceleration on the inside of the bend; thereafter the strong decrease indicates the accumulation of sluggish low-momentum, heated fluid on the inside transported there by the secondary flow. The whole pattern closely resembles the variation of wall shear stress shown in figure 5, save that the Nusselt number does not go to zero with τ_w. The minimum in Nu, occurring at the bend exit is, however, less than 20% of that at entry to the bend.

At present no measurements of local heat transfer coefficients are known for developing flow around pipe bends. Seban and McLaughlin (1953) have, however, reported such data for the flow of water in long coils where development lengths are sufficient for fully-developed flow to be established. This case

has been simulated using only four streamwise pressure planes, downstream values being successively transferred upstream until the flow pattern ceased to change.[†] The resultant circumferential distributions of Nusselt number are compared with the Seban-McLaughlin data in figure 8. The case of R/d = 5? is quite well predicted though the experiments display a somewhat greater circumferential variation than do the computations. Qualitatively, one would expect this type of difference to arise with a Boussinesq viscosity model (BVM). Real turbulence is known to be highly sensitive to small amounts of streamline curvature, heat transfer coefficients being augmented in boundary layers developing on concave surfaces and damped on convex ones. BVMs do not capture this sensitivity and it is to this failure that we may attribute the differences shown in figure 8a. A similar behaviour is also shown in figure 8b for a bend with R/d = 8.5. The differences in Nusselt number between computation and experiment on the outer half of the bend are now more marked, the computed levels being nearly 40% below the data in places. This result may reflect simply the deterioration in the model's ability to mimic the turbulent transport processes as curvature effects become progressively stronger. It should at least be noted, however, that the experimenters had several difficulties with this tighter bend. The stainless steel coil was fabricated from a straight tube and, in bending, creasing occurred on the inside of the bend, stretching on the outside (with attendant modification of the tube's electrical resistivity) and some distortion of the cross-section shape. In view of these departures in the experiment from the idealized geometry and boundary conditions, firm conclusions on this issue cannot be reached.

4. Conclusions

● A semi-elliptic solving procedure combined with the parabolic sublayer treatment adjacent to the pipe wall offers a promising route for the numerical analysis of complex three-dimensional flow in pipe bends with strong curvature.

● Although agreement is not complete, broadly satisfactory correspondence has been demonstrated with the velocity data of Enayet et al (1982) obtained in a tight 90° bend.

● The present Boussinesq viscosity model leads to an underestimate of the circumferential variation in heat transfer coefficient in fully developed flow through a coil (though for many engin.ering purposes the measure of agreement achieved would be satisfactory). The differences are believed to arise from the known insensitivity of BVMs to streamline curvature. The introduction, in the future, of a turbulence model based on second-moment closure should lead to more satisfactory predictions.

[†] This reduction in the size of the pressure array allowed us to increase the number of radial nodes to 40 and the number of circumferential nodes to 25. This refinement from the original 27 x 20 mesh gave levels of Nu which differed by at most 1% from those obtained with the coarser mesh, figure 11b.

References

Chang, S.M., Humphrey, J.A.C., Johnson, R.W. and Launder, B.E. (1983) Proc. 4th Sympos. Turbulent Shear Flows 6.20 University of Karlsruhe

Enayet, M.M., Gibson, M.M., Taylor, A.M. and Yianneskis, M. (1982) Int. J. Heat & Fluid Flow $\underline{3}$, 213

Han, T.Y., Humphrey J.A.C. and Launder, B.E. (1981) Comp. Meth. Appl. Mech. Engrg. $\underline{29}$, 81

Huang, P.G., Launder, B.E. and Leschziner, M.A. (1983) UMIST Mech. Eng. Dept. Rep. TFD/83/1

Humphrey, J.A.C. (1977) PhD thesis, Faculty of Engineering, University of London

Humphrey, J.A.C., Iacovides, H. and Launder, B.E. (1984) "Some numerical experiments on developing laminar flow in 180° circular sectioned bends" UMIST Mechanical Engineering Department Report TFD/84/2

Iacovides, H. and Launder, B.E. (1984) "PSL - An economical approach to the numerical analysis of near-wall elliptic flow" ASME J. Fluids Eng. $\underline{106}$, to appear

Jones, W.P. and Launder, B.E. (1972) Int. J. Heat & Mass Transfer $\underline{15}$, 301

Kline, S.J., Cantwell, B. and Lilley, G. (1982) (Editors) Proc. 1980-81 AFOSR-HTTM-Stanford Conference on Complex Turbulent Flows, Vol. II and III, Thermosciences Division, Stanford University

Launder, B.E. and Spalding, D.B. (1974) Comp. Meth. Appl. Mech. Engrg. $\underline{3}$, 269

Launder, B.E., Johnson, R.W. and Iacovides, H. (1983) "Convective transport in flow around a 180° bend" Annual Rep. 1981/82 on ONR RG N00D14-80-G-0130, UMIST Mech. Eng. Rep. TFD/83/2 (R)

Leonard, B.P. (1979)   Comp. Meth. Appl. Mech. Engrg. 19, 59

Levy, R., Briley, W.R. and McDonald, H. (1983)   AIAA Paper 83-055

McDonald, H. (1982)   Proc. AFOSR-HTTM-Stanford Conference on Complex Turbulent Flows, Vol. III, 1424

Patankar, S.V. (1980)   Numerical heat transfer and fluid flow, Hemisphere Publishing Corp. - McGraw Hill

Patankar, S.V. and Spalding, D.B. (1972)   Int. J. Heat Mass Transfer 15, 1787

Prandtl, L. (1925)   ZAMM 5, 136

Pratap, S.V. and Spalding, D.B. (1975)   Aero. Quart. 26, 219

Rowe, M. (1970)   J. Fluid. Mech. 43, 771

Seban, R.A. and McLaughlin, E.F. (1963)   Int. J. Heat Mass Transfer 6, 387
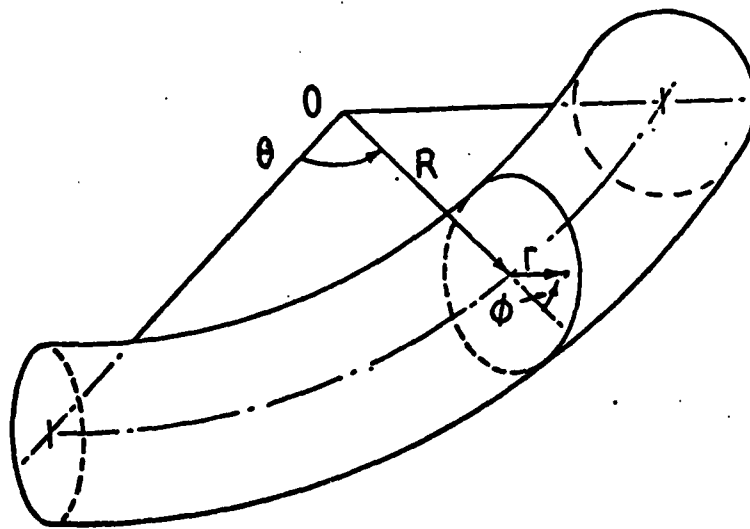
Van Driest, E.R.. (1956)   J. Aero. Soc. 23, 1007
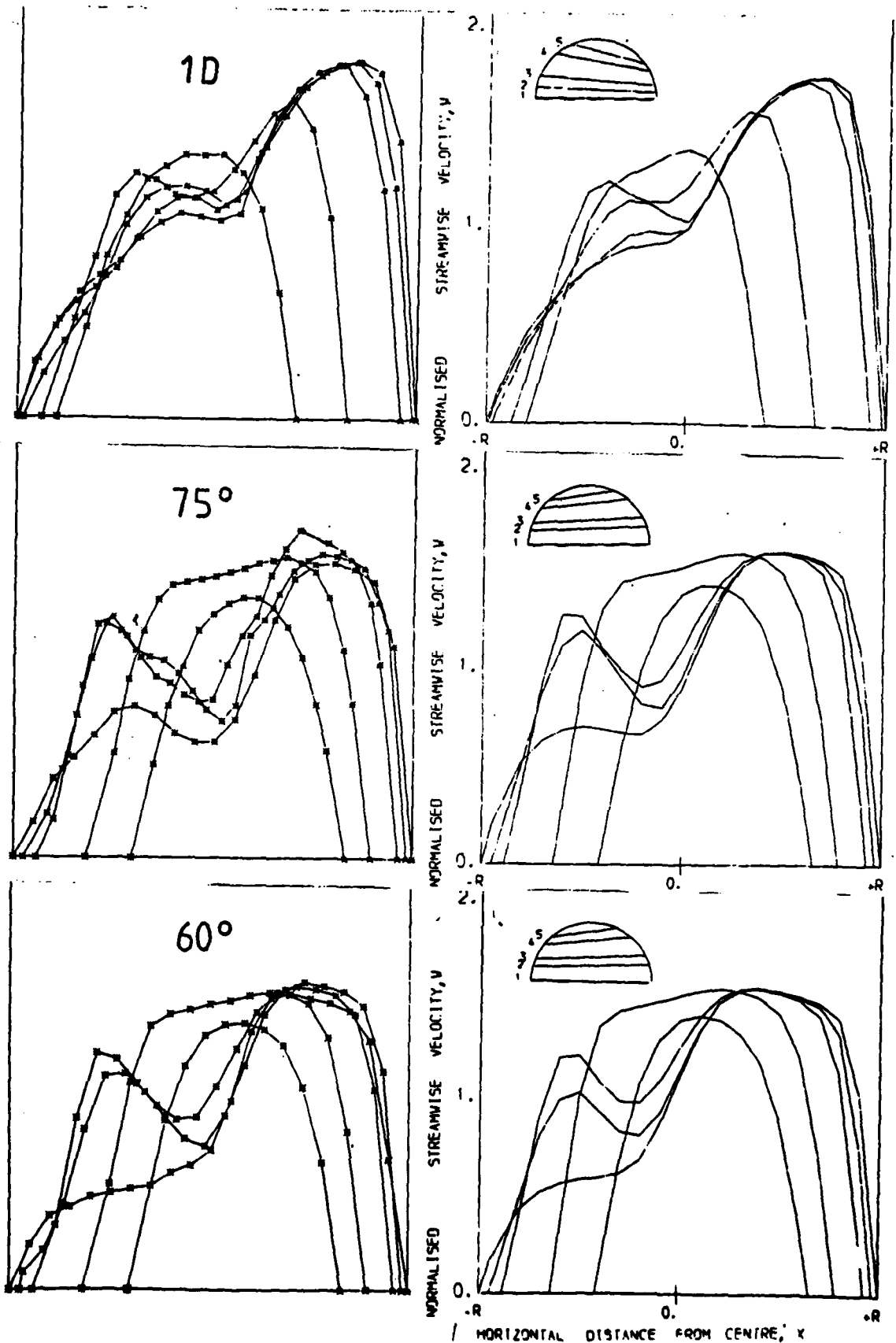
Figure 1   Toroidal coordinate system

Figure 2   Streamwise velocity profiles in laminar flow around 90° bend
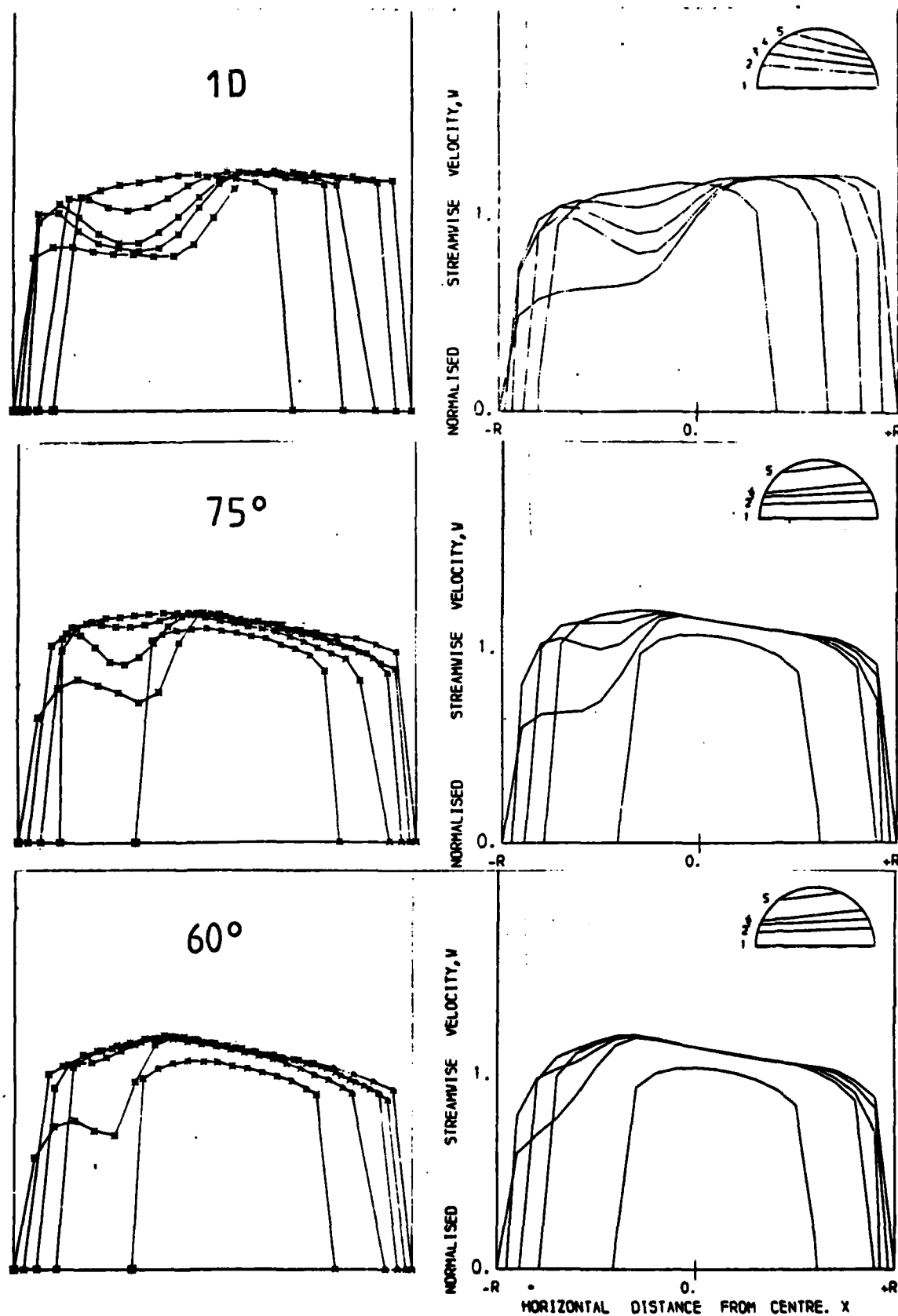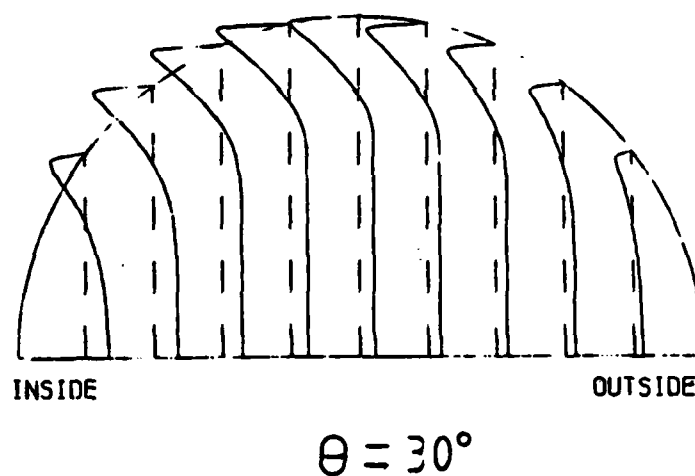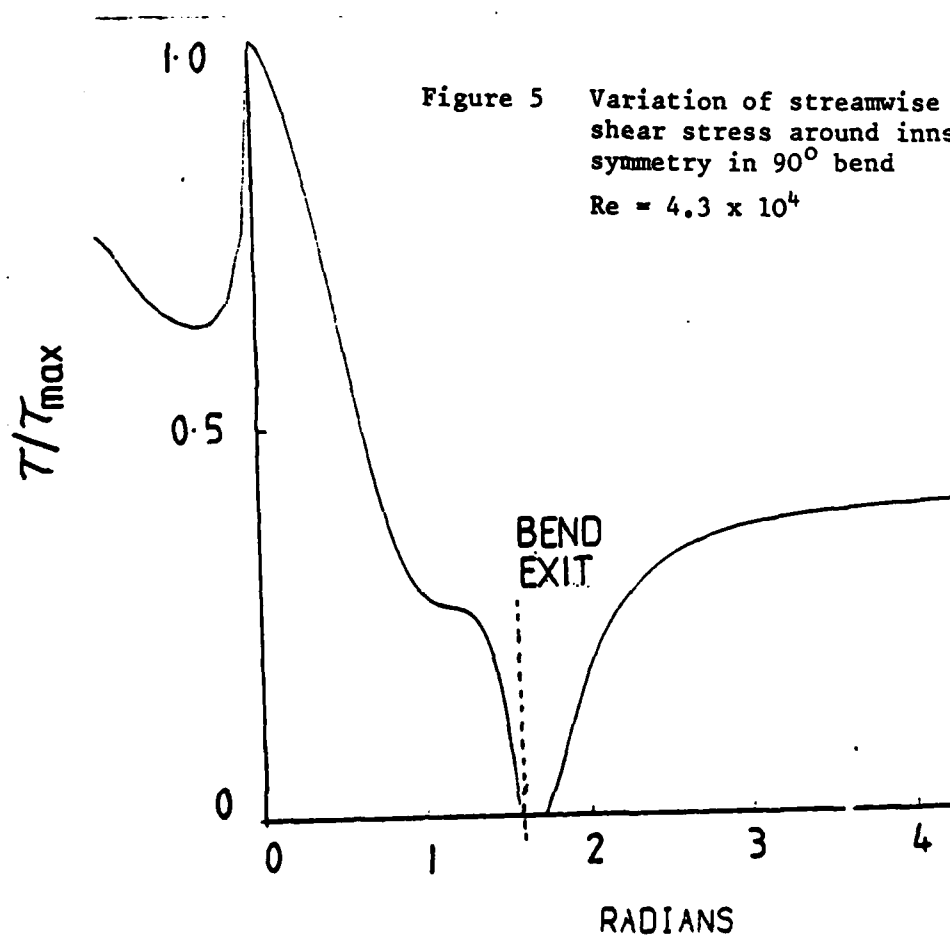Re = 1.09 x 10³ ⊸ Experiment (Enayet et al) ──Present computations

Figure 3   Streamwise velocity profiles in turbulent flow around 90° bend
Re = 4.3 x 10⁴ ← Experiment (Enayet et al) ——— Present computations

INSIDE   OUTSIDE

$$\theta = 30°$$

DISTANCE   BETWEEN   ADJACENT   DATA LINES
CORRESPONDS TO 25.0%   OF BULK   VELOCITY

Figure 4   Predicted secondary profiles for
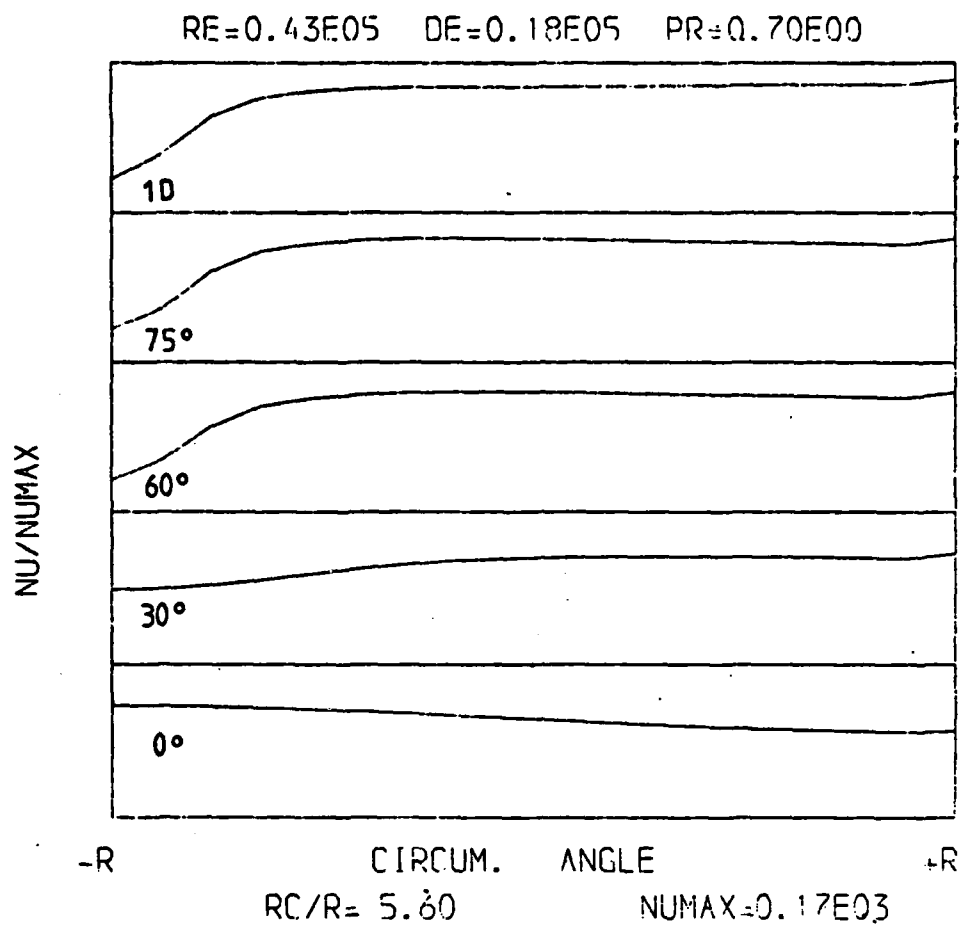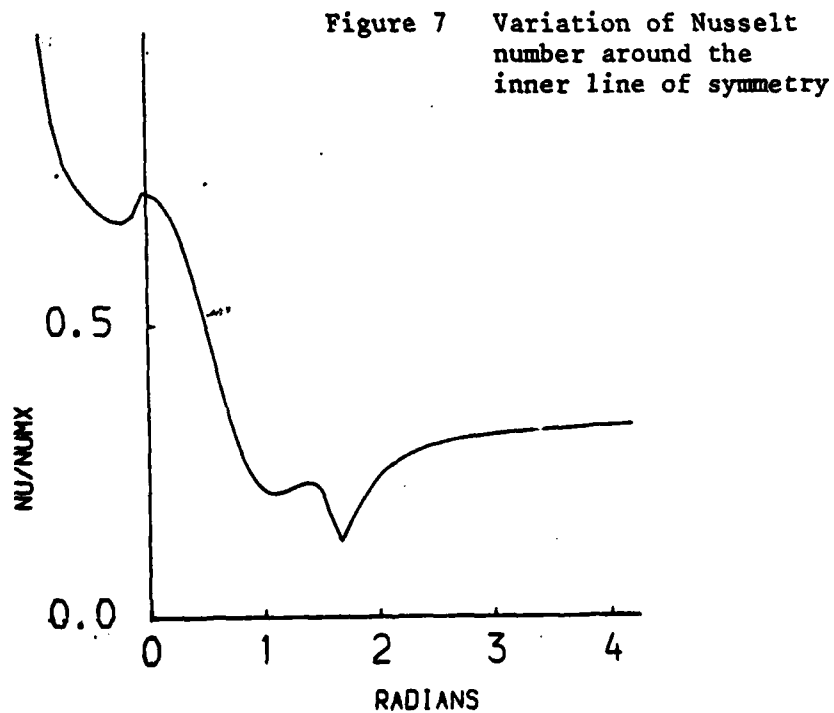   turbulent flow in a 90° bend
             Re = 4.3 x 10⁴

Figure 5   Variation of streamwise wall
             shear stress around inner line of
             symmetry in 90° bend
             Re = 4.3 x 10⁴

RE=0.43E05   DE=0.18E05   PR=0.70E00

10

75°

60°

30°

0°

NU/NUMAX

-R   CIRCUM.   ANGLE   +R
RC/R= 5.60   NUMAX=0.17E03

Figure 6   Development of convective heat transfer coefficient in 90° bend
Re = 4.3 x 10³; De = 1.8 x 10³; Pr = 0.7

Figure 7   Variation of Nusselt
number around the
inner line of symmetry

0.5

0.0

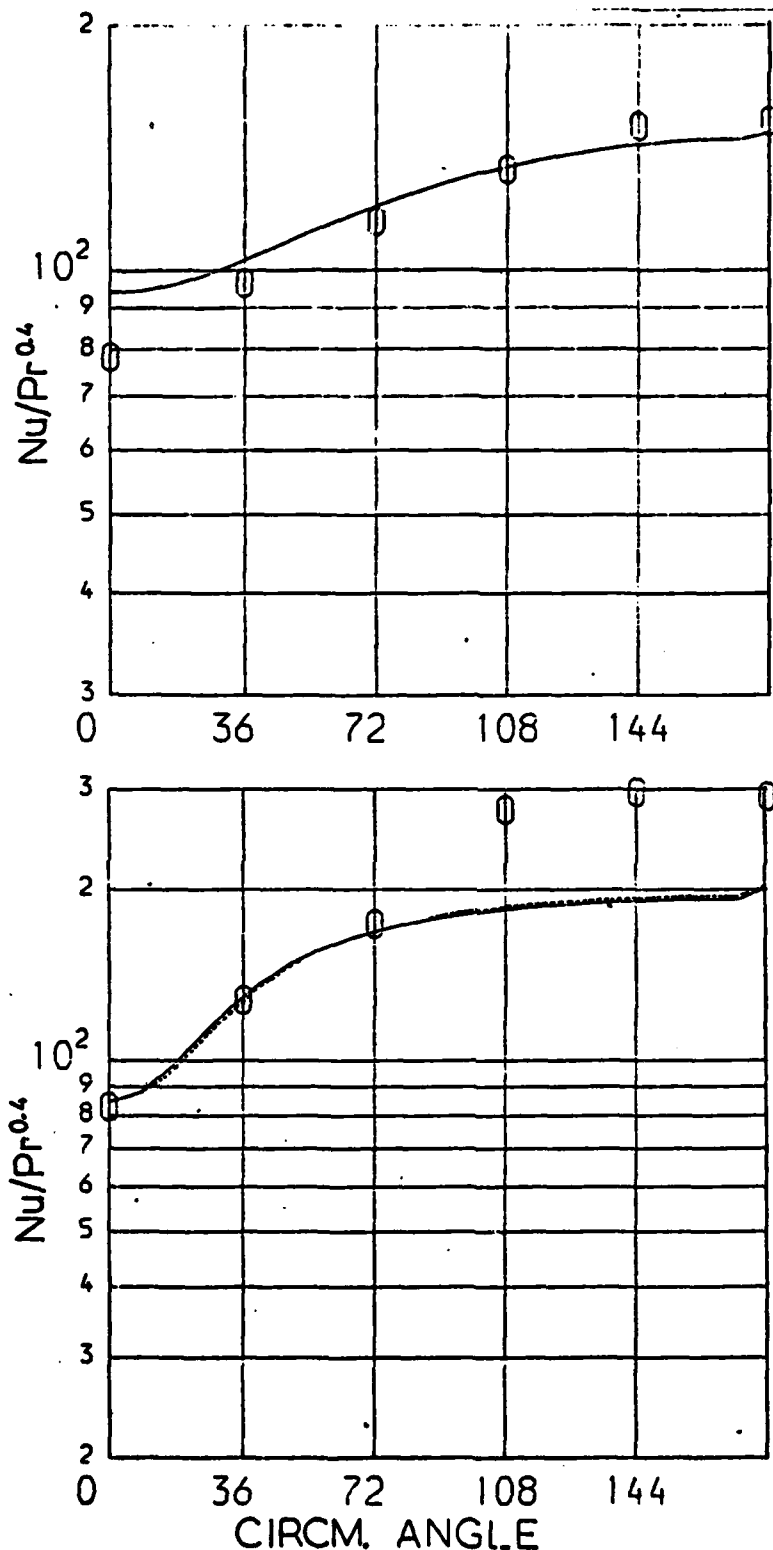NU/NUMX

0   1   2   3   4
RADIANS

Figure 8   Circumferential variation in Nusselt number in fully developed flow
through a coil

O   Experiment (Seban, McLaughlin)   ——— Present predictions

------ Refined grid (40 x 25)

(a)   R/D = 52   (b)   R/D = 8.5

APPENDIX 4

PSL - An Economical Approach to the Numerical Analysis

of Near-Wall, Elliptic Flow

by
H. Iacovides and B.E. Launder

University of Manchester Institute of Science and Technology
Manchester M60 1QD, England

Abstract

The paper points out that, in the numerical computation of elliptic
or three-dimensional turbulent flows, the neglect of pressure-variations
across the very thin viscosity affected region near the wall allows a
fine-grid analysis of this sublayer without prohibitive penalties in
core or computational time. The scheme has been successfully applied
to the three-dimensional flow around a U-bend.

1. Introduction

In the numerical study of complex, two-dimensional turbulent flows near walls, one commonly finds that a different approach to handling the near-wall low-Reynolds-number region (i.e. the viscous sublayer and "buffer" layer) is adopted, depending upon whether the flow as a whole is of boundary-layer or "recirculating" type. In the former case, because an economical, once-through marching solution can be applied, the near-wall zone is often analysed by adopting a fine grid to cover the low-Reynolds-number region. Such an approach is rarely practicable in an elliptic flow, however, because the coupling of the velocity and pressure fields requires an iterative solution; this feature means not only that computer times may typically be two orders of magnitude greater than for a boundary-layer study, but also that the dependent variables must be stored over the whole solution domain. Because of the substantial core and computer time requirements, the near-wall region is usually handled by way of wall functions (1) in which wall adjacent nodes are placed relatively far from the surface so that they lie in the region of fully turbulent fluid. The wall functions attempt to embody, through a mixture of analysis and experimental data, the integrated effects of the near-wall sublayer; in this way, no substantial near-wall mesh refinement is needed. This feature is crucial in keeping the overall core and

computing time requirements to manageable levels and is the
reason why, despite the crudeness of the physical treatment,
wall functions are nearly universally adopted. The above
remarks apply with even greater force to three-dimensional
flows.

The problem with such a simple approach to the physics is
that it is not adequate to account for the diversity of the
phenomena displayed by turbulent flow near walls. There
are, for example, many situations where the velocity vector
parallel to the wall undergoes strong skewing across the
low-Reynolds-number region, a feature which no wall-function
approach appears to have mimicked successfully.

The purpose of the present note is to recommend a new
numerical practice that facilitates the use of
fine near-wall mesh in computing elliptic and three-dimension-
al flows. This development thus opens the way to more refined
modelling of the physics of the near-wall region than has
hitherto been employed.

2. The PSL Scheme and its Application .

The PSL scheme is based on the idea that, while the flow as
a whole must be regarded as elliptic, there is a thin
parabolic sublayer (whence the acronym) immediately adjacent
to the wall across which static pressure variations are
negligible or, in the case of highly-curved surfaces, where
the variation may be obtained by assuming radial equilibrium.
This parabolic sublayer is taken to extend over the whole of
the low-Reynolds-number region where the turbulent transport
properties exhibit such a strongly non-linear variation.
If, as we have argued is desirable on physical grounds, a
fine grid treatment is employed across this region, then
major simplifications may be made to the conventional,
incompressible elliptic treatment, (2). Our own implement-
ation of the idea has been within the context of finite
volume procedures employing a staggered arrangement of
dependent variables, Fig. 1 (analogous simplifications can
clearly be adopted with an orthodox finite difference
method). Within the PSL:

    (i)   the pressure does not require storing (it
           is given by the pressure just outside the
           region);

    (ii) thus, no Poisson or pressure-perturbation
           equation has to be solved;

(iii) .the velocity component normal to the wall may be

obtained very rapidly by cell continuity rather

than by solving the normal momentum equation.

Thus, referring to Fig.1, for a Cartesian

mesh and a two-dimensional flow,

$$V(I,J) = (U(I-1,J)-U(I,J))\delta y/\delta x + V(I,J-1)$$

These are, of course, the classic boundary-layer simplifications

known for 80 years; what appears to be novel is their application

to a very thin sublayer in a shear flow that is overall not

analysable under the boundary-layer approximation. The adaptations

required to most elliptic solving schemes to incorporate the PSL

treatment will be trivial. In the codes used at UMIST the

momentum equation (or equations) for the component(s) parallel

to the wall are solved simultaneously over both the elliptic

region and the PSL; the velocity component normal to the wall

within the PSL is found next by applying continuity to the pressure

cells; thereafter, the momentum equation for this component is

solved over the elliptic region only. Finally the pressure or

pressure-correction equation is solved over the elliptic region

with corresponding adjustments also being made to the velocity

field.

There is also often scope for reducing storage associated with

velocity-component information. In many cases, at the expense

of somewhat more code reorganization, the solution can be

arranged so that velocities in the PSL are stored only on the

row contiguous with the elliptic region and along two
1-dimensional columns of nodes (which are successively over-
written), rather than in a full 2-dimensional array.

A referee has queried the use of the PSL approach in the
vicinity of a stagnation point where the variation of pressure
normal to the wall is relatively rapid. Perhaps the first
thing to emphasize is that any errors associated with pressure
variations across the buffer region will affect coarse-grid
wall-function schemes at least as much as a PSL approach.
Our experience at UMIST suggests in fact that even on the
axis of an impinging jet the PSL approximation can be applied
over most of the low Reynolds number region. Although in
our applications to date the PSL treatment has been applied
to the same number of cells in each column (viz Fig.1), this
practice is neither necessary nor optimal in some applications.
In the impinging jet, for example, a thin PSL at the stagnation
point could be expanded to cover the full height of the domain
once the jet had been deflected into a radial wall jet. Indeed
a self-adjusting scheme for the number of nodes in the PSL at
any x-position could readily be devised.

The most important field of application of the approach is
perhaps in three-dimensional flows describable by the partially
parabolic equations for there only the pressure field requires
3D storage. The scheme has been successfully applied by the
authors to the turbulent flow in a circular tube around a $90°$

each radial string of
nodes

bend. Nine nodes have been put in the parabolic sublayer along/

For identical grid densities in the fully turbulent region,

computing times are no longer (in fact somewhat less) than

with our previously used wall-function approach; core require-

ment is also little affected because most of this is

associated with the pressure field which (alone) has to be

held on a three-dimensional array (and which is identical

for the two approaches since there are no pressure nodes

within the PSL). The PSL scheme has also been applied in

high Reynolds number *laminar* flow around pipe bends where

again near the wall the velocity field undergoes very

rapid changes but the pressure is obtained adequately via

radial equilibrium.

The scheme has since been adopted by two of our colleagues

who had hitherto been using a fine-grid low-Reynolds-number

approach within two-dimensional fully elliptic treatments.

When there were no flow reversals in the near-wall layer,

the introduction of PSL reduced their computational times,

in one case by a factor of two and in the other by a factor

of three.† Benefits were much reduced when reverse flow

was present but it seems likely that these can be substantially

restored by reorganizing the solution in the PSL so that the

direction of marching is always that indicated by the velocity

at the outer edge of this sub-layer.

---

† Their numerical results obtained with PSL are insignificantly
   different from those given by the fully elliptic solution
   using an identical mesh.

3. <u>Conclusion</u>

The PSL approach allows a fine-grid resolution to be applied
to the near-wall sublayer with no significant increase in
computer time or storage, compared with a conventional wall-
function treatment. Because the former scheme facilitates
a better modelling of the turbulent transport processes, it
is thought that in many cases it may supplant the latter.

Acknowledgements

References

1.   Launder, B.E. and Spalding, D.B. 'The Numerical Computation of Turbulent Flows' Comp. Meth. Appl. Mech. and Engrg. 3, 269, 1974.

2.   Patankar, S.V. and Spalding, D.B. 'A Calculation Procedure for Heat Mass and Momentum Transfer in 3-Dimensional Parabolic Flows' Int. J. Heat Mass Trans. 15, 1787, 1972.
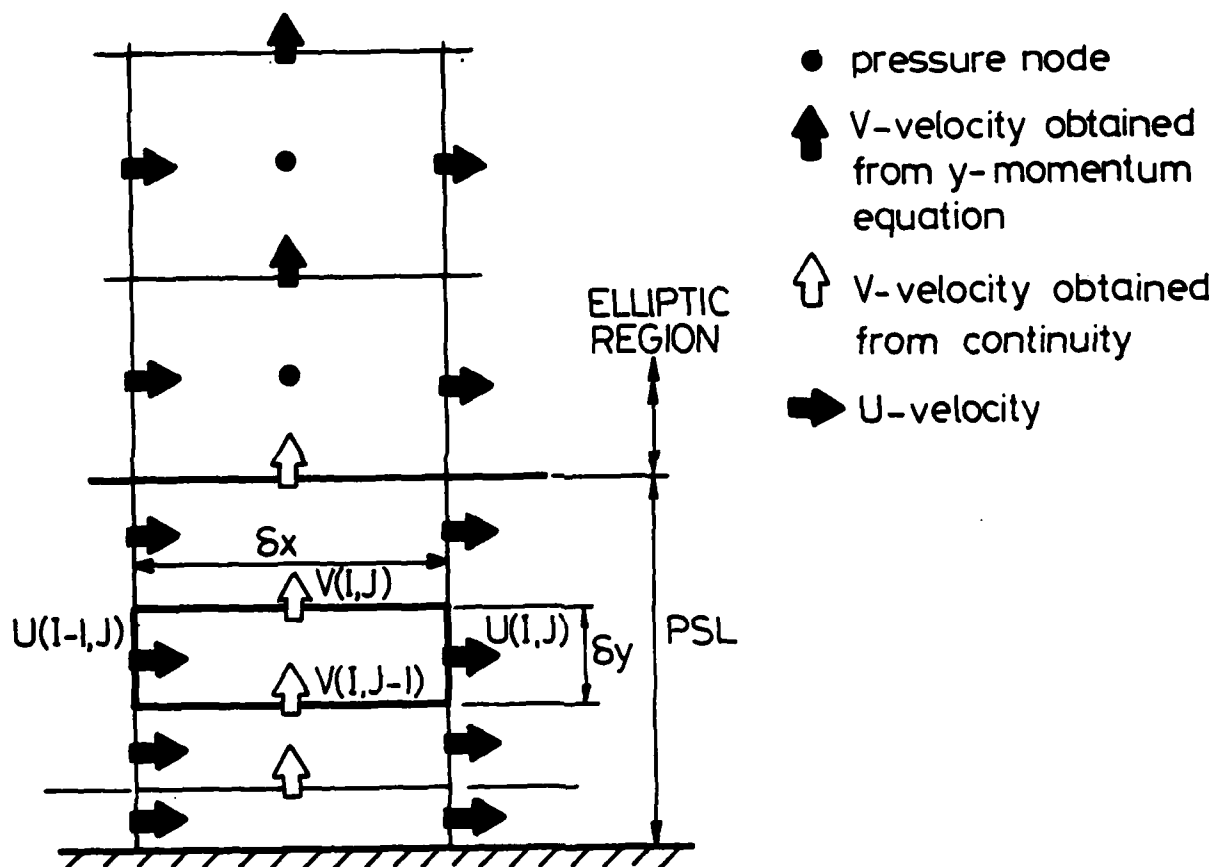
Figure 1   Treatment of Velocity
             and Pressure Nodes near
             a Wall